2023

Compound Flood Modeling of Tropical Cyclone Events in Coastal Bays and Estuaries

Nahal Maymandi

Compound Flood Modeling of Tropical Cyclone Events in Coastal Bays and Estuaries

by:

Nahal Maymandi

Presented to the Faculty of the Graduate School of

The University of Texas at Arlington in Partial Fulfillment

of the Requirements for the Degree of

Doctor of Philosophy

The University of Texas at Arlington

December 2023

To my parents, and brother. I am truly honored to have you as my family.

To all flood victims.

Acknowledgements

To begin, I would like to express my gratitude to my advisor, Dr. Michelle Hummel, for her continuous guidance and support as my supervising professor throughout my Ph.D. years. I am also thankful to my committee members, Dr. Yu Zhang, Nick Fang, and Qin Qian, for their interest in my research, providing valuable data, and insightful comments. Additionally, I appreciate the efforts of Dr. Joseph Kruger and Arifur Rahman in sharing some input data. I am grateful for the financial support provided by the National Oceanic and Atmospheric Administration's (NOAA) Climate Program Office under the COCA and SARP programs (grant NA19OAR4310347).

I value the efforts of both the current chair, Dr. Melanie Sattler, and the former chair, Dr. Ali Abolmaali, in making the UTA Civil Engineering department a place to grow. Additionally, I want to express my gratitude to my colleagues for the shared moments and their companionship throughout these years. I am also thankful to all the teachers who have contributed to my growth every day over the years.

Last but not least, thank you very much, Mom and Dad, for all the sacrifices, love, patience, guidance, and support you've provided me throughout my entire life. You have always believed in me, and without you, I couldn't have reached this point. You are the most beautiful part of my life, and it will always remain so. Thank you, my dear brother, for being great company throughout my life, even when we have been miles apart. I also appreciate the love and encouragement from my extended family.

December 13, 2023

Abstract

Compound Flood Modeling of Tropical Cyclone Events in Coastal Bays and Estuaries

Nahal Maymandi, Ph.D.

The University of Texas at Arlington, 2023

Supervising Professor: Michelle A. Hummel

Flooding due to tropical cyclones can cause severe impacts on coastal communities, particularly when multiple types of flooding (e.g., coastal and riverine) interact to create a compound flood event. In typical flood hazard assessments, these drivers of flooding are considered separately, even though they may interact and produce more severe flooding. Understanding the interactions between flood drivers is necessary to accurately plan for and respond to future flood events. This dissertation aims to improve the assessment of coupled coastal, fluvial, and pluvial flooding in coastal bays and estuaries impacted by tropical cyclones. To do this, a hydrodynamic model is developed to simulate compound flooding in the Sabine-Neches Estuary in Southeast Texas. In Chapter 2, the model is applied to survey the flooding of three historical hurricanes: Harvey, Ike, and Rita. The results show that interactions between coastal, riverine, and rainfall processes are all possible in the study area, although the relative dominance of each process can vary substantially depending on patterns of rainfall and wind. Storms accompanied by extended periods of rainfall cause the largest extent and longest duration of compound flooding. For these storms, the maximum flood extents and depths can only be simulated accurately using a coupled modeling approach, which provides more than a 70% reduction in error compared to models that simulate coastal, riverine, and rainfall processes separately. This research can inform local planning efforts aimed at reducing vulnerability to future flood events.

Climate change is projected to increase flood hazards due to sea level rise and more intense rainfall. In Chapter 3, the calibrated model is applied to simulate flooding in the Sabine-Neches Estuary during Hurricane Harvey. Future scenarios of sea level rise and rainfall are then applied to estimate how compound flooding will change in the future under 2050 and 2100 climate conditions. The combined effects of future sea level rise and rainfall cause the compound flood zone to expand and shift further inland to areas with higher population density and more development. As a result, the number of residential structures in the compound flood zone increases from 0.6% of all impacted structures in 2017 to 14% in 2100. New strategies for flood mitigation that address multiple types of flooding (e.g., coastal storm surge and high river discharge) may be necessary in these areas to reduce impacts to people and property.

Although damages in coastal areas are anticipated to worsen due to rising sea levels and subsidence, the precise impact of historical sea-level rise and subsidence on compound flooding during tropical cyclones remains uncertain. To address this uncertainty, Chapter 4 of this dissertation investigates the influence of sea-level rise and subsidence on compound

flooding during historical hurricanes and assesses how well linear superposition of individual flood drivers can predict compound flooding. The findings indicate that reductions in sea-level rise can shift the location where the riverine-rainfall influence exceeds the storm surge contribution to peak water levels. While sea-level rise typically does not change the nearshore water depth, it does impact flood depths upstream. Land subsidence in the region does not significantly lower water levels but does contribute to deeper inundation in waterways and across the land surface. Predictions of flooding using linear superposition can be inaccurate, sometimes underestimating or overestimating the depth depending on the timing and location.

Keywords: compound flooding, sea level rise, climate change, tropical cyclones, Hurricane Harvey, Hurricane Ike, Hurricane Rita, economic damage, subsidence

Contents

List of Figures

List of Tables

Chapter 1

Introduction

1.1 Problem Statement

Over the past decades, storm events have caused damage to residents, critical infrastructure systems, and the economy [3, 4]. Flooding in coastal areas may be forced by several drivers including coastal (storm surge), fluvial (river discharge), and pluvial (rainfall) [5, 6]. These drivers may interact non-linearly if they occur at the same time or within the same watershed [7]. Usually, these drivers are considered separately in conventional flood hazard assessment methods, preventing an evaluation of nonlinear interactions between coastal and watershed processes and potentially causing discrepancies between observed and modeled flood extent and depth [8, 9, 10]. Also, the coastal compound flooding frequency and severity are predicted to increase in the future due to sea level rise (SLR) [11, 12, 13] and wetter [14, 15] and more intense future tropical cyclones [16, 17, 18]. Thus, it is necessary to develop more comprehensive flood risk assessment approaches that integrate coastal, fluvial, and pluvial drivers [19].

1.2 Background

Recently, there has been a growing focus on developing numerical modeling frameworks that can account for compound flood mechanisms in coastal estuaries. While many compound modeling efforts have simulated the interactions between storm surge and river discharge (e.g., [20, 9, 10]), far fewer have investigated the pluvial contribution to flooding [21]. The extent and intensity of rainfall, along with its timing relative to peak storm surge, are important factors that influence the type and severity of compound flooding [21]. In their analysis of six tropical cyclones that impacted the Cape Fear River Estuary, [21] concluded that rainfall occurring prior to a hurricane's landfall over extensive areas in upstream watersheds produced a peak river discharge that coincided with the surge peak, leading to coastal-fluvial compounding effects. However, when rainfall was more localized or occurred at or after peak storm surge, coastal-pluvial compounding resulted.

Despite the critical role that the timing of rainfall and surge plays in determining the severity of compound flooding, the temporal dimension of flood drivers and interactions is primarily underreported in modeling studies [3, 22]. Statistical analysis of bivariate return periods for flood drivers also typically assumes that coastal surge and rainfall or river discharge peaks coincide or occur within a specified time lag [23]. While this assumption may be adequate for certain storms and estuaries, a more comprehensive analysis approach is needed to quantify the time-varying evolution of coastal, fluvial, and pluvial contri-

butions to compound flooding across a diverse range of tropical cyclone and watershed characteristics.

Although many studies have explored the interaction of storm surge, waves, and SLR for hurricanes [24, 25, 26, 27, 28], far fewer have investigated how compound flooding due to storm surge and river discharge will change in the face of SLR [29, 30, 31]. [30] developed a Delft3D model using a structured grid to simulate compound coastal and fluvial flooding of Hurricane Irene (2011) combined with SLR to quantify the vulnerability of the Hampton Roads region (VA) to storm surge and SLR. The authors concluded that the SLR impact on flood duration and intensity is site specific. Far fewer studies have explored rainfall impact on the future compound flood modeling of hurricanes [32]. Also, no literature surveys the contribution of individual forcing (coastal, fluvial, pluvial) to future compound flooding when considering SLR.

In addition to climate change factors, the risks and impacts of flooding in coastal and estuarine areas is also influenced by subsidence [33, 34]. Ignoring subsidence in flood simulations can result in an underestimation of flood extent [35]. Activities like oil and gas extraction and groundwater withdrawal contribute to subsidence in various US regions [36]. However, there are few studies that quantify subsidence over decades. [37] utilized a physics-based model to simulate 117 years of subsidence due to aquifer compression caused by groundwater extraction and incorporated time-varying subsidence rates into a hydraulic model to simulate the impact of subsidence on flooding in Houston during Hurricane Harvey. Their findings suggest that subsidence has both negative and positive effects on flooding. Given the potential impacts of subsidence on flood extent and depth, it is important to incorporate considerations of subsidence into models simulating compound flooding.

1.3 Research Goals and Objectives

In this study, we develop a coupled flood model using Delft3D-FM [38] and apply the model to simulate hurricane-induced flood hazards in the Sabine-Neches Estuary (SNE) in Southeast Texas. Our goals are to:

1. Evaluate the suitability of Delft3D-FM for compound coastal-fluvial-pluvial inundation modeling under tropical cyclone forcing;

2. Assess how the spatial structure and temporal evolution of three historical hurricanes influence the patterns of compound flood hazards in the SNE;

3. Determine which flooding mechanisms are dominant at critical water infrastructure locations in the SNE to inform planning and hazard mitigation efforts;

4. Quantify the impact of SLR on the compound inundation depth and extent during Hurricane Harvey (2017);

5. Investigate the effect of SLR and future rainfall on the contribution of flood drivers and damage costs for Hurricane Harvey;

6. Evaluate how historical SLR and subsidence have affected compound flooding in the SNE over the past century.

Our approach builds upon previous compound modeling efforts by including the effects of rainfall on the model grid and by using a single code and domain to simulate coastal, fluvial, and pluvial processes simultaneously. We also account for the time-varying evolution of compound flooding across storm events, a consideration that has been overlooked in many past studies [39]. We survey the influence of SLR, future rainfall, and subsidence on the compound flood modeling of historical hurricanes. These features enable more comprehensive flood risk assessments for communities and critical infrastructure in estuarine regions.

Chapter 2

Compound Coastal, Fluvial, and Pluvial Flooding During Historical Hurricane Events in the Sabine-Neches Estuary, Texas

2.1 Abstract

When storm surge, river discharge, and rainfall occur simultaneously or in succession, they may cause compound flooding and exacerbate impacts in coastal communities. In traditional modeling approaches, these driving processes are simulated separately, leading to discrepancies between simulated and observed data and highlighting the need for coupled modeling frameworks. Here, we develop a coupled coastal-fluvial-pluvial model for the Sabine-Neches Estuary (SNE) in southeastern Texas using Delft3D to simulate flood extent and depth during Hurricanes Rita, Ike, and Harvey. For each hurricane, four scenarios (i.e., coastal, fluvial, pluvial, and compound) are modeled to determine the relative contribution of each driving force to water levels across the domain. Our results reveal that tropical cyclones such as Harvey which are accompanied by extended periods of rainfall produce the largest extent and longest duration of compound flooding. Such storms also produce highly dynamic and evolving patterns of compound flooding over their duration, with multiple flood peaks that can inhibit response and recovery efforts. When simulating these storms, a coupled model can provide substantial improvements over coastal-, fluvial-, and pluvial-only models, decreasing root mean square error by 69%, 69%, and 79%, respectively. In contrast, storms with short-duration rainfall and moderate to severe storm surges produce less extensive compound flooding, which is typically dominated by coastal-pluvial interactions. Our results further highlight the potential for compound flooding at the locations of critical water infrastructure assets, suggesting the need for flood adaptation approaches that are robust to multiple types of flooding.

2.2 Introduction

Tropical cyclones pose a significant threat to populated coastal regions, leading to substantial economic costs and loss of life [3]. Although only 18% of the 310 billion-dollar disasters that have occurred in the US since 1980 were caused by tropical cyclones, these disasters account for 53% of total costs and 44% of total deaths [4]. In coastal bays and

estuaries, flooding associated with tropical cyclones presents a particular challenge because it may be driven by multiple mechanisms, including storm surge (coastal), river discharge (fluvial), and direct rainfall on saturated soils, impervious surfaces, and waterways (pluvial) [5, 6]. When these mechanisms occur simultaneously or shortly after one another, they may interact non-linearly and, in some cases, exacerbate the resulting inundation [7]. For example, elevated coastal water levels can inhibit the efficient drainage of rainfall and river discharge to the ocean, leading to a backwater effect [40]. The frequency and severity of compound flooding could increase in the future as a result of sea-level rise [11, 12, 13] and changes in tropical cyclones, which are projected to become more intense [16, 17, 18] and wetter [14, 15] with climate change. Thus, there is a recognized need to develop more comprehensive flood risk assessment approaches that integrate coastal, fluvial, and pluvial drivers [19].

In the past, flood hazard assessments have typically considered flood drivers separately. For example, modeling efforts meant to support emergency response and operational decision-making during hurricanes are mainly focused on storm surge hazards and do not include riverine or rainfall effects. These include probabilistic surge hazard maps produced by the National Hurricane Center using the Sea, Lake, and Overland Surges from Hurricanes (SLOSH) model [41] and real-time surge forecasts produced by the Center for Computation and Technology at Louisiana State University using the Advanced Circulation (ADCIRC) model [42]. The Federal Emergency Management Agency's (FEMA) flood zone mapping approach also considers rainfall-runoff and storm surge processes separately [43]. While these approaches provide important insight into inundation potential from individual hazards, they are unable to account for nonlinear interactions caused by two-way feedback between coastal and watershed processes and have been shown to cause discrepancies between observed and modeled flood extent and depth [8, 9, 10].

Recent research efforts have placed increased attention on the development of numerical modeling frameworks that can account for compound flood mechanisms in complex coastal estuaries. [44] provide a comprehensive review of the models and coupling approaches that have been used in the literature. Briefly, coupling may occur through simple one-way linkage, where one model provides boundary condition data for another, but no feedback occurs. In this case, one model must be chosen to serve as the base model for flood simulation. Depending on the application, the base model may be a hydrologic model that captures rainfall-runoff processes [45, 46], a hydraulic model that simulates water surface profiles and velocities [47, 48, 49, 21], or an ocean circulation model that captures hydrodynamic and meteorological processes, such as storm surge and tides [50].

Although one-way approaches are computationally efficient and provide insight into compounding effects, two-way coupling approaches are needed to simulate the complex interactions that occur at the terrestrial-coastal interface. Two-way coupling can be categorized into loosely-coupled, tightly-coupled, and fully-coupled approaches [51, 52]. Loose coupling involves the transfer of inputs between separate models using an external interface. This approach has been applied to couple the hydrologic model pWASH123D with ADCIRC, using the Earth System Modeling Framework as the coupling interface [53]. Tight coupling removes the need for external data passage by integrating the governing equations from one model into the code of another. [54] assessed coastal flood vulnerability due to sea-level rise and storms in Delaware Bay by tightly coupling a 3D ocean circulation model, a 2D shallow water model, and a topography-based hydrologic model. Fully-coupled models solve the same set of governing equations to simulate all relevant processes. Recent studies have used the Semi-implicit Cross-scale Hydroscience Integrated

System Model (SCHISM) as the basis for a 3D ocean-to-creek model to simulate compound coastal, fluvial, and pluvial flooding in bays along the US East and Gulf coasts [40, 55, 39, 22]. For example, [39] applied SCHISM to estimate the compound and individual effects of coastal, fluvial, and pluvial forcing to water levels in and around Galveston Bay during Hurricane Harvey. However, the application of tightly or fully coupled models for compound flood hazard assessment is still limited [44]. In addition, while many compound modeling efforts have simulated the interactions between storm surge and river discharge (e.g., [20, 9, 10]), far fewer have investigated the pluvial contribution to flooding [21].

The extent and intensity of rainfall, along with its timing relative to peak storm surge, are important factors that influence the type and severity of compound flooding [21]. In their analysis of six tropical cyclones that impacted the Cape Fear River Estuary, [21] concluded that rainfall occurring prior to a hurricane's landfall over extensive areas in upstream watersheds produced a peak river discharge that coincided with the surge peak, leading to coastal-fluvial compounding effects. However, when rainfall was more localized or occurred at or after peak storm surge, coastal-pluvial compounding resulted. Despite the critical role that the timing of rainfall and surge plays in determining the severity of compound flooding, the temporal dimension of flood drivers and interactions is largely under-reported in modeling studies, which often extract static grid cell or transect-based water levels to quantify compounding or transition zones [3, 22]. Statistical analyses of bivariate return periods for flood drivers also typically assume that coastal surge and rainfall or river discharge peaks are coincident or occur within a specified time lag [23]. While this assumption may be adequate for certain storms and estuary systems, a more comprehensive analysis approach is needed to quantify the time-varying evolution of coastal, fluvial, and pluvial contributions to compound flooding across a diverse range of tropical cyclone and watershed characteristics.

Tropical cyclones pose a substantial risk to water infrastructure. Flooding can cause direct damage to water and wastewater treatment plants, while hurricane-force winds can cause power outages that prevent the pumping and treatment of raw water [56, 57]. Such disruptions can lead to loss of drinking water supply for homes and businesses or result in spills of untreated wastewater to nearby waterways, presenting a risk to human and ecosystem health [58]. Recovery and repair efforts are time- and resource-intensive, often taking months or years and costing millions of dollars [56]. During Hurricane Harvey in 2017, 40 wastewater systems and 61 public drinking water systems malfunctioned, and 203 boil-water notices were issued, some of which lasted more than 3 months [59]. In addition to the impacts on residential users, the loss of reliable water supply can also hinder commercial activities and cause cascading economic impacts [60]. Given these risks, there is a strong incentive to mitigate impacts to critical water infrastructure to reduce future losses. However, current single-hazard planning frameworks do not provide the information needed to understand and plan for water infrastructure exposure during compound flood events.

In this chapter, we develop a coupled flood model using Delft3D-FM [38] and apply the model to simulate hurricane-induced flood hazards in the Sabine-Neches Estuary (SNE) in southeast Texas. Our goals are to (1) evaluate the suitability of Delft3D-FM for compound coastal-fluvial-pluvial inundation modeling under tropical cyclone forcing, (2) assess how the spatial structure and temporal evolution of three historical hurricanes influence the patterns of compound flood hazards in the SNE, and (3) determine which flooding mechanisms are dominant at critical water infrastructure locations in the SNE to inform

planning and hazard mitigation efforts. Our approach builds upon previous compound modeling efforts by including the effects of rainfall on the model grid and by using a single code and domain to simulate coastal, fluvial, and pluvial processes simultaneously. We also account for the time-varying evolution of compound flooding across storms events, a consideration that has been overlooked in many past studies [39]. These features enable more comprehensive flood risk assessments for communities and critical infrastructure in estuarine regions.

2.3 Study Area

The SNE is located in southeast Texas and forms the confluence between the Sabine and Neches Rivers and the Gulf of Mexico (Figure 2.1). This region has been impacted by numerous tropical cyclones over the past two decades, including Hurricane Rita in 2005, Hurricane Ike in 2008, and Hurricane Harvey in 2017. These events have led to substantial flooding and damage to residents, critical infrastructure, and the economy, particularly in the two largest municipalities, Beaumont (pop. 115,282) and Port Arthur (pop. 56,039) [61]. Water supplies for municipal, industrial, and agricultural users in the region are provided by the Lower Neches Valley Authority (LNVA). LNVA manages critical water infrastructure, including the Neches River Saltwater Barrier to control salinity and protect freshwater supplies and the North Regional Treatment Plant in Beaumont to treat industrial wastewater (Figure 2.1). LNVA's infrastructure has been impacted by flooding due to past storm events [62], and the agency is now considering what actions are needed to build resilience to future flooding. Comprehensive flood hazard mapping that accounts for the potential for compound flooding would provide an important resource to inform this planning effort.

Several past studies have examined compound flooding along the Texas Coast using physical [63, 39, 9], statistical [64], and combined [65, 66, 67] approaches. These studies have mainly focused on Galveston Bay, with less attention paid to the SNE. Recently, [9] developed a coupled framework using ADCIRC as the base model to simulate compound coastal and fluvial flooding in the SNE during Harvey and found that including river discharges from the Neches and Sabine River watersheds was crucial to accurate flood mapping. [64] explored the effect of compound flood-driven dependencies between storm surge and river discharge in Sabine Lake using statistical methods. They concluded that the 1% annual exceedance probability water level in Sabine Lake was 35 cm higher when considering dependencies between coastal and fluvial processes as compared to an independence assumption. However, none of the studies in the SNE included the direct influence of rainfall, which occurred at historical rates across the region during Harvey. Thus, the pluvial contribution to compound flood potential during Harvey and other past hurricane events is still not clear. In addition, although the interaction between surge and rainfall has often been cited as a driver of severe flooding during Harvey [68], it remains to be seen to what extent surge contributed to observed flooding within the SNE. An analysis of the temporal evolution of coastal, fluvial, and pluvial mechanisms and their contribution to compound flood potential during Harvey is warranted given that surge and discharge in the SNE lasted for more than 3 and 7 days [64], respectively, with non-coincident peaks.

Figure 2.1: Map of the Sabine-Neches Estuary, Texas. Red markers show the National Oceanic and Atmospheric Administration tide gauges used in this study. Blue markers show the locations of critical water and wastewater infrastructure operated by the Lower Neches Valley Authority.

2.4 Methods

2.4.1 Model development

We utilized Delft3D-FM [38] as the computational basis to model coastal, fluvial, and pluvial processes in the SNE. Delft3D-FM is a 2D-3D hydrodynamic modeling software that is capable of modeling wind, pressure, rain, river flows, surge, and tides on a single model domain and has been applied successfully in past studies of compound flooding [47, 69, 10, 70]. Delft3D-FM solves the Navier-Stokes equations and Boussinesq assumptions for an incompressible fluid in shallow water conditions on an unstructured grid to simulate water velocities and elevations in coastal, riverine, and estuarine systems [71]. The model utilizes a rain-on-grid approach to ingest rainfall data as a volume source term in each grid cell at the beginning of each time step. The rainfall term P is combined with local source and sink terms to determine the total water contribution Q per unit area:

$$Q = \int_0^h (q_{in} - q_{out})\, dz + P \tag{2.1}$$

where q_{in} and q_{out} represent discharges and withdrawals per unit volume, respectively, and are integrated over the water depth h. Q is then incorporated into the continuity equation as follows:

$$Q = \frac{\partial h}{\partial t} + \frac{\partial U h}{\partial x} + \frac{\partial V h}{\partial y} \tag{2.2}$$

where U and V are depth-averaged velocities. Drying and flooding processes are simulated by adding or removing grid cells from the flow domain based on a user-defined water depth threshold [72].

We applied the model in unsteady, 2D depth-averaged mode, as is common for compound flood modeling [69]. The computational domain covered a 2,500 km^2 inland area and included Sabine Lake, the Neches and Sabine Rivers upstream to 47 km and 28 km, respectively, and offshore areas extending up to 88 km into the Gulf of Mexico (Figure 2.2). In overland areas, the inland model boundary was defined based on hydrologic units (HUC-12). Coastal, fluvial, and pluvial forcings were fully coupled within the model domain using Delft3D-FM. However, the model did not simulate rainfall-runoff generation processes in the upstream regions of the Neches and Sabine River watersheds located outside of the model boundaries. Instead, inputs from upstream watersheds were included as discharge boundaries in the Neches and Sabine Rivers. The effects of interception, infiltration and evaporation were not modeled due to a lack of available data and based on the assumption that these effects were small compared to the influence of rainfall, as has been assumed in other studies of Harvey [73, 39].

Grid resolution varied from approximately 1,000 m offshore to 40 m nearshore and in the rivers, ship channel, and Sabine Pass, resulting in 161,623 total grid cells. Roughness was modeled using a spatially variable Manning's n based on land cover. The model was cold-started and allowed to spin up for several days prior to hurricane landfall. An adaptive time step was used for model computations based on the Courant condition [72]. A threshold of 10 cm was used for the drying and flooding algorithm, as has been applied in past studies [10].

2.4.2 Flood scenarios

The model was calibrated for a non-extreme condition in January 2016 and an extreme condition during Tropical Storm Imelda in 2019 (see Section 2.4.4). The calibrated model was then used to simulate three historical hurricane events: Rita (2005), Ike (2008), and Harvey (2017). These three hurricanes exhibit distinct tracks and patterns of rainfall, as shown in Figure 2.3. Rita made landfall east of Sabine Pass on September 24, 2005, as a Category 3 hurricane with maximum sustained winds of 100 knots, a radius to maximum wind (R_{max}) of 30 nautical miles (nm), and a forward speed of 9–11.5 mph [74, 75]. Rita produced 226 mm of total rainfall at Beaumont and a maximum surge of approximately 1.5 m at Sabine Pass [75]. Ike made landfall on Galveston Island, TX, on September 13, 2008, as a Category 2 hurricane with maximum sustained winds of 95 knots, R_{max} of 30 nm, and a forward speed of 13.5 mph [74, 76]. Within the study area, Ike produced 138 mm of total rainfall at Beaumont and a maximum storm surge of 3.9 m at Sabine Pass [77]. Ike caused major disruptions to the local water supply by damaging the Neches River

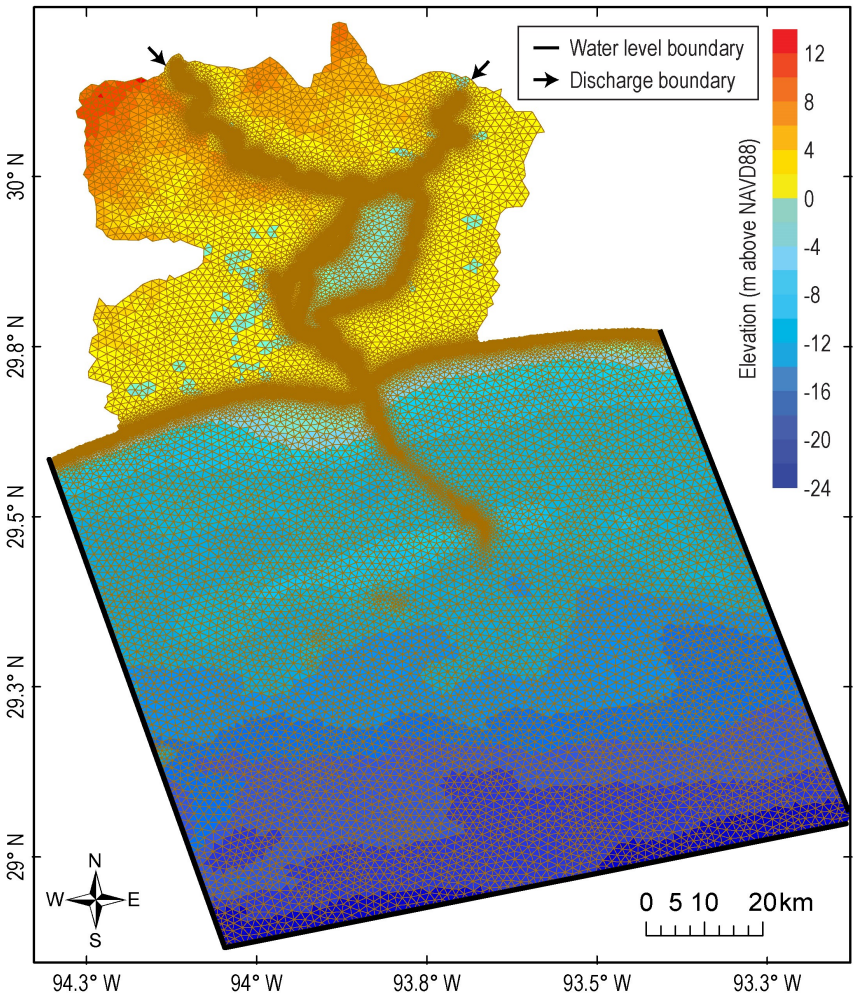

Figure 2.2: Model grid, topobathy, and boundary locations. The domain includes Sabine Lake, the Neches and Sabine Rivers upstream to 47 km and 28 km, respectively, and part of the Gulf of Mexico.

Saltwater Barrier and allowing saltwater penetration into the upstream watershed. Harvey made landfall on August 26, 2017, near Rockport, TX, as a Category 4 hurricane with maximum sustained winds of 115 knots and R_{max} of 15 nm, then again on August 30, 2017, near Cameron, LA, as a tropical storm with maximum sustained winds of 40 knots, R_{max} of 50 nm, and a forward speed of 5–7 mph [74, 78, 79]. In the SNE, Harvey produced a total rainfall of 1,207 mm at the Southeast Texas Regional Airport outside of Beaumont and a maximum surge of 1.0 m at Sabine Pass [68].

2.4.3 Data sources

Detailed topographic and roughness data is crucial for the accurate estimation of flooding since it controls surge propagation and frictional dissipation [80]. Bed level and roughness values were extracted from the TX2008 ADCIRC mesh developed to support federal flood insurance studies in coastal Texas counties following Ike. Detailed information about the data sources used can be found in [80]. To summarize, offshore bathymetry for the ADCIRC mesh was derived from the National Oceanic and Atmospheric Administration's (NOAA) depth-sounding database and navigational charts, while bathymetry for inland waterways was obtained from regional bathymetric surveys conducted by the US Army

Corps of Engineers and other agencies prior to 2005. Topographic data was taken from 10-m lidar data produced by FEMA and local surveys and published in 2005 and 2006. All bathymetric and topographic data was referenced to NAVD88. Manning's n coefficients were defined based on land cover types in the National Land Cover Database (Table S1) [81]. We made local refinements to the ADCIRC bed level and roughness data to address anomalies. For example, the data extracted from the TX2008 ADCIRC mesh captured roughness values from land use types other than water (e.g., two bridges crossing the Neches River), which we adjusted to instead represent roughness in the river channel. Channel bed levels in the upstream reaches of the Neches and Sabine Rivers, beyond the extent of bathymetric surveys, were not well-resolved in the TX2008 ADCIRC mesh. To better capture flow in the rivers, we adjusted the channel bed levels in these areas based on depth and width estimates using a simplified rectangular cross-section, which was assumed to remain constant to the upstream extent of the model.

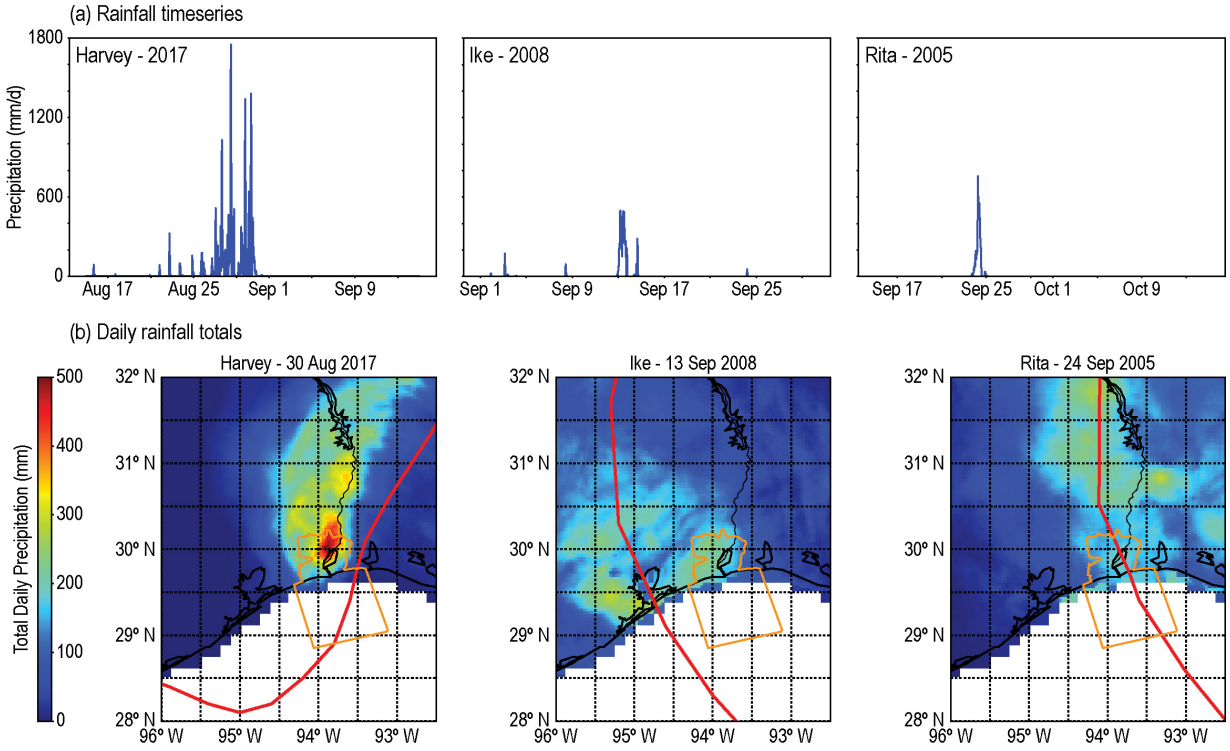

Figure 2.3: (a) Rainfall time series at Rainbow Bridge for Harvey, Ike, and Rita. (b) Total daily rainfall for Harvey, Ike, and Rita on the day of landfall. The orange outline indicates the limits of the study area, and the red lines show the hurricane tracks.

The simulation time periods and sources of meteorological and boundary forcing data for the three hurricanes and two calibration periods are summarized in Table 2.1. Wind and pressure fields with 3-hour temporal resolution were extracted from the National Center for Environmental Prediction (NCEP) North American Regional Reanalysis (NARR) using a mesh with a resolution of 34 by 30 km [82], resulting in six horizontal and four vertical grids over the study domain. NCEP NARR wind products are derived from buoy and satellite data [83]. Hourly gridded rainfall time series were derived from Next Generation Weather Radar (NEXRAD) Stage IV at 4 km resolution [84]. For Harvey, higher-resolution (1 km) radar-only Multi-Radar Multi-Sensor (MRMS) gridded data was used instead [85], as it provided a better fit for observed data. Hourly river discharge was extracted from USGS 08041780 Neches Rv Saltwater Barrier at Beaumont for the Neches River [86] and from the

National Water Model (NWM) for the Sabine River [87]. The NWM uses MRMS hourly rainfall data to estimate flows.

Water level time series from NOAA [88] at Texas Point, Sabine Pass (8770822) were used to force the model at the offshore boundary for both calibration periods. Water level data was not available at this station during Ike and Rita, so data from NOAA Sabine Pass North (8770570) was used instead. Data from the Global Tide and Surge Reanalysis (GTSR) was used to fill gaps in the NOAA water level data during Rita [89]. For the Harvey simulation, offshore water levels were extracted from Coastal Emergency Risks Assessment (CERA) hindcast modeling using ADCIRC [42], which does not include river inputs and thus avoids capturing any fluvial signal that might result from high discharge through Sabine Pass. Because CERA data was only available from August 24 to August 31, water levels were obtained from Texas Point, Sabine Pass (8770822) for the rest of the simulation. Coastal water level time series from the Sabine Pass North (8770570), Port Arthur (8770475), and Rainbow Bridge (8770520) NOAA tide gauges (Figure 2.1) were used for model calibration and validation.

Table 2.1: Summary of sources used to generate input data for the numerical model.

Period	Data	Reference
Imelda 10 Sep to 30 Sep 2019	Neches River discharge	USGS 08041780
	Sabine River discharge	NWM
	Offshore water level	NOAA 8770822
	Rainfall	NEXRAD Stage IV
	Wind and pressure	NCEP NARR
January 2016 1 Jan to 30 Jan 2016	Neches River discharge	USGS 08041780
	Sabine River discharge	NWM
	Offshore water level	NOAA 8770822
	Rainfall	N/A
	Wind and pressure	NCEP NARR
Harvey 15 Aug to 15 Sep 2017	Neches River discharge	USGS 08041780
	Sabine River discharge	NWM
	Offshore water level	NOAA 8770822 and CERA
	Rainfall	MRMS
	Wind and pressure	NCEP NARR
Ike 1 Sep to 30 Sep 2008	Neches River discharge	USGS 08041780
	Sabine River discharge	NWM
	Offshore water level	NOAA 8770570
	Rainfall	NEXRAD Stage IV
	Wind and pressure	NCEP NARR
Rita 15 Sep to 15 Oct 2005	Neches River discharge	USGS 08041780
	Sabine River discharge	NWM
	Offshore water level	NOAA 8770570 and GTSR
	Rainfall	NEXRAD Stage IV
	Wind and pressure	NCEP NARR

2.4.4 Model calibration

We calibrated the model using two separate time periods: (1) a non-extreme condition in January 2016 to ensure that the model was accurately representing typical hydrodynamic conditions in the estuary and (2) an extreme condition with overland flooding during Tropical Storm Imelda (2019) to confirm the model's ability to capture overland flow effects. The roughness coefficient was selected to calibrate the model because friction is a significant parameter in estimating water surface elevation and velocity [90]. Roughness coefficients in the waterways were adjusted iteratively for the non-extreme January 2016 period until an acceptable match was obtained between modeled and observed water levels at the three NOAA tide gauges mentioned previously. Roughness coefficients in overland areas were then calibrated by comparing simulated water surface elevations for the extreme condition during Imelda with 30 high water marks (HWMs) collected by the Dartmouth Flood Observatory [1]. We calculated the root mean square error (RMSE), coefficient of determination (R^2), Nash-Sutcliffe Efficiency (NSE), and mean absolute error (MAE) between model outputs and observations for each set of roughness coefficients to select the one that provided the best match.

2.4.5 Compound flooding decomposition

To determine the relative contribution of coastal, fluvial, and pluvial processes to tropical cyclone flooding in the SNE, we modeled four scenarios for each hurricane event: (1) coastal, (2) fluvial, (3) pluvial, and (4) compound. For the coastal scenario, offshore water levels included both tide and surge. Spatially and temporally variable wind and pressure fields were applied using gridded data. No rainfall or river discharge was included. For the fluvial scenario, offshore water levels included tides only and were derived from tidal predictions produced by NOAA using 37 tidal constituents. Hourly observed discharges were applied at the upstream extent of the Neches and Sabine Rivers. No rainfall or storm surge forcing was included. For the pluvial scenario, offshore water levels included tides only, and rainfall was applied across the whole domain. No river discharge or storm surge forcing was included. For the compound scenario, offshore water levels included both tide and surge. Gridded wind, pressure, and rainfall data were applied across the whole domain. Hourly observed discharges were applied at the upstream extent of the Neches and Sabine Rivers. For each scenario, RMSE, R^2, NSE, and MAE values were calculated to assess the ability to reproduce the observed data.

Several methods have been proposed in the literature to delineate compound or transition regions where the effects of multiple drivers interact to influence water levels [3, 39]. In this study, we apply the approach outlined by [39], which quantifies the relative contributions of pluvial, fluvial, and coastal forcings to peak water levels using the concept of disturbance (D). Because D can be calculated for each grid cell in the model domain, this approach provides a straightforward implementation to determine the spatial extent of the compound zone and regions where a single driver is dominant. For each flood driver, D is defined as:

$$D = \begin{cases} \eta & \text{if } h \geq 0 \\ \eta + h & \text{if } h < 0 \end{cases} \tag{2.3}$$

where η is the water surface elevation and h is the bed level (positive downward), referenced to the same vertical datum (NAVD88) [39]. D represents the water depth in

land areas that are initially dry and the water surface elevation in waterways that are initially wet.

For each grid cell in the model domain, we found t_{peak}, the time of maximum water level in the compound model, and calculated $D_{coastal}$ from the coastal-only model, $D_{fluvial}$ from the fluvial-only model, and $D_{pluvial}$ from the pluvial-only model at t_{peak}. Note that for Harvey, we calculated these values at two different times—one near the peak of storm surge and one near the peak of riverine discharge—to quantify the temporal changes in compound flood hazards. We then approximated the contribution C of each forcing scenario to peak water levels by calculating the ratio of the individual D to the total D at t_{peak} following the general approach proposed by [39]. For example, the coastal contribution ($C_{coastal}$) was calculated as:

$$C_{coastal} = \frac{D_{coastal}}{D_{coastal} + D_{fluvial} + D_{pluvial}} \tag{2.4}$$

Although this approach does not directly capture non-linear compound effects, it still provides insight into areas where more than one forcing may contribute at the time of peak water levels, as well as the relative importance of each forcing. The percent contribution of each forcing was also calculated at the Neches River Saltwater Barrier and the North Regional Treatment Plant to determine the main contributors to flooding at LNVA facilities.

2.5 Results

2.5.1 Model calibration

The modeled water level results for the January calibration period are plotted alongside the observed water levels at the three NOAA tide gauges in Figure 2.4. Calibrated roughness values in the waterways range from $n = 0.013$–0.015 in Sabine Pass, Sabine Lake, and the Sabine River, $n = 0.020$ in the ship channel and offshore, and $n = 0.030$ in the Neches River. The model is able to predict the observed water levels well, with average $R^2 = 0.91$, RMSE = 0.10 m, NSE = 0.78, and MAE = 0.08 m. However, water levels are slightly overpredicted at Rainbow Bridge, possibly due to the higher level of uncertainty in the Neches River bathymetric data used to create the model. During Tropical Storm Imelda, a roughness value of $n = 0.200$ in the overland areas of the Neches River floodplain provides the best correlation with observed HWMs ($R^2 = 0.87$, RMSE = 0.19 m, NSE = 0.81, and MAE = 0.10 m) (Figure 2.5a). For 84% of the HWMs, modeled water depths were within ±0.2 m of observed water depths (Figure 2.5b). Roughness values in overland areas in the rest of the domain did not influence water levels at observation points and thus were not changed from the original spatially variable values assigned based on land use.

2.5.2 Hurricane Harvey

Figure 2.6 shows the modeled versus observed water level time series for the coastal, fluvial, pluvial, and compound scenarios during Harvey. Model performance metrics (averaged across all three NOAA tide gauges) for each scenario are summarized in Table 2.2. Individual performance metrics at each tide gauge are provided in Tables S2-S5. The coastal model matches the observed water levels well until August 29, when the river influence begins to increase, first at the upstream station near Rainbow Bridge, then at Port

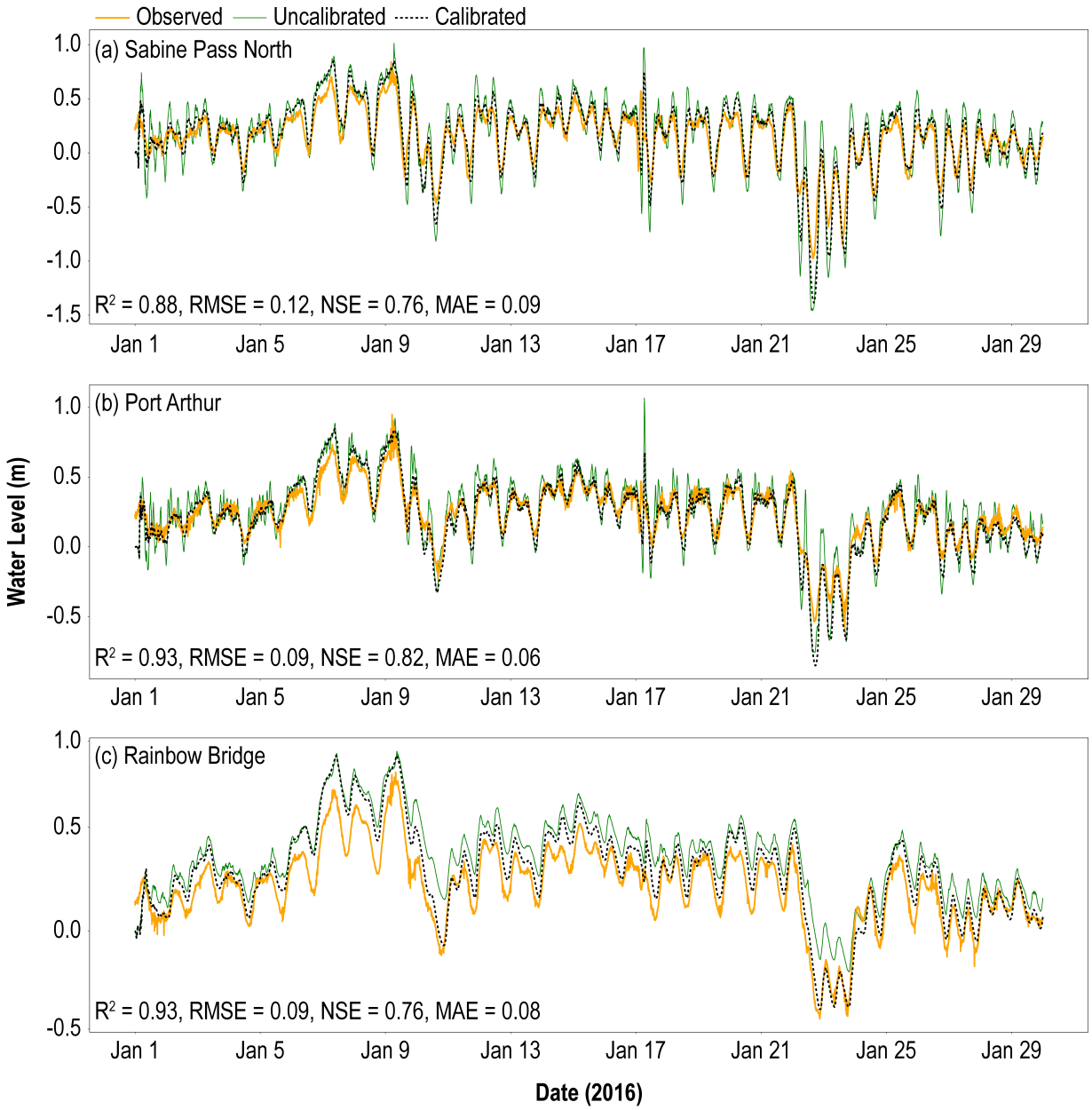

Figure 2.4: Modeled versus observed water levels for the January 2016 compound scenario (before and after calibration). Performance metrics are provided for the calibrated model. R^2 = coefficient of determination, RMSE = root mean square error (m), NSE = Nash-Sutcliffe Efficiency, MAE = mean absolute error (m).

Arthur, and finally at Sabine Pass. During this time, a compound effect is visible as the coastal model begins to underpredict the compound model results. The increasing riverine influence lasts for over a week at all stations, although its magnitude is attenuated further downstream near the estuary entrance as some of the fluvial inflow is converted into overland discharge east of Sabine Lake. Elevated river water levels are driven by heavy rainfall in the Neches and Sabine River watersheds starting on August 27 and extending through August 30 (Figure 2.3a-b, Figure S1), with daily rainfall totals exceeding 400 mm on August 30. Even after the initial surge passes, simulations that include only the coastal influence or the fluvial influence substantially underpredict the observed water levels at all stations, again indicating compound effects due to the interactions between these two

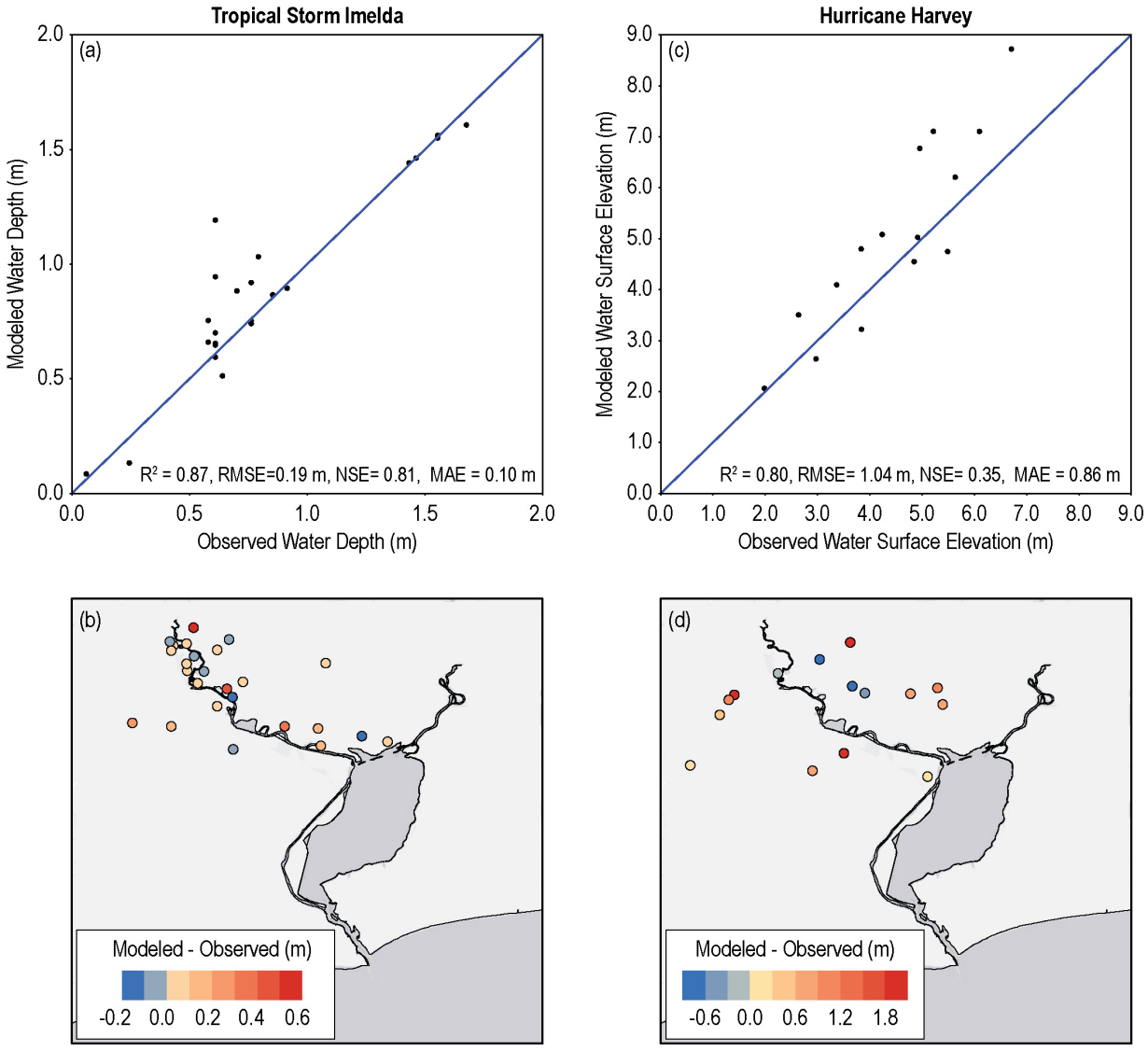

Figure 2.5: Comparison of (a) modeled and observed water depths at locations of high water marks for Tropical Storm Imelda [1] and (c) modeled and observed water surface elevation at locations of high water marks for Hurricane Harvey [2] using the calibrated compound model. Maps show the difference between modeled and observed values for (b) Imelda and (d) Harvey. R^2 = coefficient of determination, RMSE = root mean square error (m), NSE = Nash-Sutcliffe Efficiency, MAE = mean absolute error (m).

processes. The rainfall effect is greatest at the upstream station in the watershed but is still visible at Sabine Pass. The compound flood model generally predicts the observed values well (Table 2.2; $R^2 = 0.94$, RMSE = 0.09 m, NSE = 0.91, and MAE = 0.07 m), although it does cause overprediction of water levels at Sabine Pass in the days following landfall. The compound model generally shows good agreement ($R^2 = 0.80$) with HWMs collected after Harvey (Figure 2.5c), although overprediction does occur at some HWM locations outside of the Neches River floodplain (Figure 2.5d).

To further assess the importance of coastal, fluvial, and pluvial forcing across the domain during Harvey, the relative contribution of each forcing to peak water levels based on the disturbance factor is plotted for two points in time: (1) at 13:00 on August 30, as the storm surge was receding and the fluvial influence was increasing (Figure 2.7a-c),

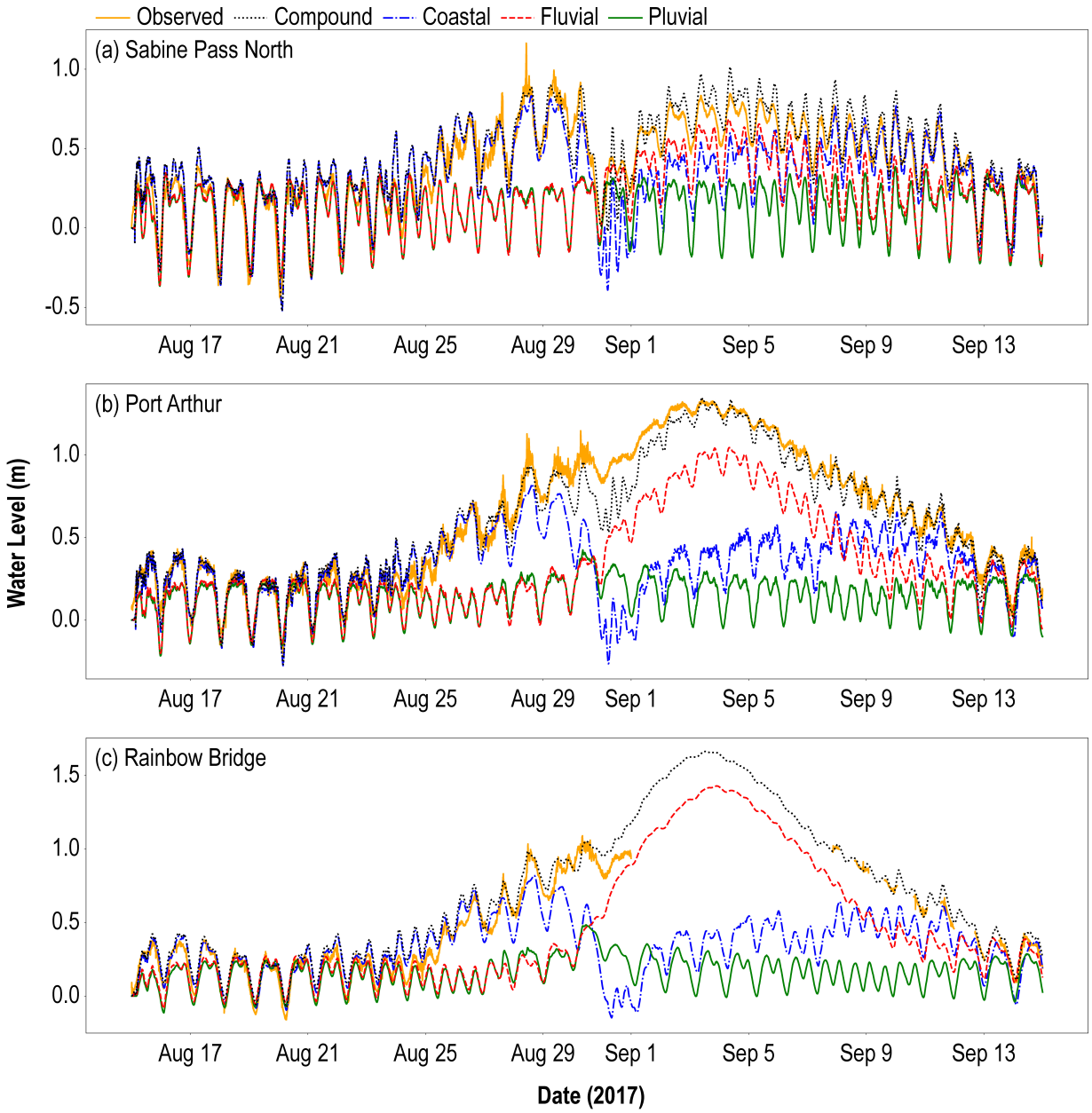

Figure 2.6: Modeled versus observed water levels at (a) Sabine Pass North, (b) Port Arthur, and (c) Rainbow Bridge for Hurricane Harvey.

and (2) at 0:00 on September 4, during the peak fluvial discharge (Figure 2.7e-g). The timing of peak water levels is plotted in Figure 2.8a. On August 30, water levels peak offshore (Figure 2.8a), where coastal surge is dominant (Figure 2.7a). Surge contributes approximately 50% to water levels in Sabine Lake and in overland areas near Sabine Pass and east of Sabine Lake. Surge also affects areas in the Neches and Sabine River watersheds to a lesser extent (Figure 2.7a). Fluvial processes are dominant at the upstream end of the Neches River, as discharge begins to increase, and contribute 30-50% to water levels in the rivers and 20% to water levels in Sabine Lake (Figure 2.7b). Rainfall is dominant outside of the river floodplains and contributes partially (40–50%) to water levels in overland areas adjacent to Sabine Pass, Sabine Lake, and the river channels (Figure 2.7c). Rainfall also contributes (20–30%) to water levels in the waterways. Classifying the dominant forcing in each grid cell using an 80% threshold as suggested by Ye et al. 2021 (Figure 2.7d), it is

Table 2.2: Summary of average model performance compared to observations for Hurricanes Harvey, Ike, and Rita. The reported values for each scenario are averaged across the three NOAA tide gauges (Sabine Pass North, Port Arthur, and Rainbow Bridge).

Hurricane	Scenario	R^2	RMSE (m)	NSE	MAE (m)
Harvey	Compound	0.94	0.09	0.91	0.07
	Coastal	0.37	0.30	0.15	0.19
	Fluvial	0.59	0.30	0.14	0.23
	Pluvial	0.28	0.44	-0.78	0.34
Ike	Compound	0.97	0.15	0.93	0.10
	Coastal	0.96	0.14	0.94	0.10
	Fluvial	0.03	0.66	-0.30	0.36
	Pluvial	0.06	0.66	-0.31	0.37
Rita	Compound	0.86	0.10	0.83	0.08
	Coastal	0.85	0.10	0.82	0.07
	Fluvial	0.22	0.26	-0.10	0.18
	Pluvial	0.21	0.27	-0.22	0.20

Note: R^2 = coefficient of determination, RMSE = root mean square error, NSE = Nash-Sutcliffe Efficiency, MAE = mean absolute error.

clear that compounding effects are widespread within the waterways, from Sabine Pass to the upstream portions of the Neches and Sabine Rivers, on August 30. During this time, coastal, fluvial, and pluvial processes all contribute to modeled water levels. Compound zones are also observed in some overland areas around Sabine Pass, east of Sabine Lake, and in small parts of the Neches and Sabine River floodplains. In these locations, coastal-pluvial interactions are the main source of flooding, although coastal-fluvial interactions are observed at the upstream end of the Neches River.

On September 4, water levels reach their peak values in Sabine Pass, Sabine Lake, the Neches and Sabine Rivers and floodplains, and the area east of Sabine Lake (Figure 2.8a). Coastal processes are again dominant offshore and contribute partially to peak water levels in Sabine Pass (30–60%) and Sabine Lake (10–20%) (Figure 2.7e). The fluvial influence is dominant in the Neches and Sabine Rivers and floodplains and in Sabine Lake (80–100%) (Figure 2.7f). It is also a significant contributor to peak water levels in the region east of Sabine Lake (50–90%), as high water levels in Sabine Lake led to overflows across the eastern part of the domain. Rainfall also contributes partially to peak water levels east of Sabine Lake and in parts of the Neches and Sabine River floodplains (20–50%) (Figure 2.7g). Given that rainfall in the study region concludes by August 31 (Figure 2.3), this pluvial contribution is likely due to a lack of infiltration and drainage, which leads to ponding in overland areas. Rainfall is also dominant outside of the river floodplains to the north and west of the study domain. As shown in the dominant forcing map for September 4 (Figure 2.7h), the compounding zone at the time of peak discharge covers much of the overland area east of Sabine Lake and smaller areas in the river floodplains and is driven by interactions between fluvial and pluvial processes. A second compound zone occurs in Sabine Pass and the downstream portions of Sabine Lake and the ship channel due to coastal-fluvial interactions.

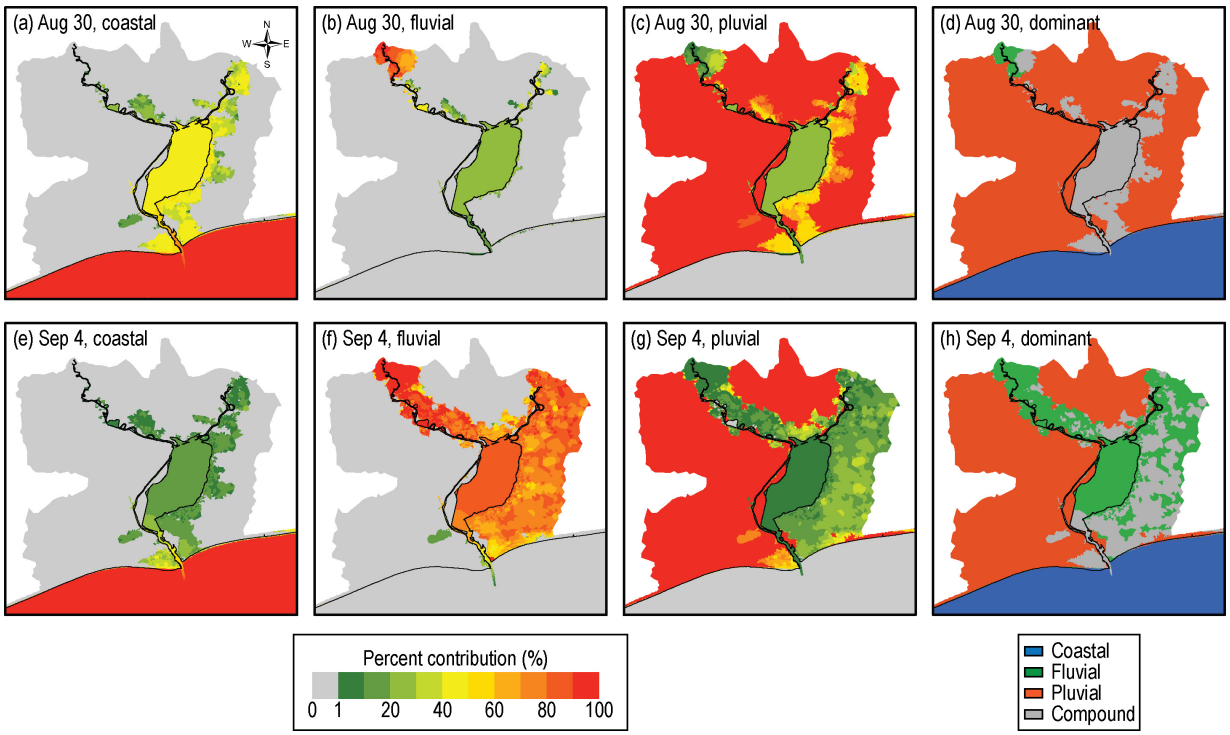

Figure 2.7: Percent contribution of (a,e) coastal, (b,f) fluvial, and (c,g) pluvial forcing to peak water levels for Hurricane Harvey at 13:00 on August 30 (top row) and at 0:00 on September 4 (bottom row). The dominant forcing, representing at least 80% of the peak water level, during each time period is shown in panels d and h. Areas in blue are dominated by coastal influence, areas in green by fluvial influence, and areas in orange by pluvial influence. Gray areas represent locations where no forcing contributes more than 80% to the peak water levels, suggesting the potential for compound effects. The legend on the left corresponds with panels a-c and e-g. The legend on the right corresponds with panels d and h.

2.5.3 Hurricane Ike

The modeled and observed water level comparisons for Ike are shown in Figure 2.9. Coastal surge is the primary contributor to peak water levels at all stations. As a result, the coastal-only model generally simulates the observations well, although it slightly overpredicts the peak water levels at Sabine Pass and Rainbow Bridge and the recession limb at all stations. A slight water level increase due to rainfall can be observed at Port Arthur and Rainbow Bridge on September 13, when rainfall intensity is greatest across the Neches and Sabine River watersheds (Figure 2.3a-b). Although all three forcings peak on the same day, the fluvial and pluvial influences are negligible compared to the extreme influence of coastal storm surge. The compound flood model performs well (Table 2.2; average $R^2 = 0.97$, RMSE = 0.15 m, NSE = 0.93, and MAE = 0.10 m) but causes slight overprediction as water levels peak and recede.

Peak water levels across much of the region during Ike were dominated by storm surge (Figure 2.10a). This includes all areas within 30–55 km of the coastline, Sabine Lake, and the Neches and Sabine River floodplains, as surge propagated to the upstream extents of the current model domain on September 13 and into the early hours of September 14 (Figure 2.8b). The fluvial influence was not dominant at any location in the domain and only contributed minimally to peak water levels (Figure 2.10b). Rainfall was the dominant

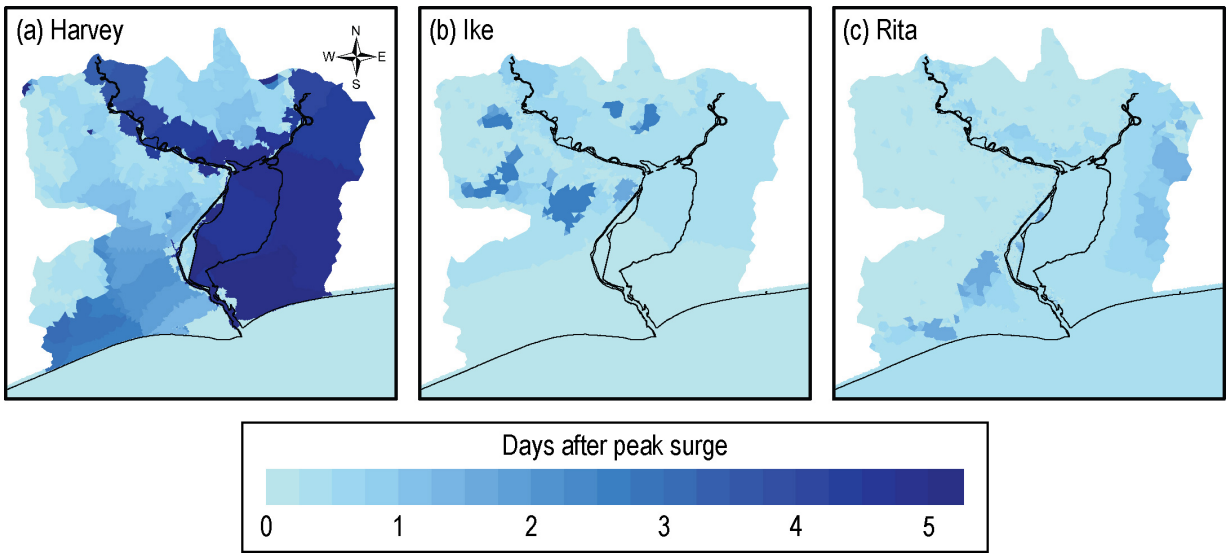

Figure 2.8: Timing of peak water levels for (a) Harvey, (b) Ike, and (c) Rita. Timing is shown as days after peak storm surge, which occurred at approximately 0:00 on August 30, 2017, for Harvey; 6:00 on September 13, 2008, for Ike; and 6:00 on September 24, 2005, for Rita.

factor in the inland areas north and west of Sabine Lake (Figure 2.10c), although the total depth of rainfall-driven flooding in these areas was minor (average water depth = 0.4 m). Peak water levels in overland areas generally occurred on September 13 along with maximum rainfall, although some areas experienced water level maxima on September 15 due to a second period of rainfall (Figures 2.3 and 2.8b). The compound region for Ike is small and only occurs at the inland extent of the storm surge effect (Figure 2.10d).

2.5.4 Hurricane Rita

Figure 2.11 shows the water level comparisons for Rita. Water levels begin to increase on September 23 and remain elevated for several days after the maximum surge on September 24. Before water levels return to pre-storm conditions, a second, smaller peak is observed during the first week of October. Both peaks appear to be driven primarily by coastal influences, as the coastal-only model shows the best agreement with the observed water levels. The compound model provides good agreement with observations (Table 2.2; average R^2 = 0.86, RMSE = 0.10 m, NSE = 0.83, and MAE = 0.08 m) and performs slightly better than the coastal-only model during the recession limb of the first peak at Port Arthur and Rainbow Bridge. However, it leads to poorer performance during the second, smaller peak at Rainbow Bridge. A small rainfall effect is seen on September 24, when rainfall intensity peaks across the domain and in the upstream watersheds (Figure 2.3a-b). In contrast to Harvey, this rainfall spike is coincident with the peak storm surge, suggesting the potential for compounding effects. A minor fluvial effect due to rainfall in the upstream watershed is visible on September 30 (several days after landfall and peak rainfall) at Rainbow Bridge and Port Arthur. However, as with Ike, the fluvial and pluvial effects are minor compared to the coastal contribution at all three gauged locations.

Rainfall is again dominant in inland areas outside the floodplains (Figure 2.12c), where water levels peak along with rainfall early on September 24 (Figure 2.8c). The average water depth due to rainfall in these areas is 0.3 m. Coastal surge propagates inland mid-

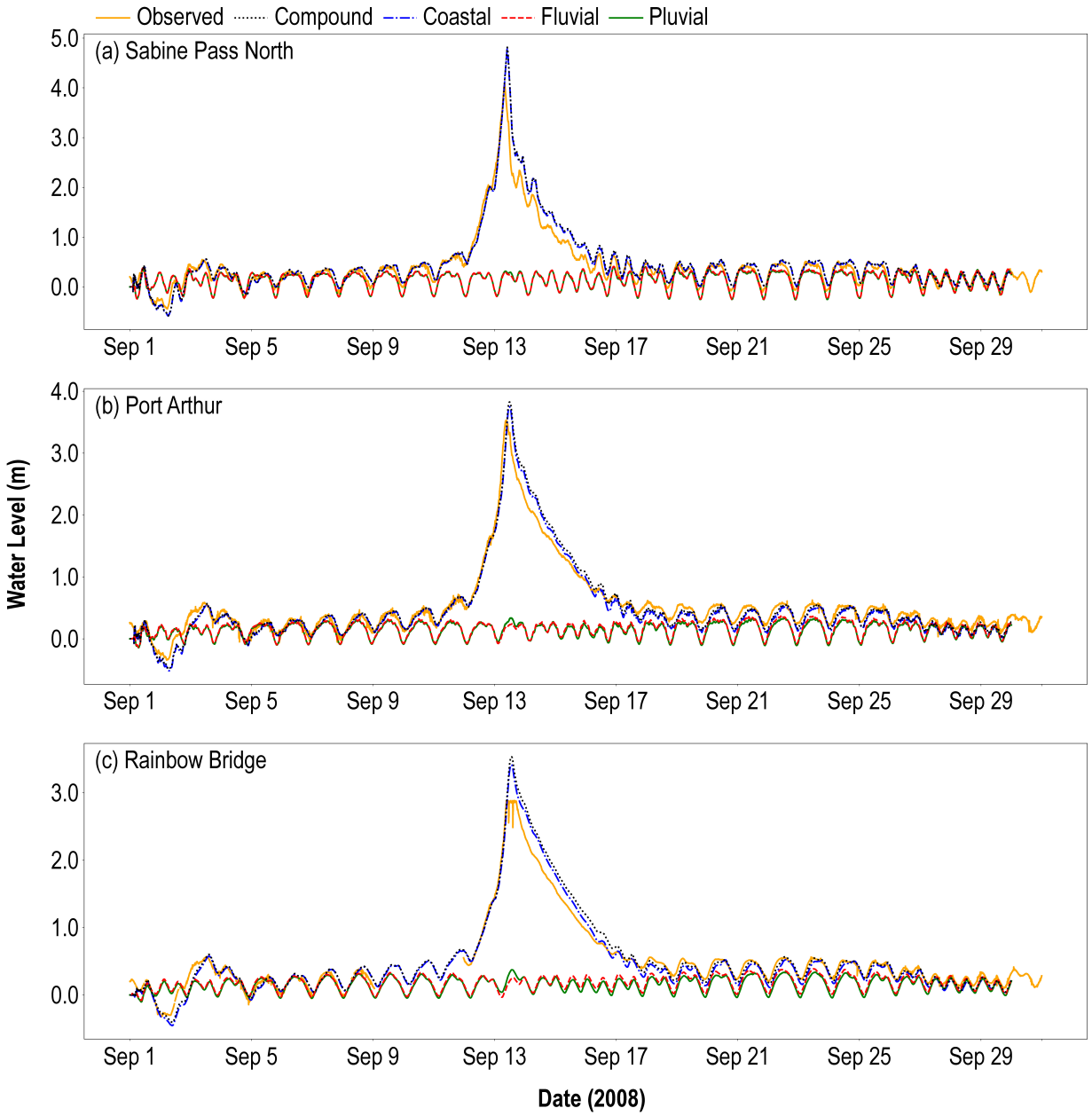

Figure 2.9: Modeled versus observed water levels at (a) Sabine Pass North, (b) Port Arthur, and (c) Rainbow Bridge for Hurricane Ike.

day on September 24 (Figure 2.8c) and is the primary contributor to peak water levels offshore and in Sabine Lake (Figure 2.12a). Coastal effects also extend upstream into the river floodplains and east of Sabine Lake, generally representing 40–80% of peak water levels. Rainfall contributes 10–50% to flooding east of Sabine Lake (Figure 2.12c), where water levels peak late on September 24 through September 25 (Figure 2.8c). As with Ike, the riverine influence during Rita is negligible, contributing a maximum of only 10% to peak water levels (Figure 2.12b). Compounding effects primarily occur along the inland extent of the storm surge, in parts of the river floodplains, and east of Sabine Lake due to surge and rainfall (Figure 2.12d).

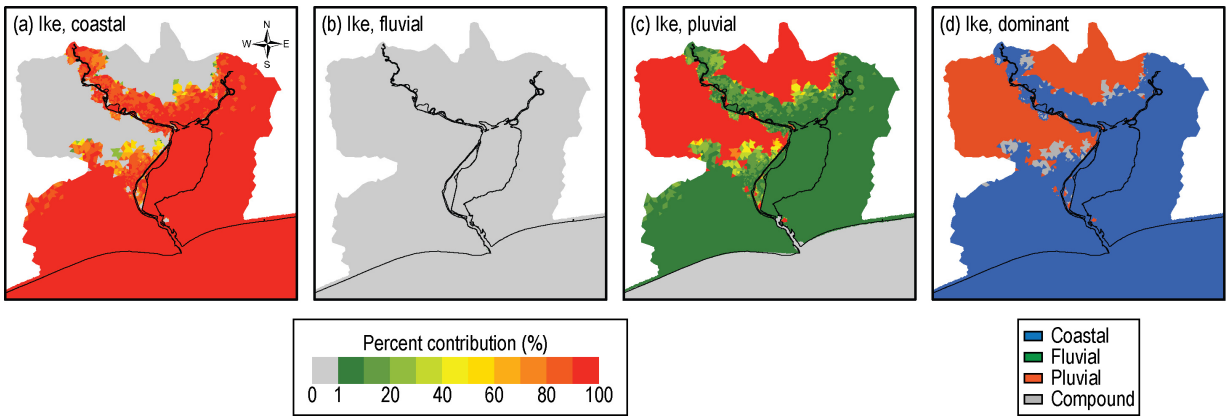

Figure 2.10: Percent contribution of (a) coastal, (b) fluvial, and (c) pluvial forcing to peak water levels for Hurricane Ike. The dominant forcing, representing at least 80% of the peak water level, is shown in panel d. Areas in blue are dominated by coastal influence, areas in green by fluvial influence, and areas in orange by pluvial influence. Gray areas represent locations where no forcing contributes more than 80% to the peak water levels, suggesting the potential for compound effects. The legend on the left corresponds with panels a-c. The legend on the right corresponds with panel d.

2.5.5 LNVA water infrastructure assets

As mentioned previously, LNVA operates critical water infrastructure that supports municipal, industrial, and agricultural customers in the region. To examine the effects of hurricane-driven flooding on LNVA assets, we extracted the disturbance factor for each forcing at the time of peak water level in the compound scenario from the grid cells closest to the locations of the Neches River Saltwater Barrier and the North Regional Treatment Plant (Table 2.3). At the Saltwater Barrier, fluvial effects are dominant (97%) for Harvey, while coastal effects are dominant (78%) for Ike. Both coastal (55%) and fluvial (35%) processes contribute to peak water levels at the Saltwater Barrier during Rita. Across all storms, the pluvial effect is minimal. In contrast, at the North Regional Treatment Plant, compounding effects due to all three forcings were observed during each storm. The fluvial scenario contributed most during Harvey (60%), the coastal scenario during Ike (55%), and the pluvial scenario during Rita (40%).

Table 2.3: Percent contribution of individual forcing scenarios to peak water levels at LNVA facilities.

Location	Hurricane	Time of Compound Peak	Coastal	Fluvial	Pluvial
Neches River	Harvey	2 Sep 2017 04:06:00	3	97	0
Saltwater Barrier	Ike	14 Sep 2008 12:54:00	78	13	9
	Rita	24 Sep 2005 18:48:00	55	35	10
North Regional	Harvey	2 Sep 2017 19:54:00	14	60	26
Treatment Plant	Ike	13 Sep 2008 19:18:00	55	18	27
	Rita	25 Sep 2005 12:00:00	30	30	40

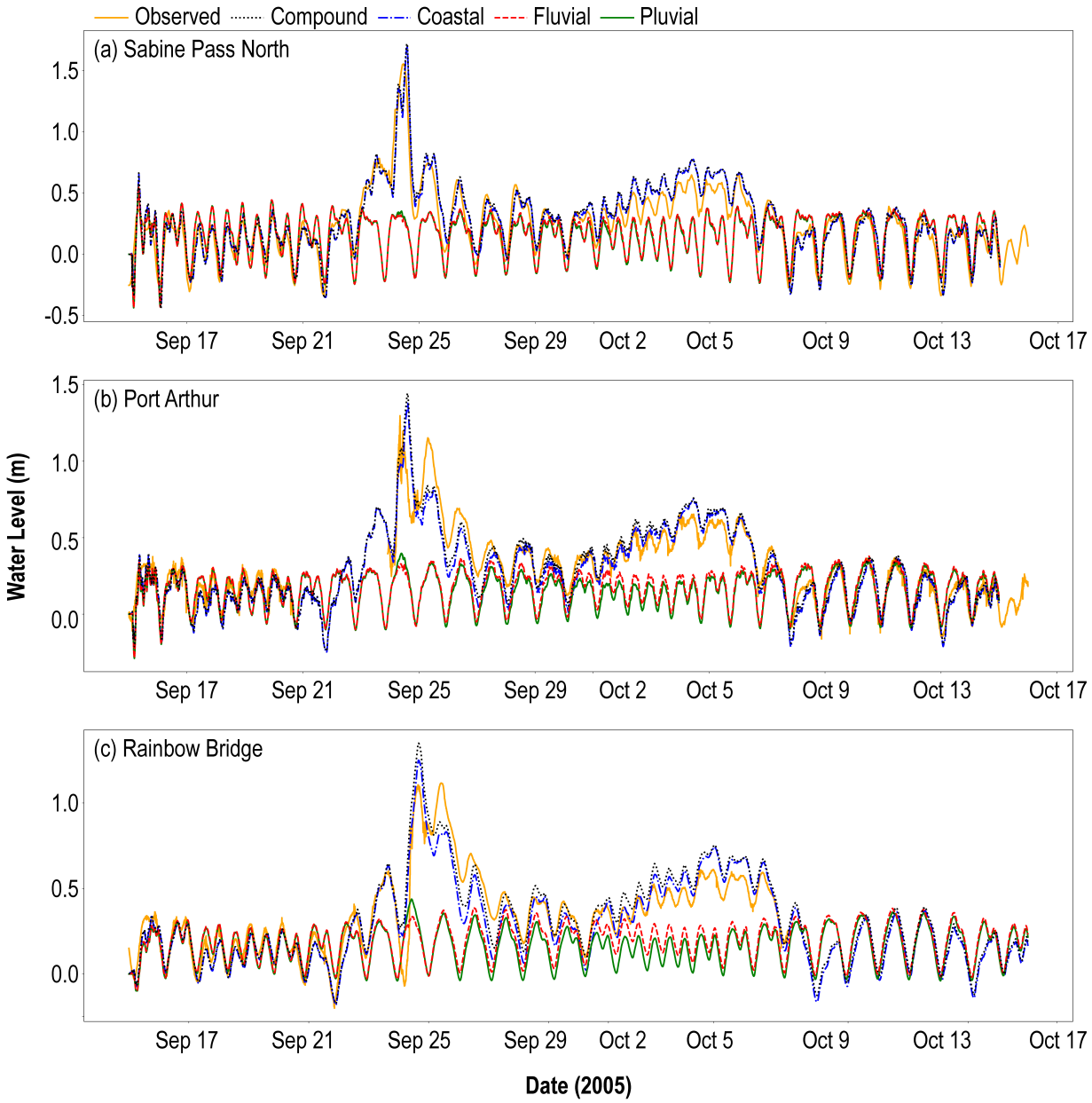

Figure 2.11: Modeled versus observed water levels at (a) Sabine Pass North, (b) Port Arthur, and (c) Rainbow Bridge for Hurricane Rita.

2.6 Discussion

The Delft3D-FM computational engine provides a means to simulate coupled coastal, fluvial, and pluvial processes within the computational domain. The compound model was generally able to predict observed water levels well across all three hurricanes, even given their disparate meteorological characteristics. For Harvey, the compound scenario provided a significant improvement over the individual forcing scenarios at the NOAA observation stations, reducing RMSE by 0.21 m compared to the coastal and fluvial scenarios and 0.35 m compared to the pluvial scenario (Table 2.2). In contrast, the compound scenario provided negligible improvements over the coastal scenario at NOAA stations during Ike and Rita, since the coastal influence was dominant in Sabine Lake and the Neches River during these storms (Figures 2.10d and 2.12d). However, compounding effects were important in

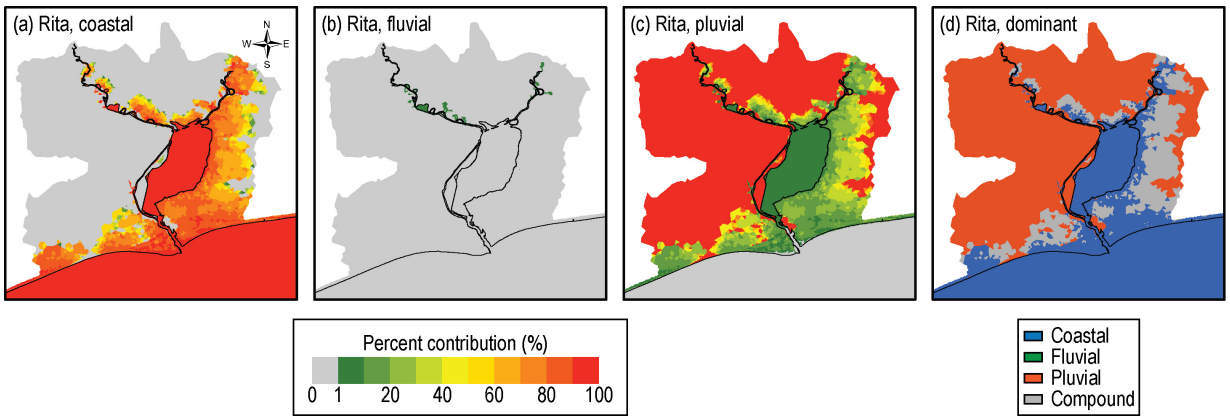

Figure 2.12: Percent contribution of (a) coastal, (b) fluvial, and (c) pluvial forcing to peak water levels for Hurricane Rita. The dominant forcing, representing at least 80% of the peak water level, is shown in panel d. Areas in blue are dominated by coastal influence, areas in green by fluvial influence, and areas in orange by pluvial influence. Gray areas represent locations where no forcing contributes more than 80% to the peak water levels, suggesting the potential for compound effects. The legend on the left corresponds with panels a-c. The legend on the right corresponds with panel d.

other parts of the domain, including in overland areas near the extent of surge penetration and east of Sabine Lake, indicating the value of using a coupled approach.

Comparing the results of our scenario modeling for Harvey, Ike, and Rita, we observe four compound flood mechanisms in the SNE during tropical cyclone events: (1) coastal-fluvial-pluvial interactions in the waterways, (2) coastal-fluvial interactions in the downstream part of the estuary near Sabine Pass, (3) fluvial-pluvial interactions in overland areas east of Sabine Lake, and (4) coastal-pluvial interactions in overland areas east of Sabine Lake. The first mechanism occurred on August 30 as Harvey made landfall east of the SNE as a tropical storm with moderate wind speeds. Harvey's storm surge coincided with ongoing heavy rainfall over the SNE and was exacerbated by increasing river discharges following almost a week of heavy rainfall in upstream watersheds. This led to coastal-fluvial-pluvial interactions in the waterways, from Sabine Lake upstream to the Neches and Sabine Rivers (Figure 2.7).

The second mechanism was also observed during Harvey but occurred several days later, on September 4. Extreme rainfall falling over multiple days across the study area and in upstream watersheds during Harvey led to extensive runoff draining into the Neches and Sabine Rivers and Sabine Lake. The resulting fluvial discharge interacted with elevated coastal water levels, unrelated to the initial surge, to produce compound flooding in Sabine Pass and the downstream portions of Sabine Lake and the ship channel (Figure 2.7).

The third mechanism, compounding due to fluvial-pluvial interactions, was observed during Harvey in overland areas east of Sabine Lake. Peak river discharge on September 4 led to outflows from Sabine Lake that interacted with saturated and undrained conditions in overland areas impacted by extreme rainfall, causing widespread flooding. Although the peak river discharge did not coincide with the period of rainfall, the antecedent saturated conditions exacerbated the flooding caused by fluvial outflows. The influence of fluvial flows on flooding east of Sabine Lake during Harvey was also demonstrated by [9] when comparing their coastal-only scenario to a scenario that included both coastal and fluvial inputs.

Finally, the fourth mechanism occurred during both Harvey and Rita as coastal and

pluvial drivers interacted. During Harvey, the initial storm surge led to overflows near Sabine Pass, east of Sabine Lake, and in small portions of the river floodplains on August 30. This coincided with heavy rainfall over the SNE, leading to concurrent coastal and pluvial impacts in limited areas. Coastal-pluvial interactions were more notable during Rita, which made landfall east of Sabine Pass as a Category 3 hurricane, with strong onshore winds driving storm surge into the estuary. Elevated water levels in Sabine Lake due to storm surge led to outflows to the east, where the pluvial effect was also high, causing a compounding effect. Coastal-pluvial compounding also occurred to a lesser extent in the river floodplains during Rita.

Based on these four mechanisms, we conclude that rainfall duration plays an important role in determining the likelihood of experiencing multiple types of compound flooding during a single storm. Tropical cyclones like Harvey that make landfall at the tail-end of an extended period of rainfall over the estuary and upstream watersheds are of particular concern, as they have the potential to produce temporal compounding with an initial surge-driven peak followed by a lagged fluvial peak. If this lagged fluvial peak occurs before the downstream watershed has time to drain or if it coincides with a subsequent period of high coastal water levels, compounding between fluvial-pluvial or fluvial-coastal drivers can result. Such events should be carefully accounted for in emergency planning efforts so residents are aware that, even after the passing of the hurricane and associated surge, river discharge into the estuary can produce a second, potentially more severe, flood peak and further delay recovery efforts. In contrast, storms like Rita that cause intense but short-duration or localized rainfall and moderate surge are likely to produce only coastal-pluvial compounding, as the fluvial influence from the Neches and Sabine Rivers will be small.

This study highlights the diversity of hazards that the SNE may face due to tropical cyclone events and suggests the need for more comprehensive flood hazard assessments that account for multiple flood drivers and their interactions. Building resilience to multiple flood drivers is particularly important for LNVA given the critical role that LNVA assets serve in maintaining surface water quality and supplies in the region. At facilities such as the North Regional Treatment Plant, protective barriers like levees or seawalls can mitigate the effects of coastal and fluvial flooding but may exacerbate the impacts of pluvial flooding by restricting off-site drainage. Dual approaches that couple protective infrastructure with pumps may be needed to effectively manage these multiple sources of flooding. Deployment of gauges to collect data on rainfall, soil moisture, and infiltration in overland areas could further constrain the role of pluvial flooding to inform mitigation activities. Given the potential for both coastal and fluvial impacts at the Neches River Saltwater Barrier, as demonstrated here, refined modeling of coastal-fluvial interactions and salinity distributions would provide insight into potential impacts on structural and mechanical components and upstream freshwater supplies.

2.7 Limitations

Detailed bathymetric survey data was only available up to the extent of dredging in the Neches and Sabine Rivers, so river cross-sections further upstream were simplified within the model. This introduced uncertainty in the modeling of water levels and velocities in the upstream reaches of these rivers. In addition, the topography and bathymetry datasets used to construct the model were mostly collected prior to 2006. As a result, changes due to natural or anthropogenic influences between the three simulated hurricane events were

not captured.

The data and assumptions used when implementing rainfall in the model could also cause discrepancies between modeled and observed water levels. Although 1-km resolution MRMS data was available for Harvey, only 4-km resolution Stage IV data was available for Rita and Ike, limiting the ability to capture high-resolution variability in the spatial distribution of rainfall. In addition, if the effects of interception, infiltration, or evaporation are not negligible, as was assumed in this and other studies of Harvey [39], water levels may be overpredicted. In fact, ignoring these processes may have contributed to the overprediction of water levels at HWMs outside of the Neches River floodplain, where the pluvial influence was dominant during Harvey (Figure 2.5d). A lack of high-resolution information on antecedent soil moisture conditions and infiltration rates thus presents a challenge for accurate modeling of rainfall-runoff processes in compound flood frameworks and could be a target for future data collection efforts.

Uncertainty in the datasets used to set the model boundary conditions are another possible source of error [91]. For most scenarios, we used NOAA tide gauge data at the offshore boundary and USGS discharge data at the upstream Neches River boundary. In past studies, NOAA data was reported to have high accuracy, with errors of approximately 1 mm [92, 67], although errors may be higher during extreme events [93]. The quality of USGS discharge measurements can range from <2% error (excellent) to >8% error (poor) [94, 67]. USGS gauges might not perform well under extremely high flow conditions that are beyond their rating curves which brings some uncertainty to discharge data. For the scenarios that used modeled data from CERA or GTSR to force the offshore boundary instead of NOAA observations, errors could result from grid resolution and input data quality. However, the datasets obtained from CERA (based on ADCIRC) and GTSR (based on Delft3D-FM) have been shown in the past to provide accurate coastal water level data to inform coastal flood studies [95, 89]. To address concerns with data accuracy and eliminate the need for observed or modeled data at the offshore boundary, the domain could be extended to cover the entire Gulf of Mexico and part of the Atlantic Ocean, thus enabling the use of hurricane wind and pressure data to generate coastal water levels offshore of Sabine Pass.

2.8 Conclusions

In this study, we developed a coupled flood model to investigate the potential for compound flooding in the SNE during three historical hurricane events (Harvey, Ike, and Rita). We used this model to assess the individual and combined effects of coastal, fluvial, and pluvial flood drivers on peak water levels in the study region. Our results reveal that tropical cyclones such as Harvey that are accompanied by extended periods of rainfall produce the largest extent and longest duration of compound flooding. Such storms also produce highly dynamic and evolving patterns of compound flooding over their duration, with multiple flood peaks that can inhibit response and recovery efforts. For such storms, a compound model that is capable of simulating storm surge, tides, river discharge, and rainfall can provide substantial improvement over single-hazard modeling approaches. Although the coastal-only model may be adequate to predict water levels in the waterways for storms such as Ike and Rita, which were accompanied by shorter-duration rainfall and more extreme surge, we identified overland areas where multiple drivers contributed to peak water levels for both storms, thus motivating the use of the compound model.

Our results also demonstrate that critical water and wastewater infrastructure in the

region is susceptible to flooding from multiple sources, depending on the characteristics of individual tropical cyclone events. This has important implications for infrastructure planning and operation, suggesting the need for adaptation approaches that address flood hazards holistically. Incorporating projected sea-level rise and changes in tropical cyclone activity and structure is also important to ensure that the design of flood protection is adequate to address both current and future threats. Although beyond the scope of the current study, this will be the focus of follow-on work.

Overall, this study highlights the importance of characterizing the spatial and temporal influence of and interactions between coastal, fluvial, and pluvial drivers to more accurately assess flood hazards in the SNE. Although our focus here is on a single estuary in southeast Texas, the modeling approach can be applied to similar bay and estuary systems where data of adequate quantity and quality are available to evaluate the local factors that contribute to compound flood potential and to inform more comprehensive flood hazard assessment in coastal communities.

Chapter 3

Impact of Climate Change on Compound Flooding During Tropical Cyclone Events

3.1 Abstract

Flood hazards associated with tropical cyclones cause severe impacts on coastal communities, including loss of life and property. In low-gradient estuaries and coastal watersheds, interactions between storm surge, rainfall, and river discharge during tropical cyclones can lead to compound flooding, potentially exacerbating impacts compared to individual drivers. The severity of tropical cyclone-driven flooding is projected to increase in the future due to sea level rise and increases in extreme rainfall associated with climate change, with yet-unknown impacts on the spatiotemporal evolution of compound flooding. This study applies a numerical flood model to simulate compound flooding in the Sabine-Neches Estuary (SNE), a low-gradient estuary on the US Gulf Coast, during Hurricane Harvey (2017) and to examine the relative influence of projected future sea level rise and increased rainfall on compound flood hazards during Hurricane Harvey under 2050 and 2100 climate conditions. We find that while water levels increase along the entire coastal-estuary-river continuum due to sea level rise and future rainfall, the magnitude of the flood peak above tidal levels decreases with sea level and can counteract the increase due to higher rainfall intensity. The combined effects of future sea level rise and rainfall create new coastal-fluvial and coastal-pluvial interactions and shift compound flood hazards further inland toward high-density developments. The number of residential structures in the compound flood zone increases from 0.6% of all impacted structures in 2017 to 14% in 2100. The shifting flood zones observed in our modeling can affect how flood mitigation is implemented in coastal regions.

3.2 Introduction

Tropical cyclones can have devastating impacts on coastal communities, leading to loss of life and property and causing extended disruptions to local and regional economies. The combined impacts of storm surge and rainfall during tropical cyclones can generate compound flooding due to the interactions between elevated coastal water levels, higher river discharge, and direct rainfall [96, 97]. Studies have demonstrated that neglecting the interactions between these flood drivers can lead to misrepresentation of flood exposure

and damages [8, 9, 10, 64]. For example, Kumbier et al. (2018) found that flood depths in the Shoalhaven Estuary in Australia during a 2016 storm event would be underestimated by up to 1.5 m if interactions between discharge and surge processes were not considered.

Tropical cyclone-induced flood hazards are projected to worsen in the warmer future climate due to the combined effects of sea level rise [98, 99, 100] and more intense rainfall associated with wetter tropical cyclones [16, 17, 18, 14, 15]. Recent projections by the Intergovernmental Panel on Climate Change (IPCC) suggest that global sea level rise could be in the range of 0.28–1.01 m by the end of the century relative to the period from 1995–2014 [101], although local relative sea level rise can vary substantially across the global coastlines due to factors such as vertical land motion [102]. Higher mean sea level allows storm surge to propagate further inland, impacting areas that were formerly outside of the flood zone, and also produces a reduction in drainage gradients that can slow or inhibit effective drainage of runoff to the coastline, leading to longer inundation duration and recovery times [103]. Previous studies that have applied global climate models to quantify potential changes in rainfall associated with tropical cyclones suggest a 10–32% increase in rainfall intensity within a 100 km storm radius by the late 21st century [104, 105, 106, 107].

Both statistical and numerical approaches have been applied to study how compound flooding will change in the future with climate change. Studies that apply statistical frameworks have suggested that the probability of compound flooding will increase in the future as a result of sea level rise and more intense rainfall [108, 109, 13]. While statistical approaches can provide important information about the frequency and magnitude of coincident flood drivers, numerical models that incorporate forcing variables as boundary conditions are needed to translate these drivers into predictions of flood extent and depth [110]. Many numerical modeling studies have demonstrated nonlinear interactions between flood drivers (e.g., storm surge and sea level rise or storm surge and river discharge) that are critical for accurate assessment of flood hazards and impacts [111, 29]. This highlights the importance of capturing the physics of the local system when attempting to predict changes in compound flooding.

Previous work has presented approaches for defining compound flood zones, or areas where interactions between rainfall, surge, and river discharge are likely to occur [3, 22]. Delineating these compound zones within a watershed can inform where coupled modeling approaches that simulate coastal and inland process are needed to accurately capture likely flood hazards. In addition, design and implementation of effective flood mitigation projects requires a complete understanding of the types of flooding that may impact a region. In compound flood zones, flood control approaches used to prevent one type of flooding may not be effective at addressing other sources of flooding. While past research has examined the role of sea-level rise and changes in coastal landscape features in modifying the location and extent of compound flood zones [11], the combined influence of sea level rise and changing rainfall patterns on flood transition zones has not yet been studied, despite its important role in guiding community and infrastructure adaptation to future flooding.

Here, we examine how the extent of compound flood zones and associated impacts may change in the future based on projections of sea level rise and changes in rainfall intensity. We apply a coupled flood model that utilizes Delft3D-FM to simulate potential flood hazards in a micro-tidal estuary under tropical cyclone forcing. We then delineate flood hazards zones based on the dominant flood driver(s) across the study area. Finally, we leverage building stock data and depth-damage curves to estimate impacts to residential structures within each zone. Our findings provide greater insight into how future climate

conditions will shape the types of flooding and impacts due to tropical cyclone events and can inform the selection of flood mitigation measures that holistically address flood hazards facing coastal communities.

3.3 Study Area

The Sabine-Neches Estuary (SNE) is located along the Texas-Louisiana border, where the Sabine and Neches Rivers converge with the Gulf of Mexico (Figure 3.1). The SNE is the freshest of Texas's estuaries and receives an average annual inflow of 14 million acre-ft from the Sabine and Neches Rivers [112]. The two major population centers, Beaumont (pop. 115,282) and Port Arthur (pop. 56,039) [113], are located along the Port Arthur Canal and the Neches River, respectively.

The SNE is vulnerable to flooding from coastal storms due to its low topographic gradient. Rates of relative sea level rise in the SNE are some of the highest in the nation, between 5.8 and 6.2 mm/yr [114]. In 2017, the region was impacted by Hurricane Harvey, which brought minor storm surge and unprecedented rainfall, causing billions of dollars in damages in the two Texas counties adjacent to Sabine Lake (Orange County to the north and Jefferson County to the west). A study by [115] estimated that human-induced climate change increased the probability of Hurricane Harvey rainfall from 1% during 1981-2000 to 6% by 2017 and 18% by 2100. Another recent study that applied a regional earth system model to examine the impacts of climate change on rainfall associated with Hurricane Harvey over the Clear Creek watershed in Harris County, Texas, found that total rainfall during the storm increased by 50% under end-of-century climate conditions, leading to greater inundation extent, depth, and duration [32]. Understanding how climate change will influence future hurricane-induced flooding in the SNE is important for mitigation planning and adaptive management in the region.

3.4 Methods

3.4.1 Numerical model

We applied a calibrated and validated numerical model built using Delft3D-FM [38] to simulate coastal, fluvial, and pluvial processes in the SNE. Delft3D-FM is a hydrodynamic modeling software that solves the Navier-Stokes equations with Boussinesq assumptions on an unstructured grid [71]. We applied the model in two-dimensional, depth-averaged mode to simulate water levels and velocities across our study domain, which covered an inland area of 2,500 km^2. The model boundaries were delineated using hydrologic units (HUC-12) in inland regions to include the lower Neches and Sabine River watersheds and adjacent overland areas contributing runoff to Sabine Lake. The grid resolution varied from approximately 1,000 m in offshore areas to 40 m nearshore and in channels, resulting in a total of 161,623 grid cells. To model surface roughness, we implemented a spatially variable Manning's roughness based on land cover. A drying and flooding algorithm with a threshold of 10 cm is applied, following the approach used in previous studies (e.g., [10]). Further information on the development, calibration, and validation of the model can be found in [116].

For this study, the model was forced at the offshore boundary using water level time series from two sources: modeled water levels from the Coastal Emergency Risks Assessment (CERA) hindcast simulation and observed water levels from NOAA [88] at Texas

Figure 3.1: Map of the Sabine-Neches Estuary, Texas.

Point, Sabine Pass (8770822). The CERA data was used for the period from August 24 to August 31, 2017, because, unlike observational data that may also capture the effects of high river discharge through Sabine Pass, the modeled data only accounts for coastal forcing. Observed water levels from NOAA were used for the remainder of the simulation period. At the upstream river boundaries, hourly discharge time series were implemented as point sources. For the Neches River, data was extracted from USGS 08041780 Neches Rv Saltwater Barrier at Beaumont [86]. For the Sabine River, data was obtained from the National Water Model (NWM), which uses hourly, 1-km radar-only Multi-Radar Multi-Sensor (MRMS) rainfall data to estimate flows. Meteorological forcing included 3-hr wind and pressure fields from the National Center for Environmental Prediction (NCEP) North American Regional Reanalysis (NARR) [82] and hourly MRMS gridded rainfall time series [85]. The model was run for several days prior to Hurricane Harvey's landfall to reach a stable state.

3.4.2 Future scenarios

We modeled three scenarios to evaluate the effects of climate change on the spatial distribution of compound flood zones in 2050 and 2100 (Table 4.1). First, we considered the effects of sea-level rise using projections from the Intergovernmental Panel on Climate Change (IPCC) for the Western Gulf of Mexico under an intermediate warming scenario. This resulted in sea-level rise estimates of 0.57 m in 2050 and 1.6 m in 2100 compared to the 2017 baseline [102]. For each sea-level rise scenario, we added the sea-level rise increment to the offshore water level timeseries for Hurricane Harvey, which allowed us to the capture local nonlinear effects of sea-level rise on water levels in our study domain.

Second, we modeled the effects of future increases in rainfall intensity using results from [32], which projected increases of 17.7% and 49.7% in future total rainfall associated with Hurricane Harvey in the 2050s and 2090s, respectively, for the Clear Creek watershed in Houston, Texas. Although there are varying estimates of the impacts of climate change on rainfall intensity associated with tropical cyclones, we selected the estimates from [32] because they were generated from the same storm (Hurricane Harvey) over the Texas coast. For each future rainfall simulation, we scaled the observed MRMS rainfall for Hurricane Harvey by the percent change in total rainfall from [32] to adjust the rain falling over our computational domain. To account for the effects of increased rainfall in upstream watersheds on river discharge at the river boundaries, we applied a calibrated HEC-HMS model developed by USACE for the Neches River watershed. USACE validated the HEC-HMS model for Harvey using USGS-observed discharge. We modified the HEC-HMS model for future scenarios by applying the rainfall coefficient for mid-century and end-of-the-century (the same percentages from above) to the historical rainfall of Harvey offered in the USACE model.

Finally, we simulate a combined scenario that considers both future sea-level rise and rainfall intensity in 2050 and 2100 to evaluate how interactions between intensifying coastal and hydrological processes influence patterns of compound flooding. For each of the sea-level rise, rainfall, and combined scenarios, we ran several sub-scenarios to simulate the individual and combined influences of coastal, fluvial, and pluvial processes. The coastal-only scenario included surge and wind/pressure, with no river discharge or rainfall. The fluvial-only scenario included river discharge due to upstream runoff in areas outside of the model domain and tidal water levels at the offshore boundary, with no surge, wind/pressure, or rainfall. The pluvial-only scenario included rainfall over the model domain and tidal water levels at the offshore boundary, with no surge, wind/pressure, or river discharge. The compound scenario included all processes to account for potential nonlinear interactions. These scenarios and their forcing conditions are summarized in Table 4.1.

3.4.3 Compound flood delineation

To delineate compound flood zones and zones where a single flood driver is dominant, we apply the approach outlined by [39]. For each grid cell in the model domain, we find the time of maximum water level in the compound model, t_{peak}. We then determine the water depth above tide DAT due to each flood driver by subtracting the water level at t_{peak} from a tide-only simulation from the water level at t_{peak} for each of the individual forcing simulations (coastal-, fluvial-, pluvial-only). Finally, we calculate the percent contribution C of each forcing scenario to peak water levels. For example, the coastal contribution ($C_{coastal}$) is calculated as:

Table 3.1: Summary of future flood scenarios.

Scenario	Sub-Scenario	Offshore WL	Rivers	Rainfall	W/P
SLR	Coastal	NOAA/CERA + SLR	N/A	N/A	NCAR
	Fluvial	NOAA tide + SLR	HEC-HMS	N/A	N/A
	Pluvial	NOAA tide + SLR	N/A	MRMS	N/A
	Compound	NOAA/CERA + SLR	HEC-HMS	MRMS	NCAR
Rainfall	Coastal	NOAA/CERA	N/A	N/A	NCAR
	Fluvial	NOAA tide	fut. HEC-HMS	N/A	N/A
	Pluvial	NOAA tide	N/A	fut. MRMS	N/A
	Compound	NOAA/CERA	fut. HEC-HMS	fut. MRMS	NCAR
SLR + Rainfall	Coastal	NOAA/CERA + SLR	N/A	N/A	NCAR
	Fluvial	NOAA tide + SLR	fut. HEC-HMS	N/A	N/A
	Pluvial	NOAA tide + SLR	N/A	fut. MRMS	N/A
	Compound	NOAA/CERA + SLR	fut. HEC-HMS	fut. MRMS	NCAR

$$C_{coastal} = \frac{DAT_{coastal}}{DAT_{coastal} + DAT_{fluvial} + DAT_{pluvial}} \tag{3.1}$$

Although this approach uses a linear addition method to calculate to total DAT and does not account for nonlinear interactions between flood drivers, our aim in delineating the flood zones is to identify regions where more than one forcing may contribute to peak water levels. If $C > 80\%$ for any single flood driver in a grid cell, we classify that driver as dominant. If $C < 80\%$ for all drivers, the grid cell is classified as compound.

3.4.4 Damages

We applied the Federal Emergency Management Agency's (FEMA) Flood Assessment Structure Tool (FAST) to calculate flood damages to residential structures [117]. Peak flood depth maps from the modeled scenarios were used as input to FAST, along with building stock data from the National Structure Inventory version 2 dataset (NSI2) [118]. NSI2 uses parcel and structure footprint data to improve the precision of building locations and includes building-specific data on foundation type, total number of stories, ground elevation, foundation type, number of stories, occupancy type, and replacement costs. Building and content loss values (in 2021 dollars) are calculated using depth-damage curves from FEMA's Hazus model [119]. In this study, losses for residential structures were summed within each delineated flood zone (coastal, fluvial, pluvial, or compound) to estimate the total flood damage per zone.

3.5 Results

3.5.1 Compound flooding due to future sea level rise

Time series of water levels are shown for the historical condition (2017) and the future conditions (2050 and 2100) with sea level rise at four locations along a transect stretching from the mouth of Sabine Pass at the Gulf of Mexico to the Saltwater Barrier in the Neches River upstream of Beaumont (Figure 3.2a). For the historical condition, water

levels reach a peak of 1.1 m NAVD88 on September 4 in Sabine Pass. With sea level rise in 2050 and 2100, the influence of storm surge on August 29 produces a higher water level than subsequent discharge, which causes a muted response. Although water levels increase across the storm event with sea level rise, the gradients associated with the rising and falling limbs become more gradual. Similar patterns are seen in Sabine Lake. The magnitude of the flood wave increases further upstream in the Neches River and is visible across all sea level rise scenarios. However, the increase in the peak water level is small (0.13 m in 2050 and 0.39 m in 2100 at Neches River US) compared to the projected change in sea level (0.57 m in 2050 and 1.6 m in 2100). To further emphasize this point, water depth above tide, calculated by subtracting the maximum simulated tidal water level at each station from the total water level in the compound forcing scenario, is shown in Figure 3.2b. Across all stations, the water depth above tide decreases with sea level rise. This effect is mainly seen after peak storm surge on August 29, when upstream discharge begins to impact the region. Water depth above tide decreases by 0.2 m in Sabine Pass and nearly 0.6 m in Sabine Lake by 2100. At the Neches River US location, water depth above tide is as much as 1.2 m lower with sea level rise in 2100. This demonstrates that while water levels will be higher with sea level rise, the increase in water levels will not be commensurate with the increase in sea level rise, highlighting the importance of using dynamic physical modeling when evaluating future impacts.

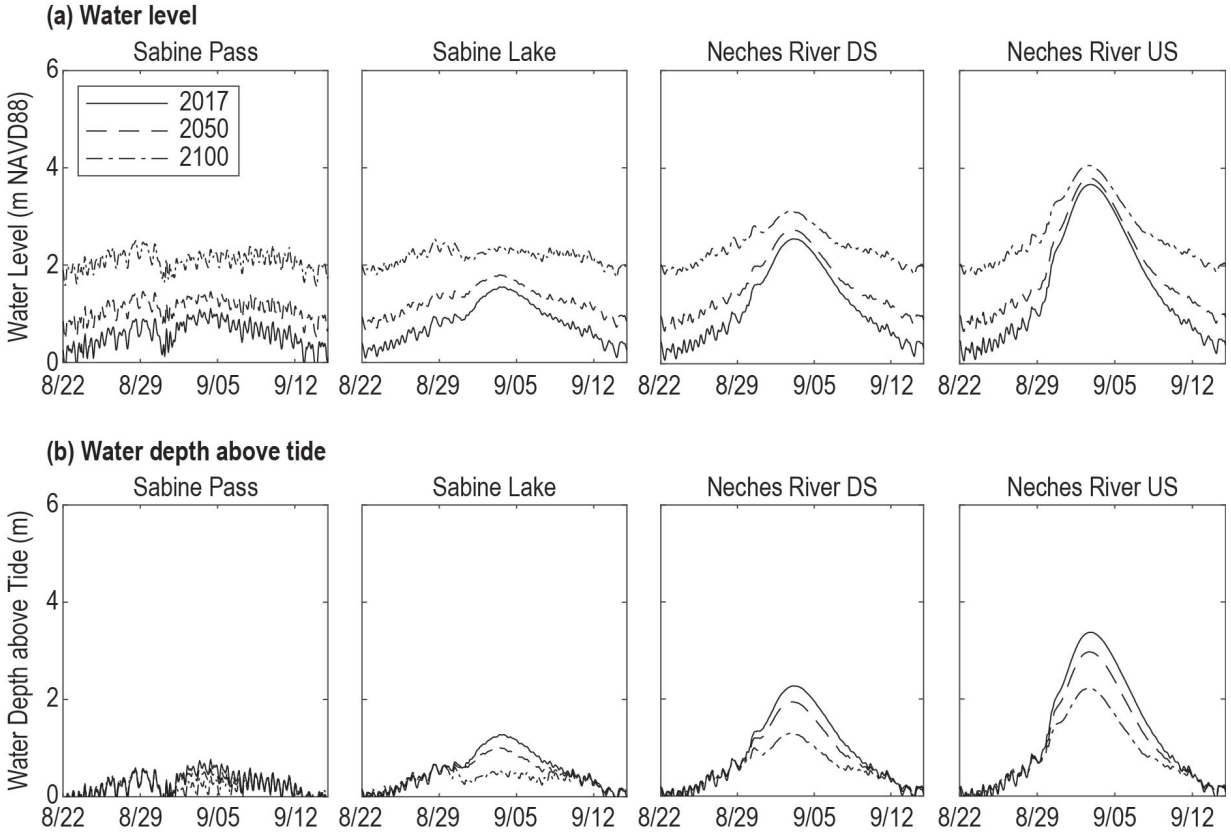

Figure 3.2: Time series of (a) water levels and (b) water depth above tide for the historical condition (2017) and the future conditions (2050 and 2100) with sea level rise at four locations along the transect shown in Figure 3.1. Water depth above tide is calculated by subtracting the maximum simulated tidal water level at each station from the total water level in the compound forcing scenario.

The impacts of sea level rise on the dominant processes driving flooding across the

SNE are summarized in Figure 3.3. Figure 3.3a shows the percent contribution of coastal, fluvial, and pluvial forcing to peak water levels during Hurricane Harvey, while Figure 3.3b shows the resulting flood zone delineations. In 2017, the coastal contribution is dominant offshore but generally contributes less than 20% to total water levels in the rest of the domain, including the waterways and adjacent areas (Figure 3.3a). In Sabine Pass, the coastal influence is higher (up to 60%). Water levels in Sabine Lake and much of the Neches and Sabine River watersheds are dominated by the fluvial influence, with minor contributions from coastal and pluvial processes. Areas to the north and west of the domain are dominated by pluvial processes. Compound fluvial-pluvial flooding occurs to the east of Sabine Lake, while compound interactions between coastal and fluvial processes occur in Sabine Pass and along the Port Arthur Canal.

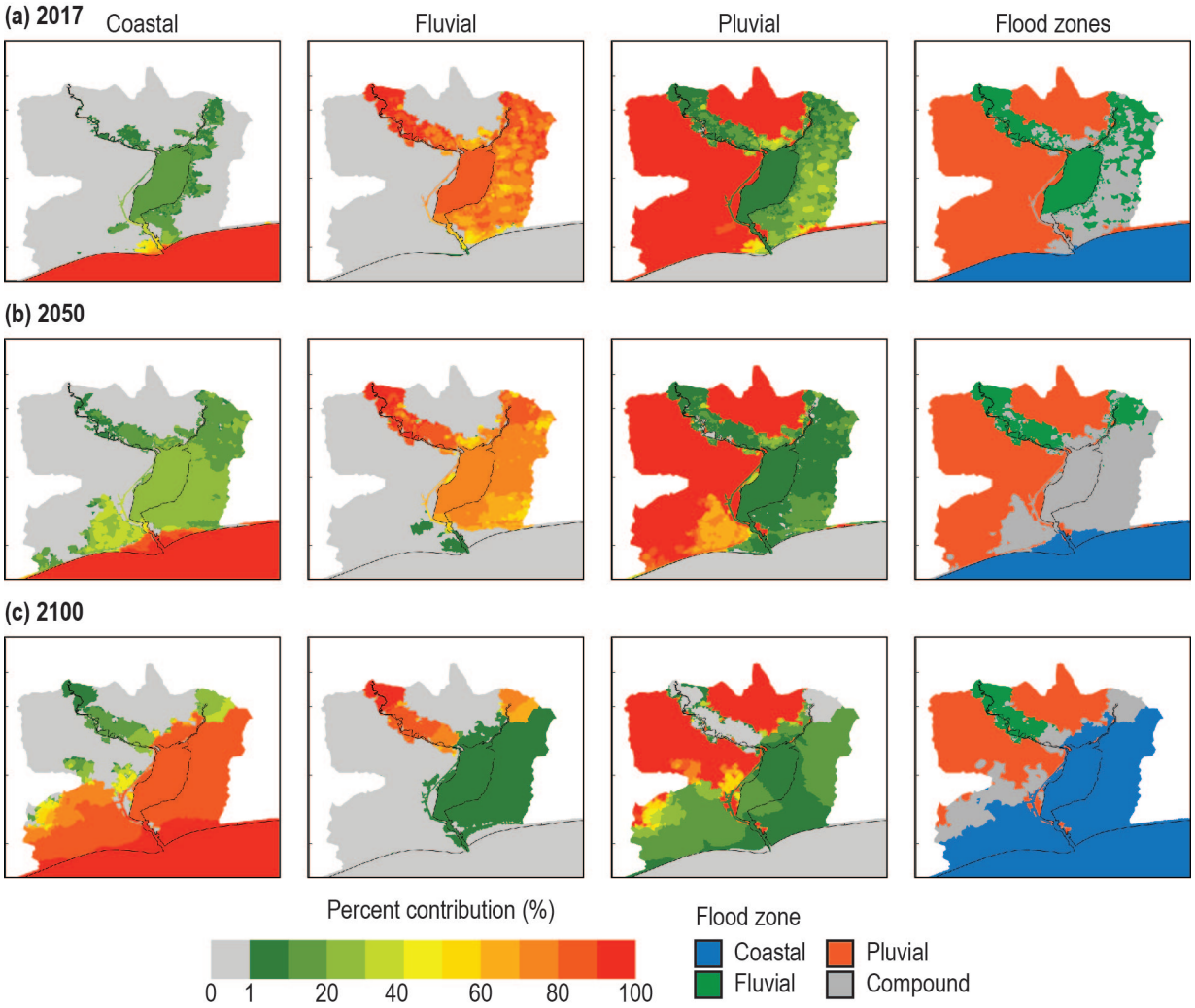

Figure 3.3: Percent contribution of coastal (first column), fluvial (second column), and pluvial (third column) forcing to peak water levels for Hurricane Harvey considering (a) historical conditions in 2017, (b) the influence of future sea level rise in 2050, and (c) the influence of future sea level rise in 2100. The dominant forcing, representing at least 80% of the peak water level, is shown in the fourth column. Areas in blue are dominated by coastal influence, areas in green by fluvial influence, and areas in orange by pluvial influence. Gray areas represent locations where no forcing contributes more than 80% to the peak water levels, suggesting the potential for compound effects.

Projected sea level rise from 2017 to 2050 causes the coastal influence to expand, contributing up to 30% to total water levels in Sabine Lake and areas to the east and up to 40% west of Sabine Pass (Figure 3.3a). The compound flood zone extends through Sabine Lake and into areas to the east (Figure 3.3b), where the primary interacting drivers shift from pluvial-fluvial to coastal-fluvial. Coastal-pluvial interactions create a smaller compound flood zone west of Sabine Pass. Coastal processes are dominant in only a small portion of the domain in and around Sabine Pass. By 2100, the coastal influence expands substantially due to sea level rise. Sabine Pass, Sabine Lake, and the Port Arthur Canal are dominated by coastal processes, which also extend to downstream areas in the Sabine River watershed, areas east of Sabine Lake, and areas west of Sabine Pass. The fluvial influence decreases substantially, only impacting the Neches and Sabine River watersheds and contributing less than 20% to water levels in Sabine Lake and to the east. The pluvial influence is still dominant in inland areas in the north and west of the study domain. Given the coastal-dominated influence in much of the study domain, the compound flood zone shrinks substantially and is limited to a few small areas in the river watersheds and to the west of the study domain. As expected, the impact of sea level rise is most pronounced in the coastal areas, and its effects diminish further upstream in the river watersheds.

3.5.2 Compound flooding due to future rainfall

Figure 3.4 shows the time series of water levels and water depth above tide for 2017 and the future rainfall conditions in 2050 and 2100. Future rainfall leads to an increase in the flood peak across all locations. The peak also shifts earlier in time, by up to 26 hours at the Neches River stations by 2100. The water depth above tide increases by 18–24% across stations for a corresponding increase in rainfall of 18% in 2050 and by 51–68% with an increase in rainfall of 50% in 2100.

Modeled increases in rainfall in 2050 and 2100 lead to a reduction in the compound flood zone in the SNE (Figure 3.5). Areas east of Sabine Lake that were formerly compound fluvial-pluvial are converted to fluvial-dominated, as the discharge at the upstream boundary of the Neches and Sabine Rivers increases due to increased runoff upstream. The compound coastal-fluvial zone at the downstream end of Sabine Lake and into Sabine Pass becomes slightly smaller in 2050 and 2100, as the fluvial influence increases upstream. However, changes to the compound flood zone across the region are small compared to the impacts from sea level rise.

3.5.3 Compound flooding due to future sea level rise and rainfall

Figure 3.6 shows the time series of water levels and water depth above tide for 2017 and the future conditions with sea level rise and increased rainfall in 2050 and 2100. When both sea level rise and future rainfall are considered, water depth above tide is reduced compared to the historical condition in Sabine Pass (by 0.1 m in 2050 and 0.2 m in 2100) and Sabine Lake (by 0.1 m in 2050 and 0.4 m in 2100). In the Neches River, the influence of higher discharge in 2050 and 2100 leads to an increase in water depth above tide of up to 0.6 m at Neches River US. This increase is muted compared to the rainfall-only scenario, which resulted in an increase of 2 m at the same station. In addition, the increase in water depth above tide is limited to a short time period associated with the rising limb and peak of the flood wave.

When the combined effects of sea level rise and rainfall are considered, the compound flood zone increases substantially (Figure 3.7). In 2050, the expansion of the coastal

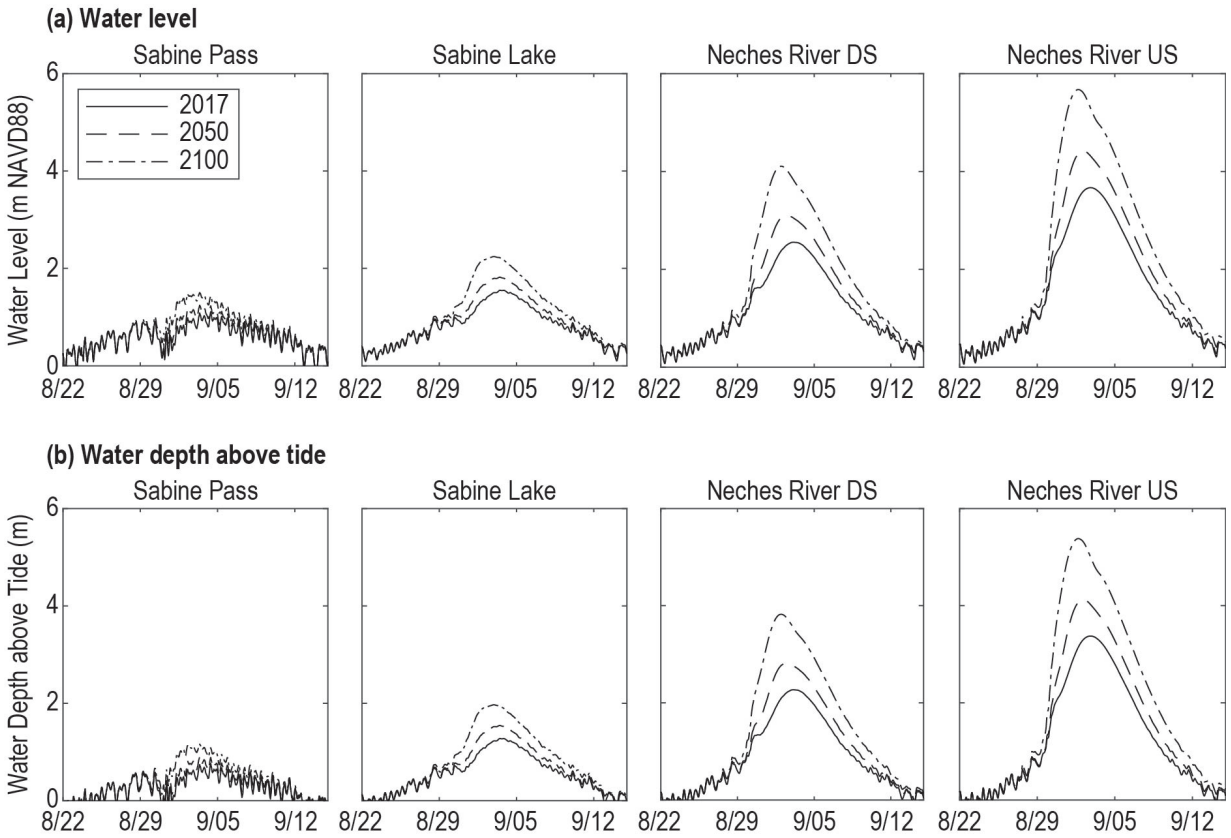

Figure 3.4: Time series of (a) water levels and (b) water depth above tide for the historical condition (2017) and the future conditions (2050 and 2100) with increased rainfall at four locations along the transect shown in Figure 3.1. Water depth above tide is calculated by subtracting the maximum simulated tidal water level at each station from the total water level in the compound forcing scenario.

influence due to sea level rise leads to a reduction in the fluvial-dominated zone in Sabine Lake. In addition, coastal processes expand to the region east of Sabine Lake, leading to coastal-fluvial interactions. Pluvial processes generally play a minor role in the compound zones, except in the area west of Sabine Pass where coastal-pluvial compounding occurs. By 2100, the coastal influence expands in areas west of Sabine Pass, east of Sabine Lake, and into the Sabine River watershed. At the same time, increased rainfall causes the fluvial influence to increase in the Neches River watershed and continues to contribute substantially to the water levels in Sabine Pass and areas to the east. In fact, in most of the coastal-fluvial compound zones, the fluvial contribution to total water levels (70-80%) is greater than the coastal contribution (20-30%). Unlike the sea level rise only scenario, which produces a larger increase in the coastal-dominated zone, the combination of sea level rise and increased rainfall causes an expansion of the compound flood zone.

3.5.4 Residential damages

Figure 3.8 summarizes the percent of the study area in each flood zone (panel a), along with the residential buildings impacted by flooding (panel b) and the associated building and content damages (panel c) per zone. In 2017, coastal-dominated areas comprise less than 1% of the domain (excluding offshore areas), impacting only one residential structure (Figure 3.8). 23% of the study area is fluvial-dominated, affecting 646 structures, while

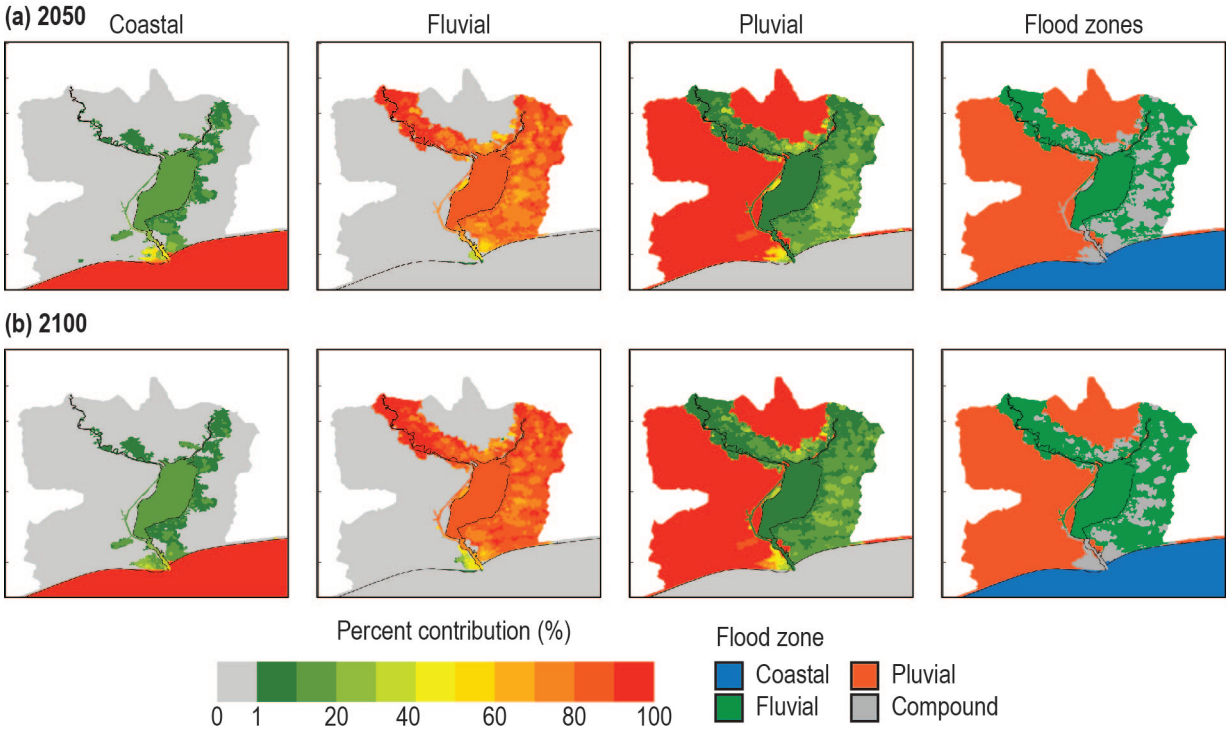

Figure 3.5: Percent contribution of coastal (first column), fluvial (second column), and pluvial (third column) forcing to peak water levels for Hurricane Harvey considering (a) the influence of future rainfall in 2050 and (b) the influence of future rainfall in 2100. The dominant forcing, representing at least 80% of the peak water level, is shown in the fourth column. Areas in blue are dominated by coastal influence, areas in green by fluvial influence, and areas in orange by pluvial influence. Gray areas represent locations where no forcing contributes more than 80% to the peak water levels, suggesting the potential for compound effects.

the majority of the area (59%) and structures (51,960) are impacted by pluvial-dominated processes. The compound zone covers 19% of the study area, impacting 299 structures. The total estimated number of residential structures impacted by flooding across all zones is 52,906, which is consistent with FEMA housing assistance data that reports that assistance was approved for 50,583 households in Jefferson and Orange counties following Hurricane Harvey [120]. The residential damage (building and contents) is estimated at $4.2 billion, with 98% of damages occurring in the pluvial-dominated zone. The NFIP claims paid for residential structures in Jefferson and Orange counties after Hurricane Harvey total $1.1 billion [121]. Previous studies indicate that only 22% of households in the region impacted by Harvey were insured through NFIP [122], and individual payouts through NFIP are limited to $250,000 USD for building damages and $100,000 USD for content damages [63]. These factors could account for the discrepancies between our modeled damages and actual NFIP payouts.

With sea level rise by 2050, the compound zone doubles in area to 37% as the coastal influence increases and the fluvial- and pluvial-dominated zones shrink (to 10% and 50%, respectively). However, the expansion of the compound zone occurs primarily in waterways or less-developed areas. As a result, the number of impacted residential structures increases to 579 in the compound zone, but this still only accounts for 1% of all impacted structures and 1% of total damages. With higher sea level rise in 2100, just under half of the model

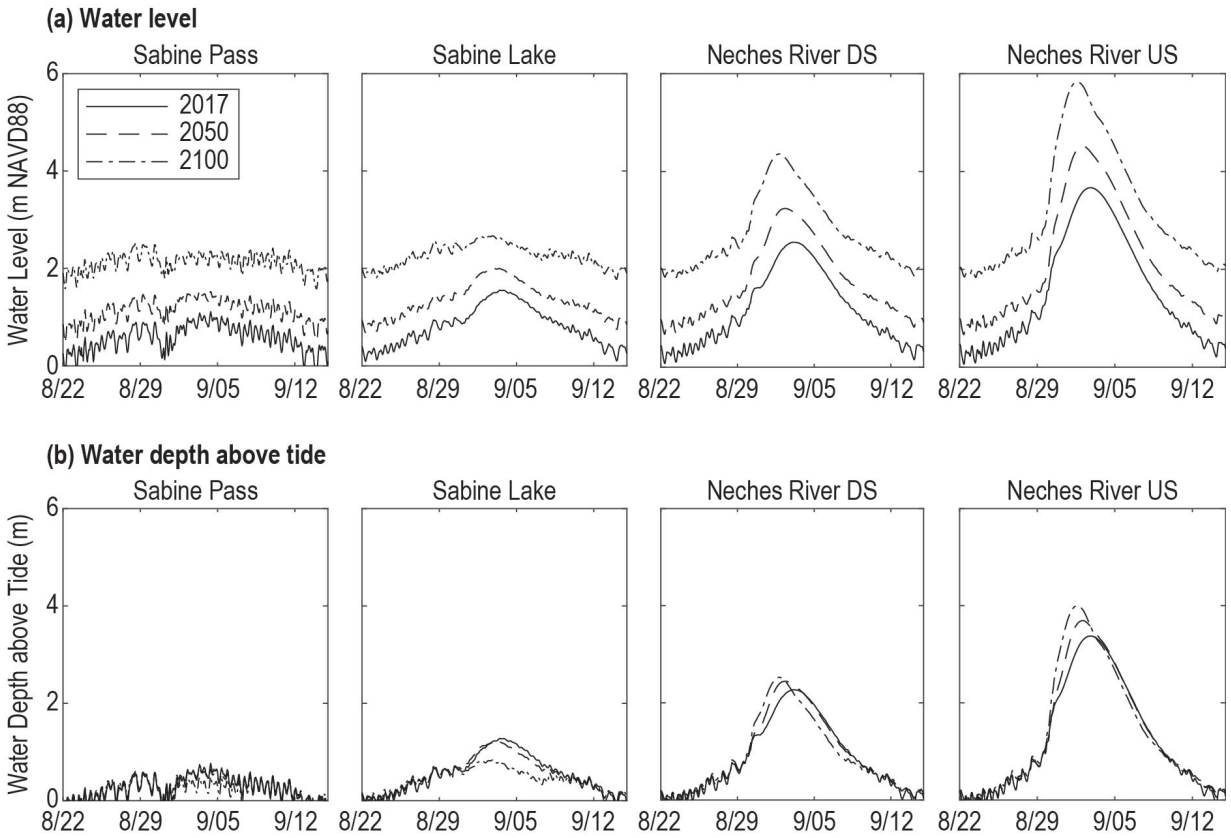

Figure 3.6: Time series of (a) water levels and (b) water depth above tide for the historical condition (2017) and the future conditions (2050 and 2100) with sea level rise and increased rainfall at four locations along the transect shown in Figure 3.1. Water depth above tide is calculated by subtracting the maximum simulated tidal water level at each station from the total water level in the compound forcing scenario.

domain (46%) is coastal-dominant, and the number of structures in the coastal-dominant zone increases to over 740. The area of the compound zone decreases to less than the area modeled for 2017 (15% of the model domain), but, at the same time, the number of structures exposed to compound flooding is 24 times higher than in 2017, while the total damages are 28 times higher. Because the major population centers in the SNE are located further inland along the Neches River, the shift in the compound zone to this area leads to substantially greater building exposure to compound flooding even as the overall area of the compound zone decreases.

As rainfall intensity increases from 2017 to 2050 and 2100, the compound zone shrinks from 19% to 14% to 10%, while the fluvial-dominated zone increases from 23% to 28% to 35%. Even as the size of the compound zone decreases, the number of impacted structures located within the compound zone increases by 1,209 between 2017 and 2100, resulting in over six times more damage. In the fluvial-dominant zone, six times as many residential structures are impacted in 2100 versus 2017, leading to a five-fold increase in damages.

For the combined scenario, increases in both rainfall and sea level cause a substantial expansion of the compound flood zone, to 33% in 2050 and 46% in 2100. This leads to a 32-fold increase in impacted structures and a 42-fold increase in damages by 2100. The coastal-dominant area also increases to 12% by 2100 but impacts relatively few structures (156). The fluvial-dominant zone decreases to 9% of the model domain by 2100, but the total number of impacted structures and associated damages increase by seven and six

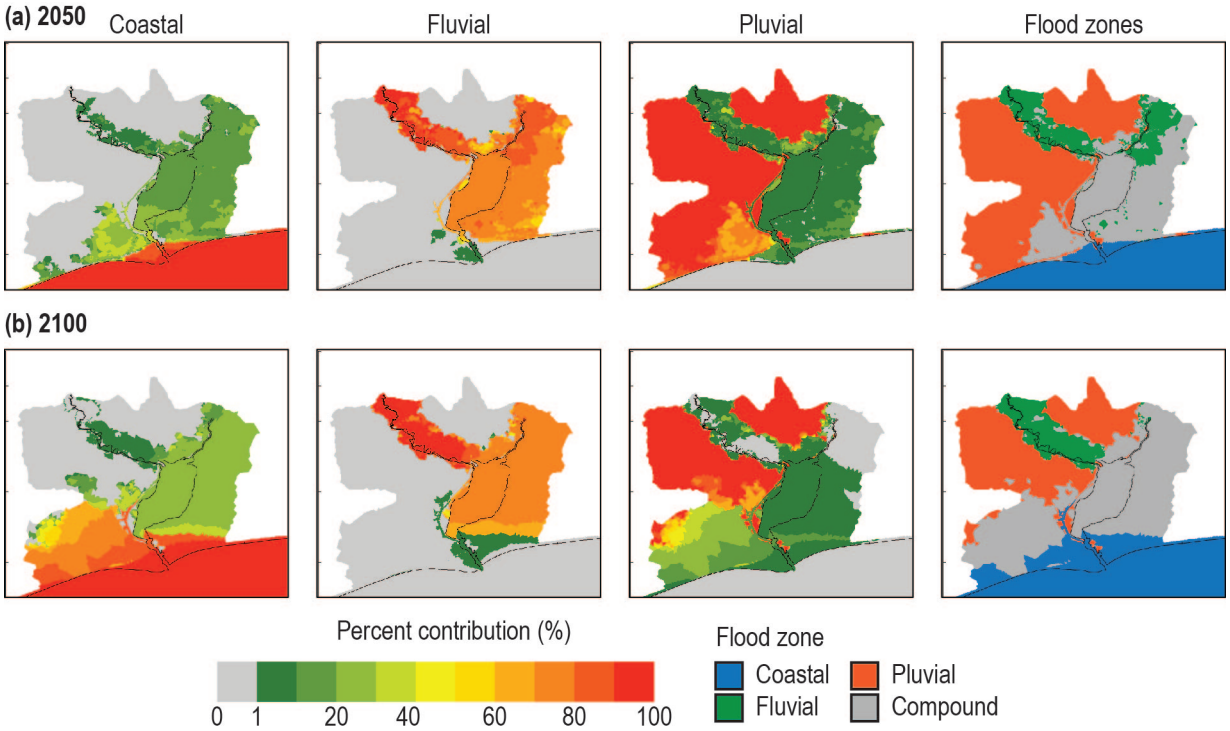

Figure 3.7: Percent contribution of coastal (first column), fluvial (second column), and pluvial (third column) forcing to peak water levels for Hurricane Harvey considering (a) the influence of future sea level rise and rainfall in 2050 and (b) the influence of future sea level rise and rainfall in 2100. The dominant forcing, representing at least 80% of the peak water level, is shown in the fourth column. Areas in blue are dominated by coastal influence, areas in green by fluvial influence, and areas in orange by pluvial influence. Gray areas represent locations where no forcing contributes more than 80% to the peak water levels, suggesting the potential for compound effects.

times, respectively, due to higher flood depths driven by the increased rainfall intensity. Across all scenarios, the pluvial-dominant zone accounts for the majority of impacted structures and damages, as most homes in Jefferson and Orange counties are located outside of the major river floodplains and far enough inland to avoid major impacts due to storm surge.

3.6 Discussion

The water level results along the coastal-estuary-river transect demonstrate nonlinearities due to sea level rise, leading to a decrease in water depth above tide with increasing sea level. This effect is not observed during the storm surge peak on August 29, but begins shortly after and continues through the recession limb of the flood peak. Higher sea levels lead to a reduction in the drainage gradient from upstream to downstream (Figure 3.9) and can create a backwater effect that forces the discharge from upstream to expand into low-lying areas east of Sabine Lake and in the river floodplains, creating an attenuating effect for the flood peak in the waterways. For future rainfall scenarios, the historical drainage gradient increases as sea level remains constant and the river water levels increase. The water depth above tide decreases from upstream to downstream as the estuary width increases in Sabine Lake and water is able to move into adjacent low-lying areas. The

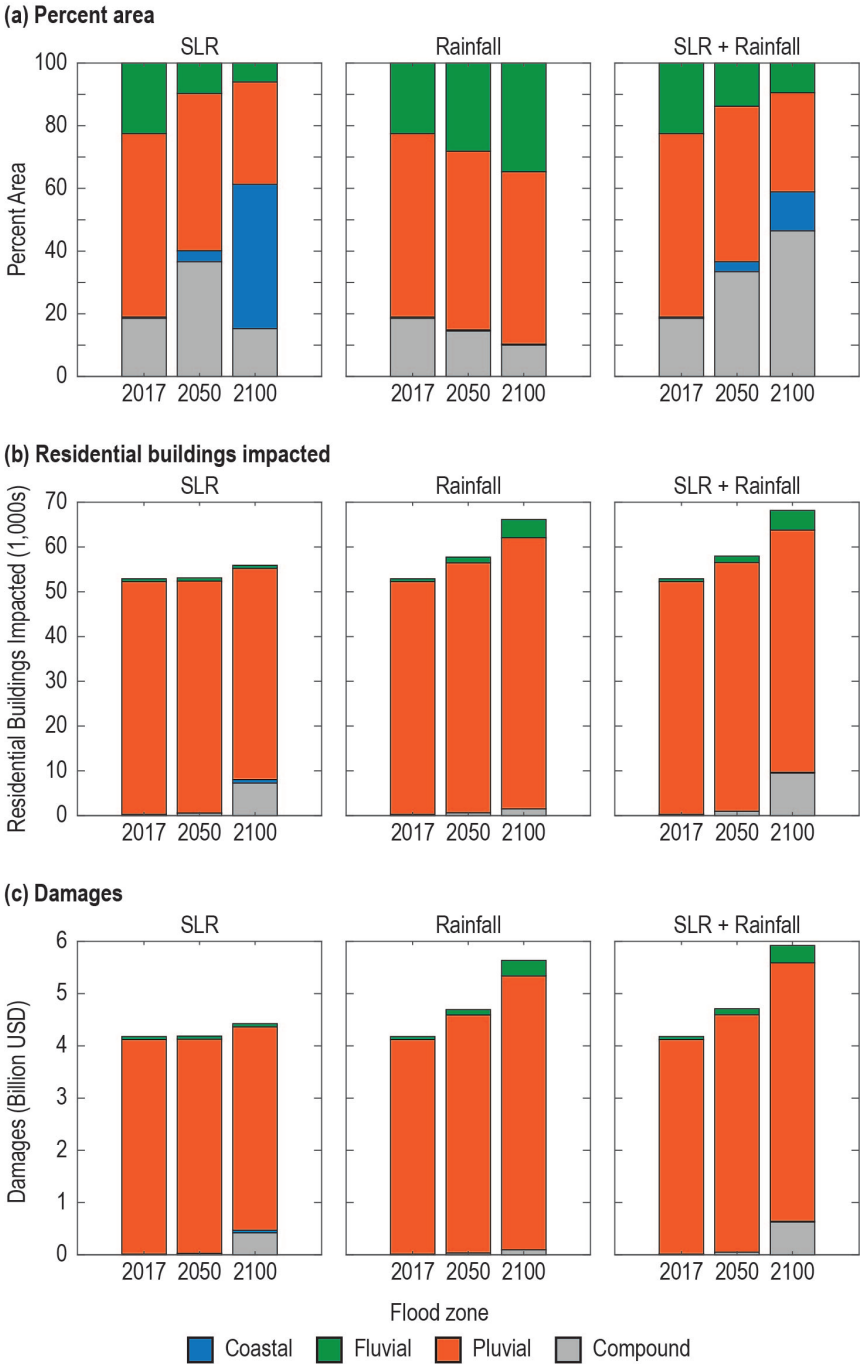

Figure 3.8: (a) Percent of inland study area in each flood zone, (b) number of residential buildings impacted by flooding in each flood zone, and (c) total residential flood damages (building plus contents) in each flood zone for the future sea level rise (left column), future rainfall (middle column), and future sea level rise and rainfall (right column) scenarios.

combined influences of sea level rise and rainfall produce little change in the gradient over the 2017 scenario and generally offset any changes in the water depth above tide across the entire transect. This highlights the importance of conducting detailed modeling studies that include future coastal and rainfall-runoff processes, as simple superposition of tides, surge, sea level rise, and river discharge can neglect nonlinearities and misrepresent potential hazards.

Future sea level rise and rainfall will affect where coastal, fluvial, and pluvial processes

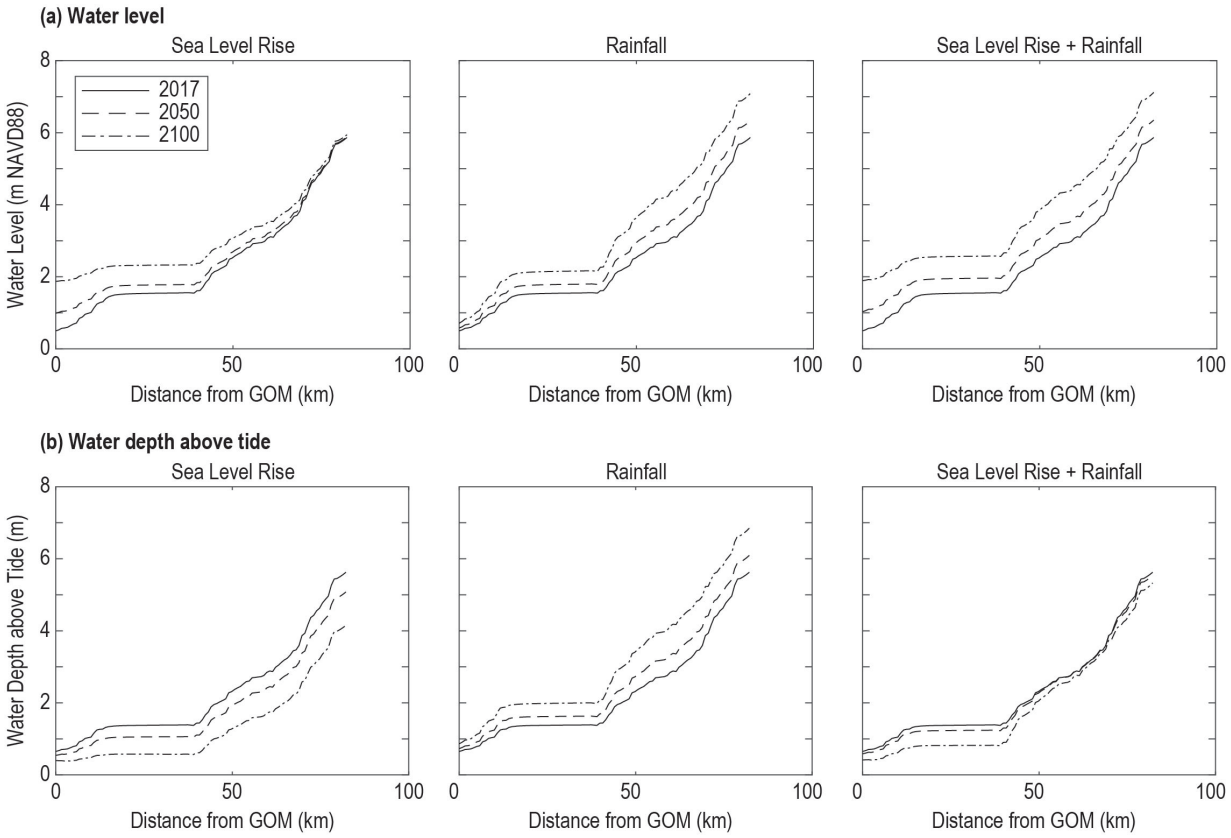

Figure 3.9: Transects of (a) water levels and (b) water depth above tide for the historical condition (2017) and the future conditions (2050 and 2100) with sea level rise and increased rainfall along the coastal-estuary-river continuum shown in Figure 3.1. Water depth above tide is calculated by subtracting the maximum simulated tidal water level at each station from the total water level in the compound forcing scenario. Values shown are extracted at the time of peak discharge at 00:00 on September 4.

are dominant across the SNE and where compound interactions occur. For example, with sea level rise alone, Sabine Lake shifts from fluvial-dominant in 2017 to compound in 2050 to coastal-dominant in 2100. Future rainfall intensity leads to a small expansion of the fluvial-dominant zone across the eastern part of the domain. When both processes are combined, the compound flood zones increases substantially across the domain, from 19% in 2017 to 33% in 2050 to 46% in 2100. Given the distribution of development in the SNE, changes in the location and extent of the coastal, fluvial, and compound zones do not translate into substantial changes in the number of residential properties impacted or associated damages in each zone. The majority of homes are located in the pluvial-dominant zone across all scenarios, although projected sea level rise in 2100 does lead to a noticeable increase in homes in the coastal-dominant and compound zones.

Within each zone, the dominant flood processes can bring unique hazards. Coastal flood zones may experience dangerous storm surge, which can cause excessive horizontal loading and damage to structures. This surge-driven flooding is often short-lived and recedes once the storm passes and winds calm down. Fluvial flood zones may experience longer-duration flooding, particularly in large watersheds where extensive upstream areas are also impacted by hurricane-induced rainfall. Pluvial flood zones experience rapid-onset flooding that can pose a risk to people living outside of FEMA-designated flood zones. In coastal and fluvial zones, the construction of seawalls, levees, or other structures can provide protection

from storm surge and rising river levels. However, in pluvial zones, these structures may exacerbate flooding by limiting runoff to nearby waterways. Flood mitigation planning that accounts for the interactions between coastal, fluvial, and pluvial processes and interactions can help ensure that the selected mitigation approaches comprehensively address all flood drivers without exacerbating individual hazards.

Based on our findings, Orange County and Port Arthur will experience more flooding in the future, which shows the necessity of constructing flood protection structures in these areas. Some infrastructures are already planned to be constructed in these areas. For example, USACE is planning to build a seawall to provide flood protection for Orange County around Sabine River which is in the design phase. Also, there are plans to upgrade the levee that surrounds Port Arthur. The result of our research can help infrastructure managers in the region to understand the source of flooding in future hurricanes in terms of potential risks and how those might change in the timeline of 80 years and guide them with mitigation plans. Coupling the numerical modeling approach with probabilistic assessments of storm characteristics would provide more robust understanding of the likelihood of different flood patterns and could inform more rigorous flood mitigation planning and design.

The results of this study should be interpreted in light of several limitations. For our analysis, we focus on flooding due to Hurricane Harvey, which brought substantial devastation to the SNE. This allows for an understanding of how future changes in tropical cyclone properties could affect the distribution of flood hazards. A more comprehensive assessment of compound flood risk in the SNE would require consideration of a range of storm conditions. Sampling from synthetic storm libraries developed for the region (e.g., [123]) could facilitate such efforts. In addition, although we considered plausible future rainfall scenarios based on the existing literature for Hurricane Harvey, the numerical flood model could be further coupled with a regional earth system model to simulate spatially and temporally variable rainfall changes over the SNE, as outlined in [32].

3.7 Conclusions

In this study, we applied a compound flood model to study the effects of future sea level rise and rainfall on flood hazards associated with Hurricane Harvey in the Sabine-Neches Estuary in Southeast Texas. We used the model to evaluate changes to the flood peak along the coastal-estuary-river continuum and to assess the location and extent of compound flooding across the region. We further coupled the compound flood model with building stock data and depth-damage curves to examine impacts to residential structures caused by the dominant flood processes. Our findings suggest that sea level rise will reduce the water depth above tide in the waterways due to the expansion of flooding in adjacent low-lying areas. Even when future rainfall is considered along with sea level rise, the water depth above tide still decreases across much of the domain except in the river channels. Compound flood models that include future coastal and rainfall-runoff processes can simulate nonlinearities in water level dynamics that cannot be captured through the superposition coastal and watershed processes and future conditions (e.g., sea level rise). Our results also indicate that while compound flood zones expand substantially under future scenarios, the number of residential structures in the compound flood zone does not increase proportionally, as most structures are located in areas that remain pluvial-dominant from 2017 to 2100. This suggests that flood risk messaging should include those living outside designated coastal or riverine flood hazard zones, where flood insurance is

less common despite the potential for substantial damages.

Chapter 4

Effect of Sea Level Rise and Subsidence on Hurricane-induced Flooding

4.1 Abstract

Tropical cyclone (TC) flooding has caused devastation for coastal communities in recent years, leading to loss of life and damage to homes, businesses, and critical infrastructure. The frequency and severity of compound flooding associated with TCs are projected to increase in the future due to sea-level rise (SLR). At the same time, ongoing subsidence due to oil and gas extraction and groundwater withdrawal can affect flow paths and flood severity in coastal regions. Despite these concerns, the extent to which TC-driven compound flooding has been altered in response to historical sea-level rise and subsidence remains uncertain. In this study, we applied a coupled coastal-fluvial-pluvial hydrodynamic model (Delft3D-FM) to assess the impacts of sea-level rise (SLR) and subsidence on compound flooding events during three recent hurricanes (Harvey, Ike, and Rita) in the Sabine-Neches Estuary of Southeast Texas. The results suggest that a decrease in SLR can shift the balance between riverine/rainfall and surge forces during hurricanes. Typically, SLR does not affect the water depth above tide in downstream areas (near shore) but does alter the inundation depth upstream. Generally land level decreases in the study region due to subsidence increases water depth. Linearly superimposing water level contributions from coastal, fluvial, and pluvial sources may either underpredict or overpredict flooding, depending on time and location, and does not produce precise predictions of inundation depth.

4.2 Introduction

Rising sea levels due to climate change present a challenge for communities in coastal bays and estuaries [124, 125]. The Intergovernmental Panel on Climate Change (IPCC) reports an approximate 28 cm increase in sea level over the past century along contiguous US coastlines [102]. Approximately ten million individuals currently reside in US coastal areas [126], suggesting a growing risk to the population as flood hazards increase in magnitude and extent. There is thus a pressing need for comprehensive flood risk analyses that take into account the compounding effects of sea level rise to predict impacts to populations and critical infrastructure systems.

Despite extensive research on flooding, damages, and population impacts due to tropical cyclones, few studies have addressed the impacts of rising sea levels on tropical cyclone-induced compound flood hazards [127, 128]. Many existing studies apply a straightforward linear addition approach when incorporating SLR into predictions of floodwater levels, without accounting for the potential nonlinear effect of SLR on estuarine water levels (e.g., [129, 130]). More advanced studies have applied hydrodynamic modeling approaches to capture nonlinear effects due to changing interactions with the coastline[30]. [30] demonstrated that the bathtub approach overestimates inundation compared to applying SLR using hydrodynamic modeling.

In addition to SLR, subsidence due to oil, gas, and groundwater extraction can substantially heighten the risk and impact of flooding from storms in coastal and estuarine areas [36, 34, 33]. [35] found that overlooking subsidence while applying flood-forcing drivers in flood risk assessment led to a 10% underestimation in flood extent in the Tohoku region. However, data on subsidence in limited in many areas, and there are few studies that quantify the impacts of subsidence on flooding over decades. Using a physics-based model, [37] simulated 117 years of land subsidence triggered by groundwater extraction, leading to aquifer compression. The impact of subsidence was incorporated into a hydraulic model to simulate flooding during Hurricane Harvey in a Houston watershed. Their results indicated a dual impact of subsidence on flooding, encompassing both adverse and advantageous effects. Within our study area, [131] calculated spatially variable rates of subsidence from 0.17 to 12.20 mm per year. Given the potential magnitude and variability in subsidence across coastal regions, it is crucial to account for subsidence in simulation models of compound flooding.

In this chapter, we investigate the impacts of SLR and subsidence on the extent of inundation caused by Hurricanes Rita, Ike, and Harvey, utilizing a compound flood model. We also evaluate the precision of using linear superposition to predict the combined effects of multiple flood drivers. The primary research questions are: 1) How did historical SLR and subsidence from 1920 to the date of the hurricanes affect the flooding experienced in the study region? and 2) What advantage does compound flood modeling provide over a simple linear superposition approach that combines the individual effects of separate flood drivers? Our choice of the three hurricanes is driven by two key factors. First, these events have caused significant flooding and extensive damage to residents, critical infrastructure, and the local economy along the Texas coast over the past two decades. Secondly, these hurricanes exhibit distinct characteristics. Hurricane Ike, for instance, was characterized by a substantial storm surge and minimal rainfall, whereas Hurricane Rita involved a combination of moderate rainfall and storm surge. Hurricane Harvey was marked by extreme rainfall and a relatively minor storm surge.

4.3 Methods

For this study, we focused our modeling on the Sabine-Neches Estuary (SNE) in Southeast Texas (Figure 4.1). We applied a coupled flood model built using the Delft3D hydrodynamic software to model water levels and velocities across the domain during hurricane events. The model was calibrated and validated as explained in [116].

Figure 4.1: Map of the Sabine-Neches Estuary, Texas. Yellow markers show a path from downstream to upstream that results are extracted from

4.3.1 Sea level rise data

To quantify the impact of SLR on observed flooding in the SNE region during hurricanes, we utilized NOAA 8770570 SLR data and determined the change in sea level from 1920 to the time of the hurricane occurrence (0.51 m for Rita, 0.53 m for Ike, and 0.58 m for Harvey) from the SLR trendline ($SL = 0.006\,year - 11.97$). This calculated SLR value was then subtracted from the offshore water level time series in the calibrated model.

Three different scenarios were defined to survey the effect of SLR on historical hurricanes. In the surge scenario, offshore water levels included both tide and surge, collected from NOAA/CERA. Spatially and temporally variable NCAR wind and pressure fields were applied using gridded data. No rainfall or river discharge was included. For the rainfall/riverine scenario, offshore water levels included tides only and were derived from tidal predictions produced by NOAA using 37 tidal constituents. Hourly observed discharges were applied at the upstream extent of the Neches and Sabine Rivers, collected from USGS

and NWM, respectively. Rainfall was applied across the whole domain (MRMS data for Harvey and Stage IV data for Ike and Rita). In the compound scenario, offshore water levels included both tide and surge. Gridded wind, pressure, and rainfall data were applied across the entire domain. Hourly observed discharges were applied at the upstream extent of the Neches and Sabine Rivers.

Table 4.1: Summary of flood scenarios.

Scenario	Offshore WL	Rivers	Rainfall	W/P
Surge	NOAA/CERA WL - SLR	N/A	N/A	NCAR
Riverine/Rainfall	NOAA tide - SLR	USGS/NWM	MRMS/Stage IV	N/A
Compound	NOAA/CERA WL - SLR	USGS/NWM	MRMS/Stage IV	NCAR

4.3.2 Subsidence data

To quantify the impact of subsidence on observed flooding in the SNE region during hurricanes, we subtracted the subsidence that occurred since 1920 from the current bed level, which was primarily measured in 2008, in the hydrodynamic model. Gridded subsidence data with a resolution of 1 km square was obtained from [131] at Lamar University (see Figure 4.2). Vertical change rates (subsidence and uplift) were determined from the oldest National Geodetic Survey (NGS) elevations for almost 340 benchmarks assuming that the elevation published was measured when the benchmark station was monumented. The average rate of subsidence was determined over up to 70 years, depending on when the benchmarks were monumented. Subsidence in Figure 4.2 does not take sea level rise into account, just land subsidence or uplift. This is because of the conversion program used by the NGS to convert the earliest orthometric heights (elevations) and datums to the one used in the survey (NAD83 GEOID09) referenced to the NAVD88 vertical datum. The maximum subsidence in the study region is -1.22 m and the maximum uplift is 0.17 m over the last century.

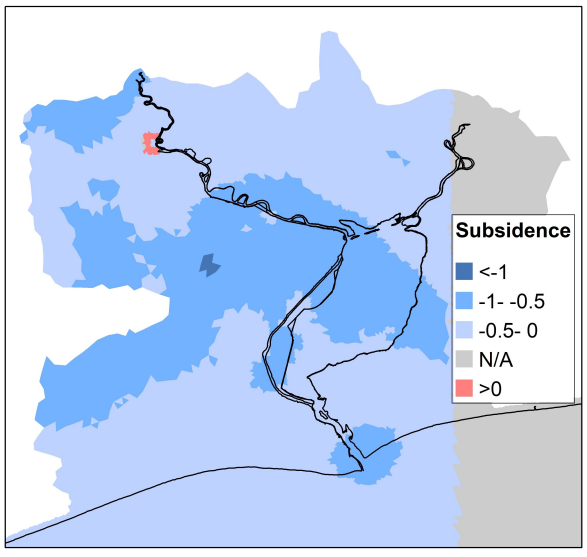

Figure 4.2: Subsidence in meters from 1920 to 2008 (time of bed level data collection)

4.4 Results

4.4.1 Influence of SLR on compound flooding

Figures 4.3 and 4.4 show transects of Harvey water depth above the tide (left column) and water levels (right column) for (a) 1920 without sea level rise and (b) 2017 with sea level rise. The x-axis in these figures shows a coastal-estuary-river continuum starting from downstream of Sabine Pass and ending in the upstream of Neches River shown in Figure 4.1. Water depth above tide is calculated by subtracting the simulated tidal water level at each location from the total water level. Values are extracted at the time of peak surge at 07:00 on August 29 for Figure 4.3, and at the time of peak riverine/rainfall at 07:00 on September 2 for Figure 4.4. For Harvey, in both years under consideration, SLR did not significantly alter the overall inundation patterns of waterways (Figures 4.3 and 4.4). It had a minimal impact on the downstream values while having a more pronounced effect on the upstream values. During the peak of the surge, the water depth above the tide level increased upstream, measuring 3.2 meters in 1920 as opposed to 2.7 meters in 2017 (Figure 4.3). The point where the riverine/rainfall diagram intersects with the surge (S) diagram moved 23 km toward downstream in 1920, indicating that the location where the rainfall/riverine effect is more than the surge effect moved to Sabine Lake upstream, whereas in 2017, it was in the middle of the Neches River. Notably, even at the peak surge, the surge value remained relatively constant throughout the path, yet the rainfall/riverine effect had already commenced to a significant degree at this time and intensified moving upstream. The superposition method overestimated the inundation depth by almost 0.5 meters in both years. Therefore, even for events like Hurricane Harvey, which had a significant rainfall/riverine effect and a minor S effect, compound flooding cannot be disregarded. This is due to some nonlinear interactions in the upstream area. Consequently, modeling flood drivers separately and combining their effects linearly does not yield accurate inundation estimates in the Neches River.

When considering the rainfall/riverine peak, SLR did not influence inundation since the water depth above tide was zero for surge-only simulation in both scenarios (Figure 4.4). However, the rainfall/riverine water depth above tide in the upstream was higher in 1920, measuring 6.8 meters compared to 6.2 meters in 2017. The superposition results coincided with the rainfall/riverine and compound scenarios for both years since the rainfall/riverine effect was dominant and the surge effect was negligible.

For Ike, SLR does not impact the overall trend observed in the diagrams for both years (Figures 4.5 and 4.6). It negligibly affects downstream values while having a more significant effect upstream. During peak surge conditions, the water depth above the tide due to surge decreases from downstream (near the coast) to upstream (Figure 4.5). Rainfall/riverine forcing causes no change in water depth above tide except in the far upstream. Notably, in the far north, a decrease in rainfall/riverine effect is observed, a phenomenon resulting from reverse flow dynamics in the river during Hurricane Ike. This reduction in rainfall/riverine effect does not significantly alter the compound scenario water depth above tide, but it does cause a noticeable decrease in the water depth above tide predicted by the superposition method. Generally, the results of compound flooding are very similar to those of surge alone, with superposition water depth above tide matching compound water depth above tide across the path except in the upstream sections of the Neches River.

At the riverine/rainfall peak, the rainfall/riverine water depth above tide increases towards the upstream, with almost identical values regardless of SLR presence (Figure

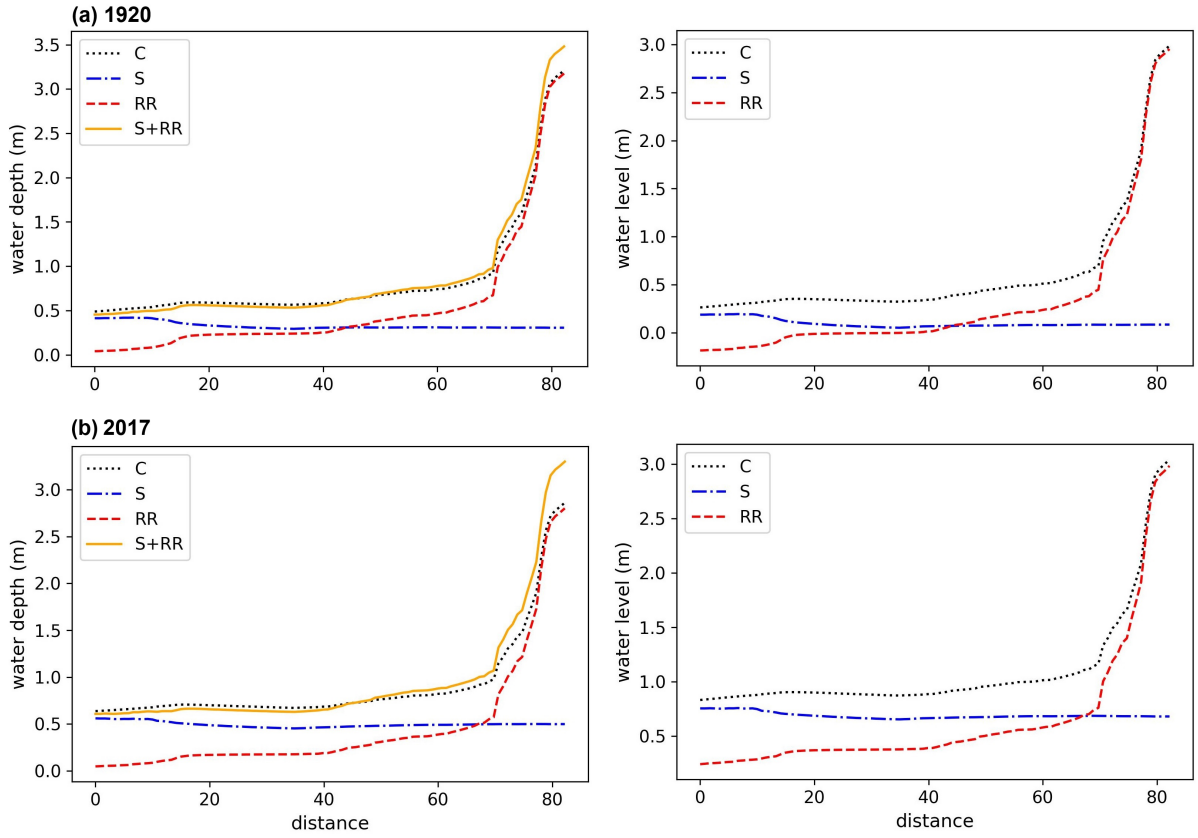

Figure 4.3: Transects of Harvey water depth above the tide (left column) and water levels (right column) for (a) 1920 without sea level rise and (b) 2017 with sea level rise along the coastal-estuary-river continuum (starting from downstream ending in the upstream) shown in Figure 4.1. Water depth above tide is calculated by subtracting the simulated tidal water level at each location from the total water level. Values shown are extracted at the time of peak surge at 07:00 on August 29.

4.6). Rainfall/riverine forcing raises the water depth above tide by approximately 1.2 meters in the extreme upstream end compared to downstream. Interestingly, surge water depth above tide increases upstream, indicating that the effect of the surge has not yet dissipated, and affects the upper watershed even two days after the hurricane passes the SNE region. The values for the compound scenario only align with the surge simulation downstream, but it does not align with either the rainfall/riverine or the surge scenarios in any other areas. Also, the superposition method tends to overestimate water depth above tide, highlighting the importance of modeling the compounding effects of all forces to accurately predict flooding.

For Rita, at the time of the surge peak, water depth above tide and water level are observed to decrease from the downstream areas toward the upstream (Figure 4.7). This is an effect of the surge moving inland from the offshore area. There is a notable increase in water depth above tide in the upstream portions of the Neches River, indicating that the effect of rainfall/riverine forcing had already begun at the upstream location concurrent with the peak of the surge. SLR generally increases water levels for surge, rainfall/riverine, and compound simulation by 0.6 meters, 035 meters, and 0.55 meters downstream, respectively. Upstream, it raises levels by 0.5 meters, 0.2 meters, and 0.4 meters, respectively. During the riverine/rainfall peak, the rainfall/riverine peak is seen to occur six days fol-

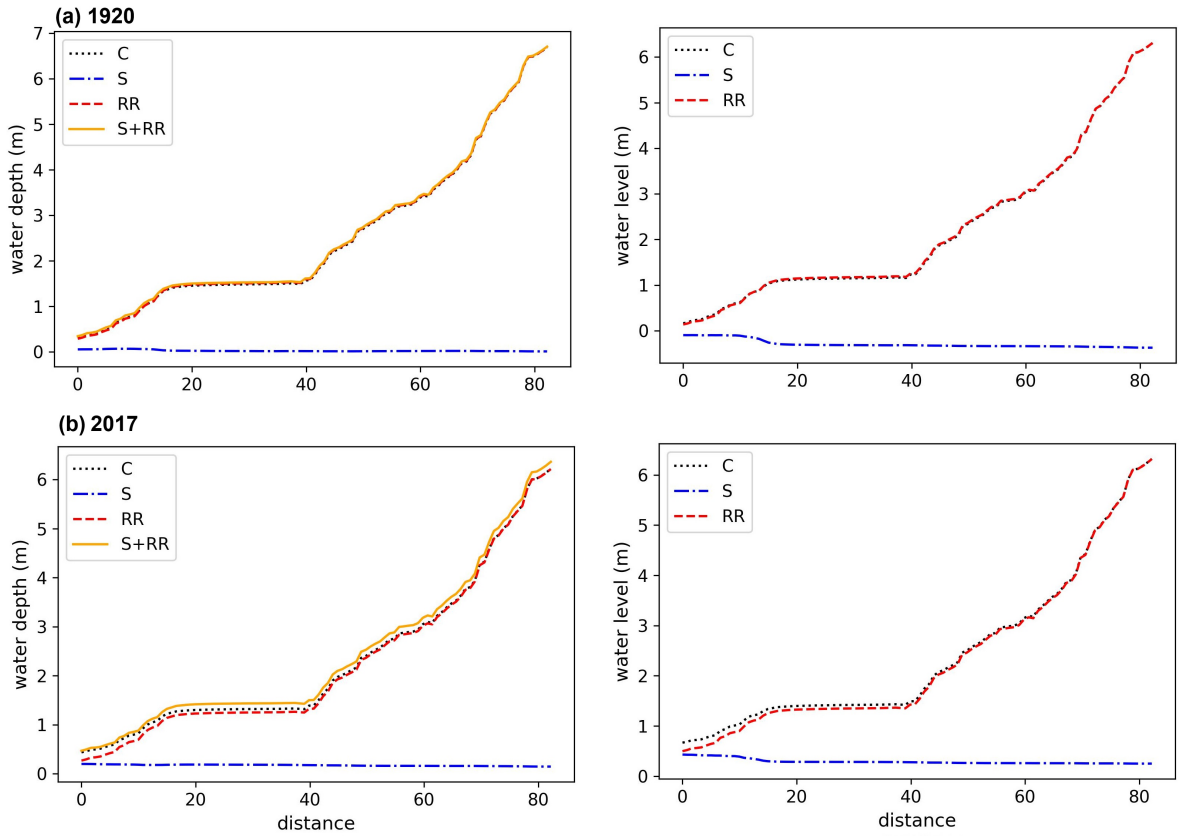

Figure 4.4: Transects of Harvey water depth above the tide (left column) and water levels (right column) for (a) 1920 without sea level rise and (b) 2017 with sea level rise along the coastal-estuary-river continuum (starting from downstream ending in the upstream) shown in Figure 4.1. Water depth above tide is calculated by subtracting the simulated tidal water level at each location from the total water level. Values shown are extracted at the time of peak riverine/rainfall at 07:00 on September 2

lowing Hurricane Rita's transit near the SNE area due to additional rainfall that fell after Rita in the upstream (Figure 4.8). This riverine/rainfall peak results from rainfall events occurring upstream, which contribute to the increased riverine flow and subsequent rise in water levels. SLR typically increases water levels for surge, rainfall/riverine, and compound simulation by 0.5 meters, 0.45 meters, and 0.5 meters downstream, respectively. Upstream, it raises levels by 0.5 meters, 0.1 meters, and 0.25 meters, respectively.

4.4.2 Influence of subsidence on compound flooding

Figure 4.2 illustrates that land levels are predominantly decreasing across the domain. Figure 4.2 shows the transects of Harvey 2017 water level/depth difference (left column) and water levels (right column) at the time of (a) surge peak (07:00 on August 29) and (b) riverine/rainfall peak (07:00 on September 2) along the coastal-estuary-river continuum starting from downstream of Sabine Pass ending in the upstream of Neches River shown in Figure 4.1. During Hurricane Harvey, the water level decreases only slightly due to subsidence, which primarily increases water depth (Figure 4.9). The difference in water depth reflects the extent of subsidence, areas with greater subsidence experience a larger increase in water depth, while areas with less subsidence see a smaller change in water depth. At the time of the surge peak, including the factor of subsidence leads to a reduction

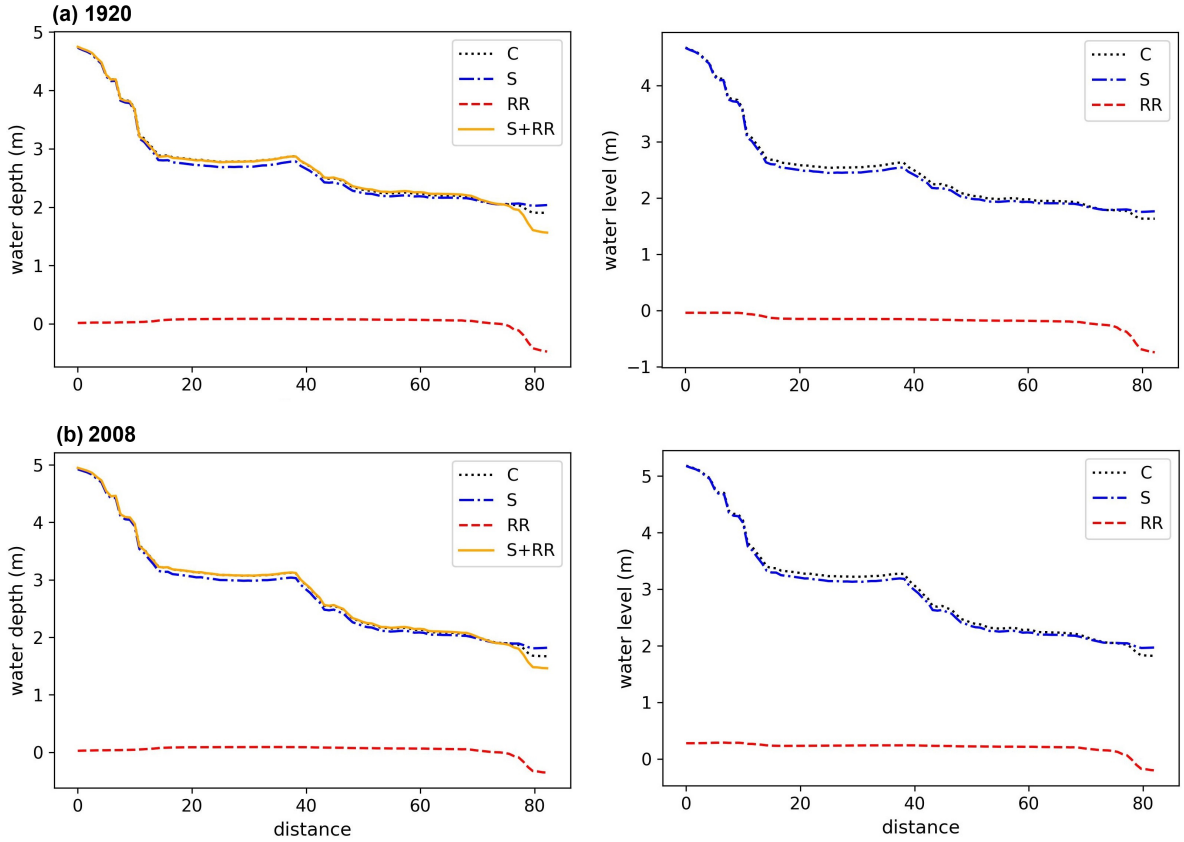

Figure 4.5: Transects of Ike water depth above the tide (left column) and water levels (right column) for (a) 1920 without sea level rise and (b) 2008 with sea level rise along the coastal-estuary-river continuum (starting from downstream ending in the upstream) shown in Figure 4.1. Water depth above tide is calculated by subtracting the simulated tidal water level at each location from the total water level. Values shown are extracted at the time of peak surge at 09:00 on September 13

in water level at the very upstream end. This is likely due to the drainage of water upstream resulting from a decrease in bed level downstream of Neches River and Sabine Lake, which in turn causes more overflow from water bodies in these areas. During the peak of rainfall/riverine, a more significant decrease in water level (up to 40 cm) is observed in the Neches River. This greater decrease is also attributed to higher subsidence levels in Sabine Lake and the downstream portions of the Neches River, which leads to more overflow from these areas, and more drainage of water from waterways into land areas.

For Ike, at the time of the surge peak, water level shows a marked decrease from downstream to upstream starting with a decreasing trend up to downstream of Sabine Lake then water levels move toward zero again. This is a result of a significant offshore surge impacting the area (Figure 4.10). This surge, arriving at SNE from the ocean, coincides with river discharge occurring in reverse which causes a flow from downstream toward upstream. Land subsidence exacerbates the situation, allowing for a higher volume of water to overflow from Sabine Lake, which, in turn, causes water depth to decrease in the waterway. During the peak period of riverine/rainfall, there is a general increase in water level from downstream to upstream, attributed to intense rainfall/riverine forces at the upstream end in both years (Figure 4.10 (b) right panel). At the time of the rainfall/riverine peak, the reverse river flow ceases, and water begins to move from the

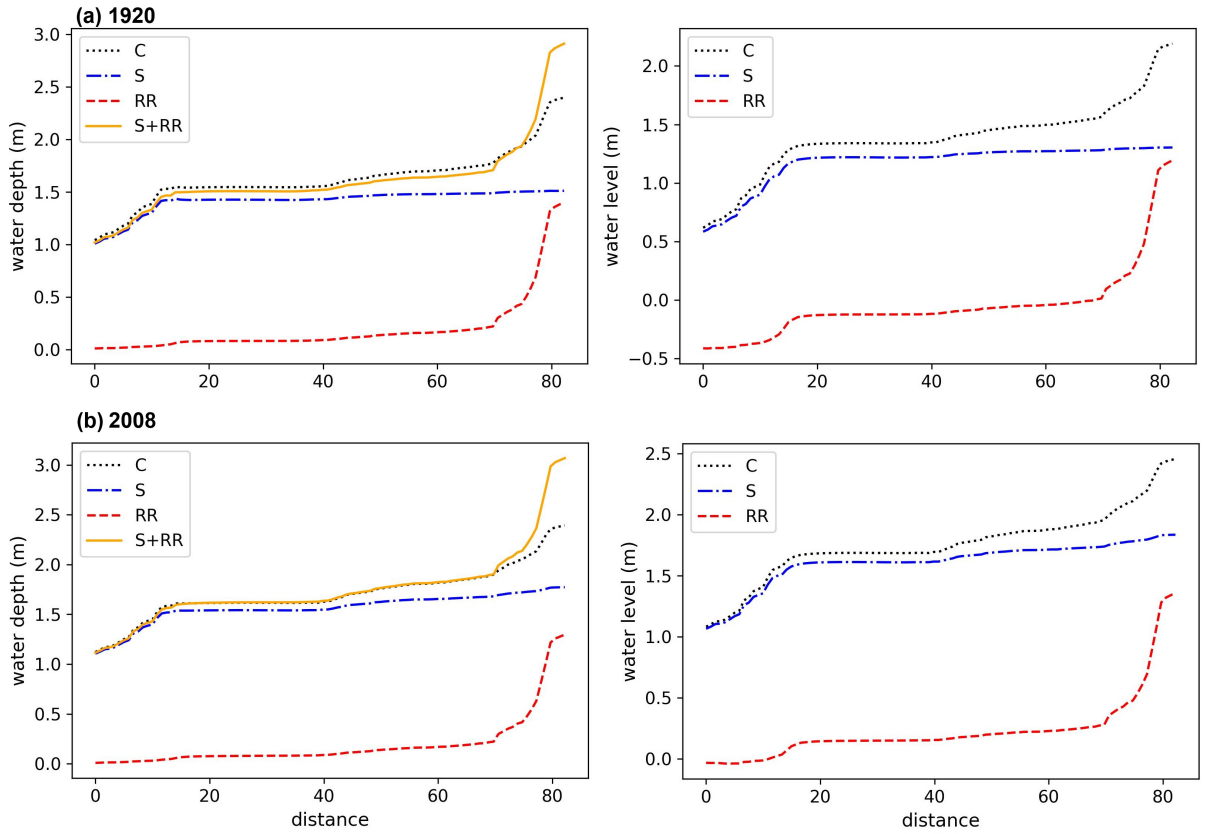

Figure 4.6: Transects of Ike water depth above the tide (left column) and water levels (right column) for (a) 1920 without sea level rise and (b) 2008 with sea level rise along the coastal-estuary-river continuum (starting from downstream ending in the upstream) shown in Figure 4.1. Water depth above tide is calculated by subtracting the simulated tidal water level at each location from the total water level. Values shown are extracted at the time of peak riverine/rainfall at 04:00 on September 15

upper reaches towards the lower reaches of the Neches River. Despite a slight decrease in water level, there is predominantly an increase in water depth (Figure 4.10 (b) left panel). The changes in water depth are reflective of the varying levels of subsidence: greater subsidence corresponds with a more substantial increase in water depth, while lesser subsidence corresponds with a minor change in water depth.

Similar to Hurricane Harvey, for Hurricane Rita, there is a slight decrease in water level, which primarily leads to an increase in water depth (Figure 4.11). During the peak of the surge, water level decreases from the downstream to the upstream areas as a result of the surge coming from the offshore area (Figure 4.11 (a) right panel). However, there is a minor increase in water level in the upstream region of the Neches River, indicating that the effect of rainfall/riverine forcing had already commenced in the upstream at the time of the surge peak. At the time of the riverine/rainfall peak, there is a slight decrease in water level and an increase in water depth (Figure 4.11 (b) left panel). Taking subsidence into account causes a lowering of water levels at the furthest upstream point. This is probably because water drains upstream due to a decrease in the bed level downstream of the Neches River and Sabine Lake, subsequently leading to increased overflow from water bodies in these regions.

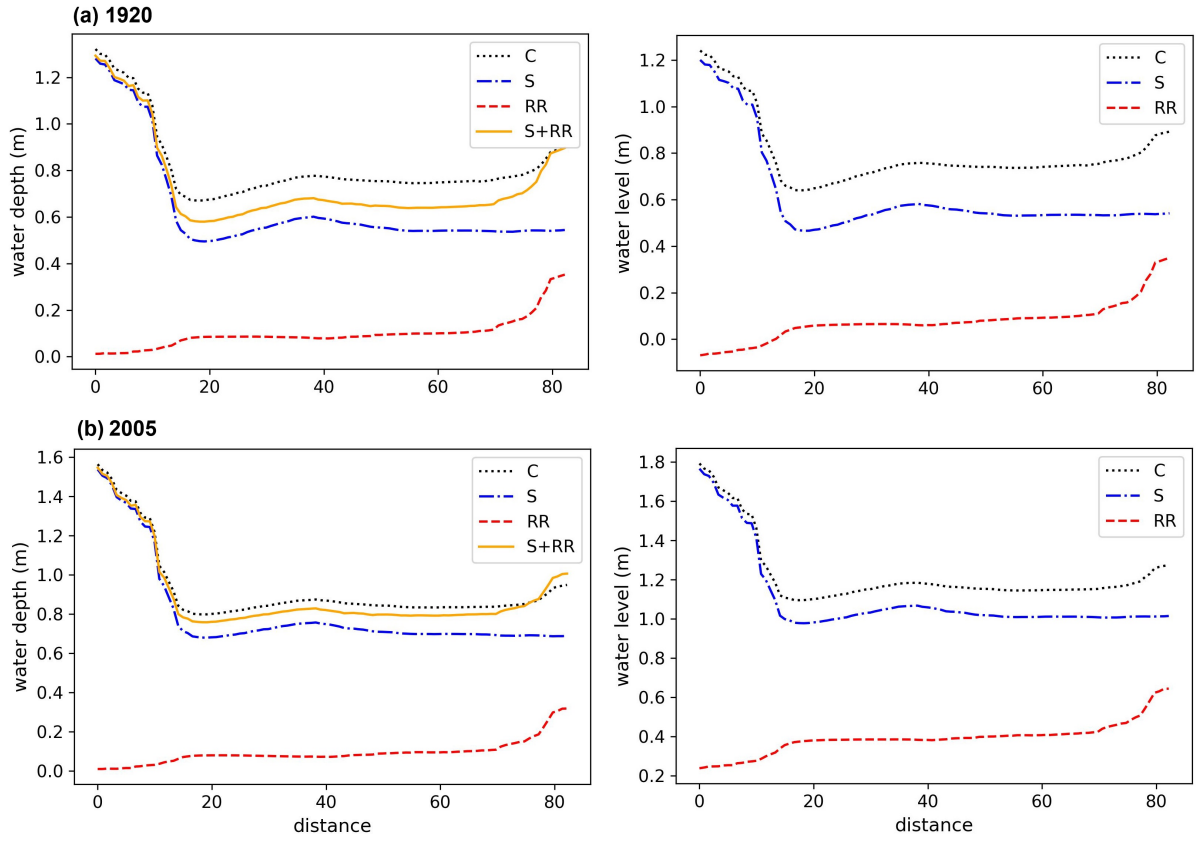

Figure 4.7: Transects of Rita water depth above the tide (left column) and water levels (right column) for (a) 1920 without sea level rise and (b) 2005 with sea level rise along the coastal-estuary-river continuum (starting from downstream ending in the upstream) shown in Figure 4.1. Water depth above tide is calculated by subtracting the simulated tidal water level at each location from the total water level. Values shown are extracted at the time of peak surge at 12:00 on September 24

4.5 Discussion

This research investigates how sea level rise and subsidence influence compound flooding during Hurricanes Harvey, Ike, and Rita. These hurricanes with different natures are known for their devastating impacts over the past two decades. Hurricane Ike brought about a substantial storm surge but minimal rainfall, while Hurricane Rita exhibited a blend of moderate rainfall and storm surge. In contrast, Hurricane Harvey was defined by a large amount of rainfall despite having a relatively minor storm surge.

The exclusion of SLR altered the position where the rainfall/riverine effect surpassed the surge effect, shifting it 23 km downstream from the Neches River to the upstream of Sabine Lake at the peak of the surge for Harvey. However, a similar shift did not occur for Rita and Ike. This difference might be attributed to Harvey's relatively lower surge level compared to Ike and Rita, which is further reduced by excluding SLR. SLR has a low effect on the water depth above tide in downstream areas for Harvey. It also influences Rita's water depth above tide in downstream areas minimally, although it decreases downstream water depth above tide in the surge and compound simulations for Rita.

Generally, SLR causes a nonlinear increase in water level across the entire region. Areas near the coast experience a greater rise in water level due to SLR compared to those upstream of the Neches River. In the case of Hurricane Harvey, during both the peak

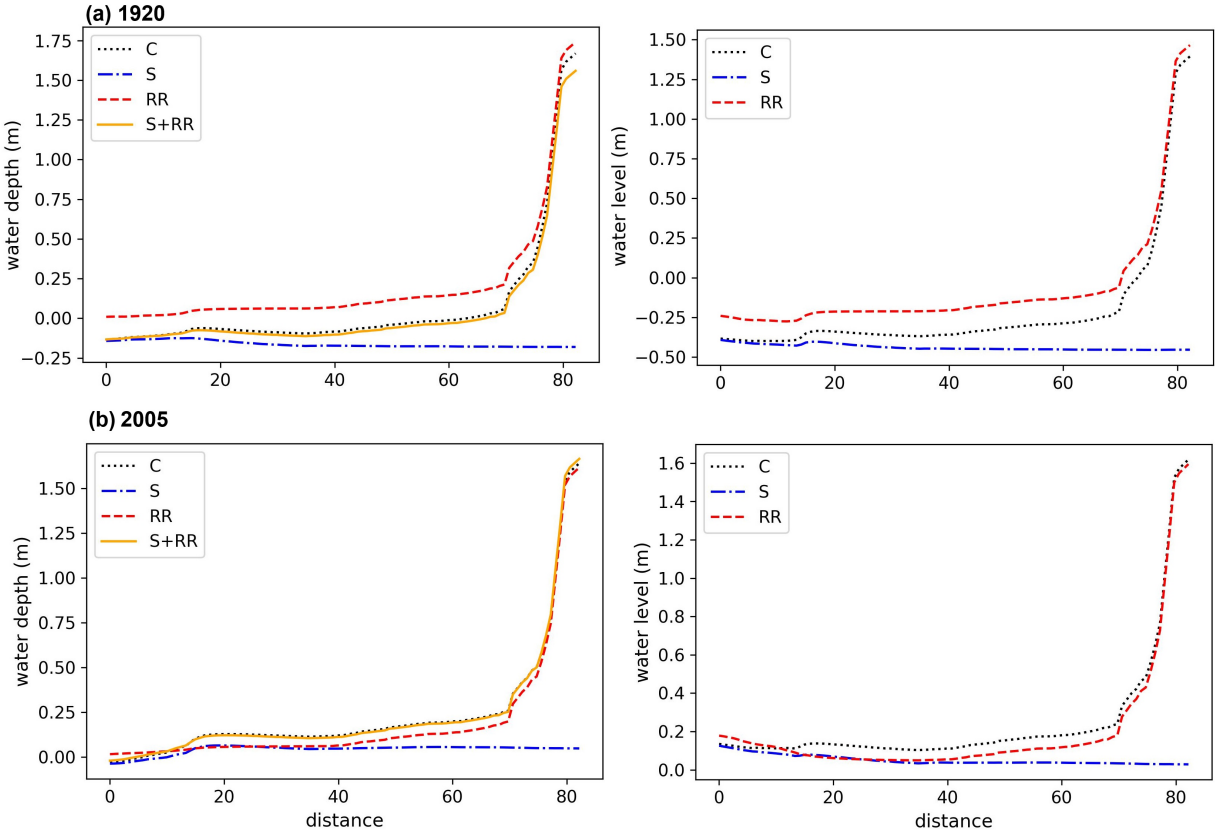

Figure 4.8: Transects of Rita water depth above the tide (left column) and water levels (right column) for (a) 1920 without sea level rise and (b) 2005 with sea level rise along the coastal-estuary-river continuum (starting from downstream ending in the upstream) shown in Figure 4.1. Water depth above tide is calculated by subtracting the simulated tidal water level at each location from the total water level. Values shown are extracted at the time of peak riverine/rainfall at 04:00 on September 30

surge and rainfall/riverine, the combined water level increase due to SLR is 0.5 meters downstream of Sabine Pass and 0.1 meters upstream of Neches River. For Hurricane Ike, SLR raises water level by 0.5 meters downstream and 0.05 meters upstream during the surge peak, while during the rainfall/riverine peak, it increases by 0.5 meters and 0.2 meters, respectively. For Hurricane Rita, SLR leads to a compound water level increase of 0.5 meters downstream and 0.35 meters upstream at the surge peak. During the rainfall/riverine peak, it results in a water level rise of 0.5 meters downstream and 0.25 meters upstream. Overall, the water level rise downstream is nearly consistent for all hurricanes (∼0.5 meters) during both surge and rainfall/riverine peaks. So, hurricanes' nature does not affect the increase in downstream water level due to SLR. The water level increase upstream varies among hurricanes at different times.

Subsidence typically causes a decrease in water levels throughout the region, except in downstream of Sabine Pass where the water level remains unchanged. During Hurricane Harvey, the water level upstream of Neches River drops by 0.25 meters at both surge and rainfall/riverine peak times. For Hurricane Ike, the upstream water level decreases by 0.3 meters and 0.2 meters, respectively. In the case of Hurricane Rita, there is a consistent decrease of 0.1 meters at both peak times. The rate of decrease in upstream water level due to subsidence doesn't seem to be connected to hurricane nature and it should be more

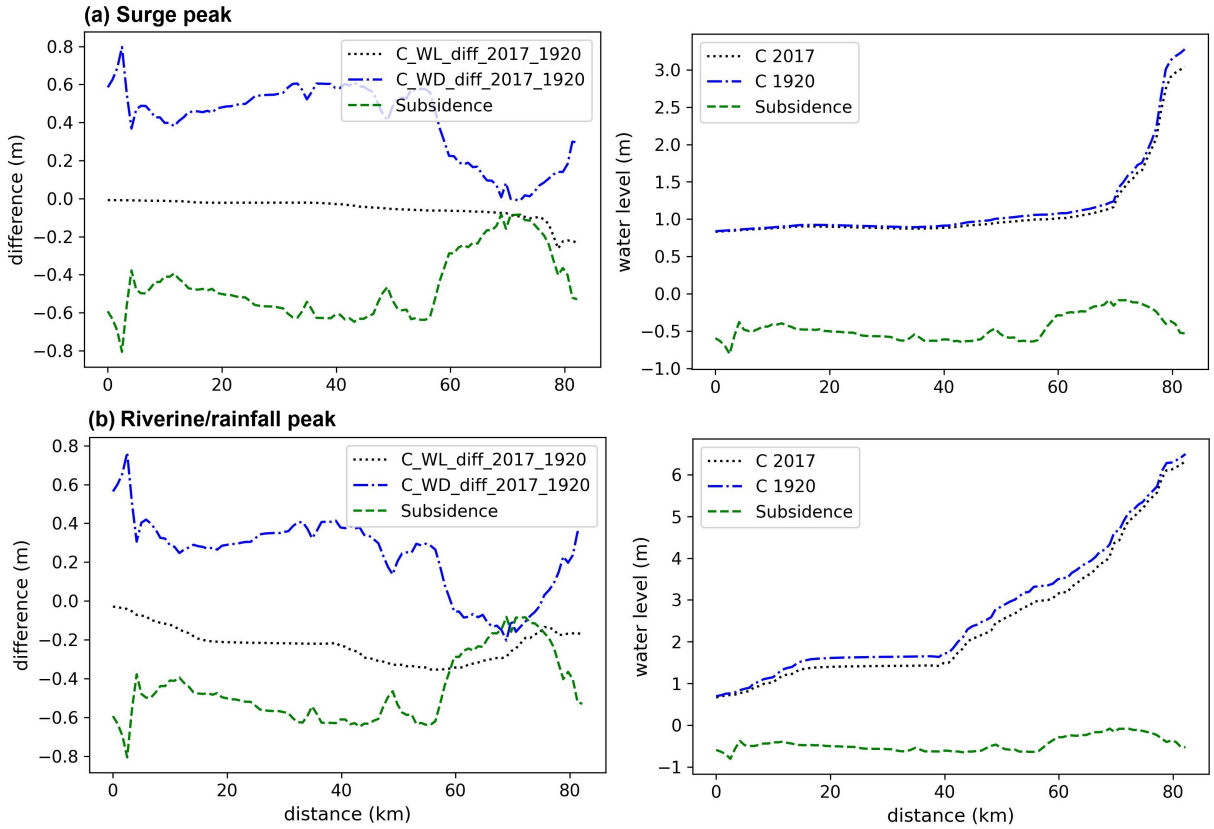

Figure 4.9: Transects of Harvey 2017 water level/depth difference (left column) and water levels (right column) at the time of (a) surge peak (07:00 on August 29) and (b) riverine/rainfall peak (07:00 on September 2) along the coastal-estuary-river continuum (starting from downstream, ending in the upstream) shown in Figure 4.1. On the left panel, the black line displays the water level change, and the blue line shows the water depth change. On the right panel, the black line represents the water level in 2017, and the blue line illustrates the water level in 1920. The green line indicates a delta change in bed level.

related to the change in the flow of water in the downstream areas.

At the rainfall/riverine peak time during Hurricane Harvey, the most significant decrease in water level occurs in the upstream section of Sabine Lake (0.4 meters). This is attributed to the notably high subsidence rates in this area, leading to water overflow from waterways to land areas. Additionally, during Ike at the surge peak time, the most substantial reduction in water level happens in the downstream section of Sabine Lake, with a reduction of 0.75 meters. This is primarily caused by reverse water flow in the Neches River and the high subsidence rates in Sabine Lake, Sabine Pass, and the downstream section of the Neches River, resulting in increased overflow and drainage into land areas. In other scenarios and peak times, the most significant decrease in water level occurs in the upstream section of the Neches River due to high subsidence in downstream.

Subsidence does not influence the water level downstream of Sabine Pass, whereas SLR leads to a decrease of approximately 0.5 meters in water levels downstream. This is mainly due to the relatively minimal subsidence rate in offshore areas, while SLR has a profound impact on offshore water levels. SLR maintains the general water level trend, but subsidence alters it significantly. This distinction emerges because the most substantial

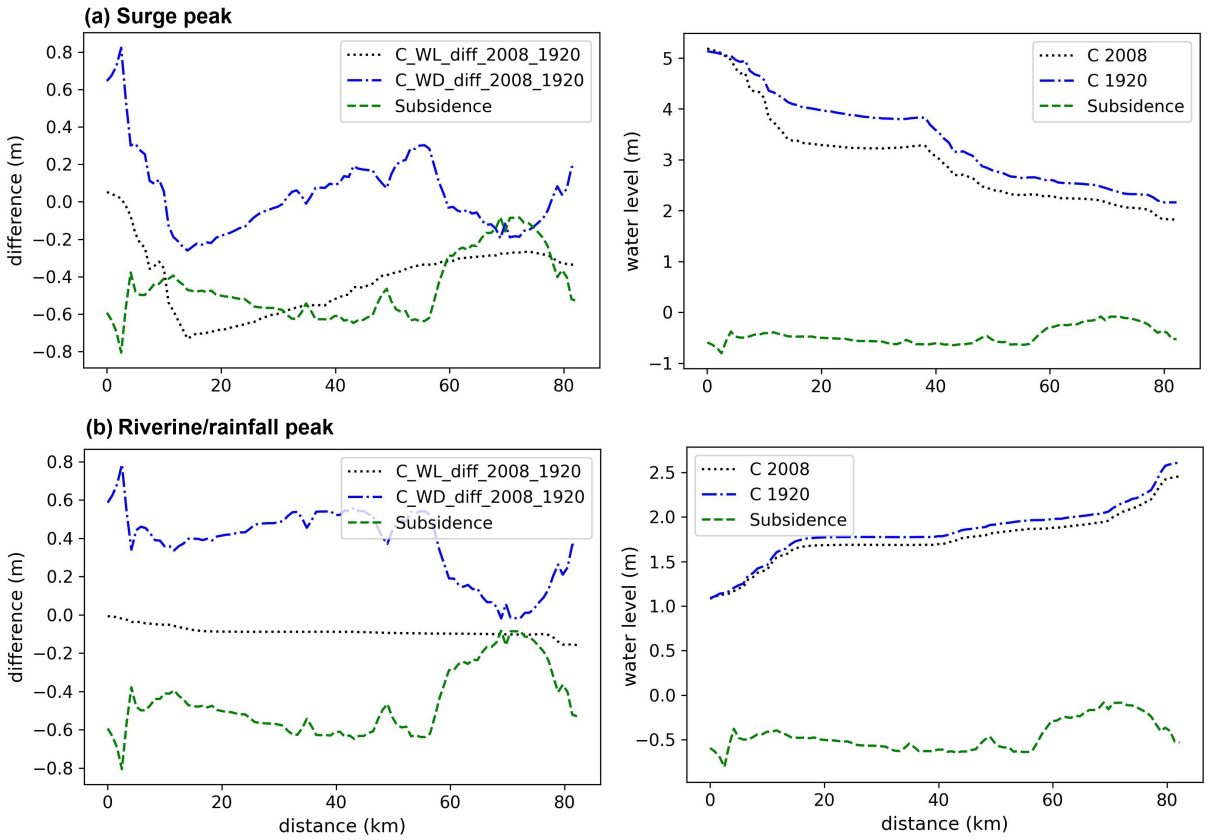

Figure 4.10: Transects of Ike 2008 water level/depth difference (left column) and water levels (right column) at the time of (a) surge peak (09:00 on September 13) and (b) riverine/rainfall peak (04:00 on September 15) along the coastal-estuary-river continuum (starting from downstream, ending in the upstream) shown in Figure 4.1. On the left panel, the black line displays the water level change, and the blue line shows the water depth change. On the right panel, the black line represents the water level in 2008, and the blue line illustrates the water level in 1920. The green line indicates a delta change in bed level.

subsidence occurs in the central region of the study area, whereas SLR affects offshore water levels downstream. SLR leads to increased water levels, ranging from 0.05 meters to 0.5 meters, whereas subsidence decreases water levels by up to 0.75 meters.

4.6 Conclusion

In this chapter, we have examined the impacts of sea level rise and land subsidence over the past century on the inundation patterns of three historical hurricanes: Rita, Ike, and Harvey. We also evaluated the precision of using linear superposition to predict the combined effects of multiple flood drivers. Our findings indicate that there are no consistent patterns to the accuracy of linear superposition, as it can both overestimate and underestimate actual inundation. For example, in the case of Ike, the superposition underestimates the water depth by 0.4 meters at the time of the peak surge and overestimates it by 1 meter at the time of the rainfall/riverine peak. This inconsistency underscores the necessity of considering compound flooding in hydrodynamic models by integrating all relevant forces simultaneously to achieve spatiotemporal accuracy.

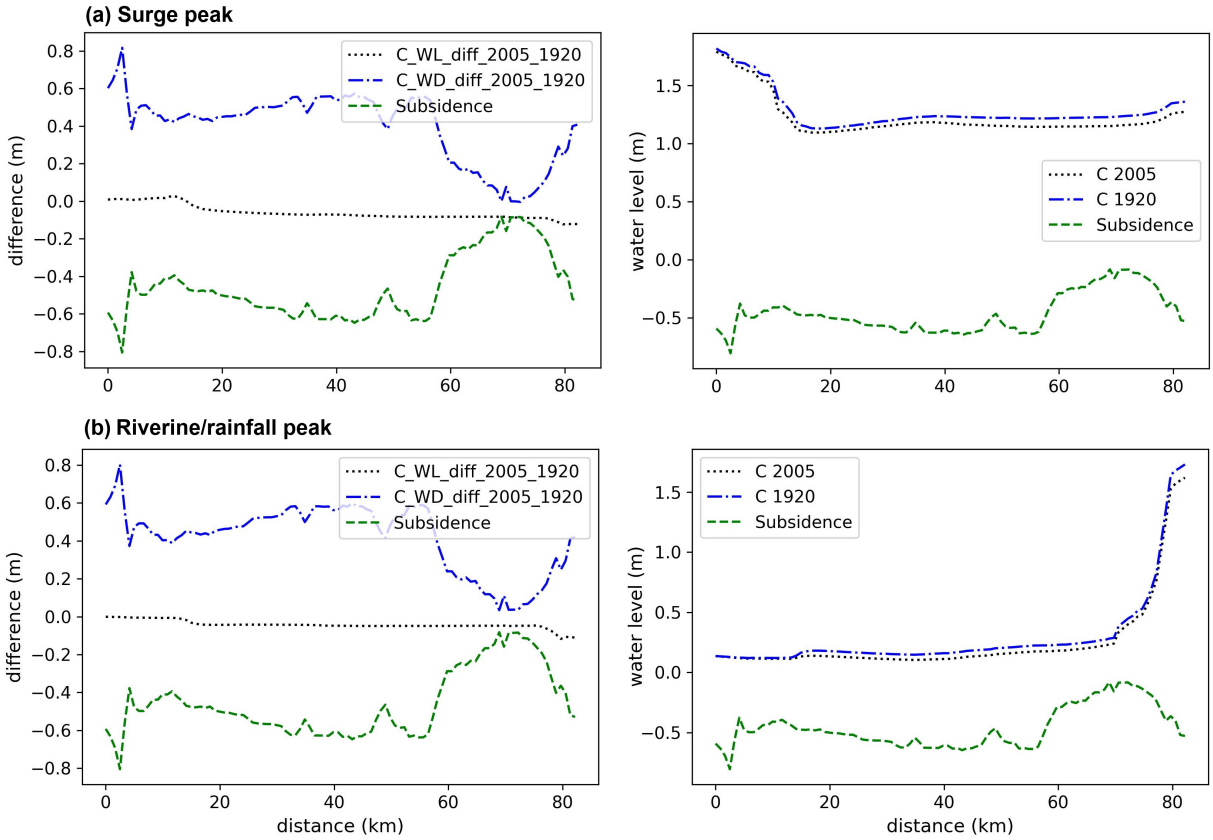

Figure 4.11: Transects of Rita 2005 water level/depth difference (left column) and water levels (right column) at the time of (a) surge peak (12:00 on September 24) and (b) riverine/rainfall peak (04:00 on September 30) along the coastal-estuary-river continuum (starting from downstream, ending in the upstream) shown in Figure 4.1. On the left panel, the black line displays the water level change, and the blue line shows the water depth change. On the right panel, the black line represents the water level in 2005, and the blue line illustrates the water level in 1920. The green line indicates a delta change in bed level.

SLR generally has a minimal impact on downstream water depth above the tide for Harvey. It is also the case for Ike while SLR decreases the downstream water depth above tide for Rita. SLR does not significantly alter the overall trends observed in the data. However, it may increase the water depth above tide or water level slightly in the upstream areas. Notably, SLR can alter the dynamics between riverine/rainfall and surge forces during hurricanes, especially evident in cases like Hurricane Harvey, where fluvial and pluvial forces are pronounced. For Hurricane Harvey, characterized by strong rainfall influence, the effects of riverine/rainfall were already visible upstream at the time of surge peak. It was also the case for Hurricane Rita with moderate rainfall. In contrast, during Hurricane Ike, which was marked by a significant surge, the surge impact maintained its presence in the mid to upper watershed regions even at the rainfall/riverine peak, which occurred two days after Ike had passed SNE. By this point, the impact of the surge was substantially diminished for both Harvey and Rita.

Generally, subsidence in the SNE results in a decrease in land levels over the century. Interestingly, subsidence minimally decreases the water level, which leads to an increase in water depth. Water depth mirrors subsidence; where subsidence is high, the increase

in water depth above tide is significant, and vice versa. The only exception is Hurricane Ike, which experienced a drastic decrease in water levels at the time of the surge peak in waterways, and the water depth decreased at that time as well. This is mainly rooted in the high surge from the coast, the reverse flow occurring in the Neches River, and the significant subsidence in Sabine Lake and the Neches River downstream, which lead to a substantial overflow of water from waterways in these areas.

In this analysis, we considered the SLR and subsidence impact due to extreme storm events. However, it is also important to understand how subsidence and SLR could affect less intense, more frequent flooding within the region as well, as there could be different patterns in the flow, water level, and depth. Subsidence data was collected and measured at two points in time, which introduces some uncertainty to the model. This limits our ability to project time-varying rates of subsidence, which may not be constant over the last century.

Chapter 5

Conclusion

For the analyses presented in this dissertation, a coupled flood model was developed to simulate compound flooding events in the Sabine Neches Estuary (SNE) in Southeast Texas during three historical hurricane events (Harvey, Ike, and Rita). We applied fluvial, pluvial, and surge forces separately and simultaneously to observe their effects on compound flooding.

In Chapter 2, we highlighted the significance of understanding the spatial and temporal interaction between coastal, fluvial, and pluvial forcing during hurricanes characterized by multiple interacting flood drivers, such as surge, river discharge, and rainfall. Depending on the storm's characteristics, various types of compound flooding can persist over an extended period. For instance, Hurricane Harvey generated several forms of compound flooding (pluvial-fluvial, coastal-pluvial, coastal-fluvial, and coastal-pluvial-fluvial), each occurring at different times and locations within the domain. Consequently, even after the initial flood hazard subsides, additional flooding may endure for days or weeks after landfall, influencing response and recovery efforts. While the coastal-only model adequately predicts water levels during storms like Ike and Rita, characterized by short periods of rainfall and extreme surges, it falls short in areas where multiple forces contribute to peak water levels for both storms. Our results also highlight the vulnerability of critical water and wastewater infrastructure in SNE to multiple flood drivers, necessitating holistic adaptation approaches to address flood hazards comprehensively. These findings emphasize the importance of adopting a compound model framework for coastal flood hazard assessments.

In Chapter 3, we incorporated future projections of SLR and rainfall data into the compound flood model to analyze the future flood hazards stemming from Hurricane Harvey in the SNE region. Furthermore, we combined the compound flood model with detailed information on building stock and depth-damage curves, enabling a thorough examination of the impact on residential structures caused by the predominant flood processes. Compound flood models that incorporate future coastal and rainfall-runoff processes can simulate nonlinearities in water level dynamics that cannot be captured solely through the overlay of flood drivers, especially under future conditions such as sea level rise. The findings reveal that sea level rise reduces the water depth above tide in the waterways, primarily due to the overflow of flooding into adjacent low-lying areas. This phenomenon persists even when combining sea level rise and rainfall in the model. Furthermore, our results suggest that while compound flood zones expand significantly in future scenarios, the number of residential structures within these zones does not increase proportionally. This discrepancy arises because most structures are situated in areas that remain predominantly affected by rainfall-related flooding from 2017 to 2100. Findings from this work

can inform efforts to develop appropriate flood mitigation and adaptation plans for communities and critical infrastructure systems that address multiple types of flooding and are robust under future conditions.

In Chapter 4, we examined the impact of SLR and land subsidence over the past century on the inundation depth during historical hurricanes. SLR doesn't notably affect the water depth downstream above the tide for hurricanes Harvey and Ike. However, it decreases downstream water depth for Hurricane Rita. SLR does not significantly change the overall trends observed in the data. Yet, there might be a slight increase in water depth or level in the upstream regions due to SLR. Omitting the effect of SLR could alter the interplay between riverine/rainfall and surge forces during hurricanes, as observed in the case of Hurricane Harvey. Over the past century, land levels have typically decreased. This decrease typically does not significantly affect water levels but leads to increased water depths. An exception to this trend occurred during the peak surge time for Hurricane Ike when both water level and depth decreased mainly due to reverse flow in the Neches River and increased overflow from Sabine Lake. Consequently, subsidence substantially elevates inundation depth and can alter the flow dynamics of water bodies (e.g., by causing increased overflow into adjacent low-lying areas). This issue is important and should be considered in both infrastructure design and modeling. Additionally, comprehensive contingency and mitigation plans are needed, along with enhanced monitoring of subsidence to track ongoing changes topography. Effectively managing and mitigating the consequences of SLR and subsidence can reduce future impacts and damages.

Bibliography

[1] Dartmouth Flood Observatory. (2019) DFO Flood Event: 2019-USA-4797. [Online]. Available: http://floodobservatory.colorado.edu/Events/4797/2019USA4797.html

[2] U.S. Geological Survey. (2022) Flood Event Viewer. [Online]. Available: https://stn.wim.usgs.gov/FEV/2017Harvey

[3] M. V. Bilskie and S. Hagen, "Defining flood zone transitions in low-gradient coastal regions," *Geophysical Research Letters*, vol. 45, no. 6, pp. 2761–2770, 2018.

[4] National Oceanic and Atmospheric Administration. (2022) Billion-dollar weather and climate disasters. [Online]. Available: https://www.ncdc.noaa.gov/billions/summary-statstemporal-comparison-div

[5] D. J. Wuebbles, D. W. Fahey, and K. A. Hibbard, "Climate Science Special Report: Fourth National Climate Assessment Volume I," Tech. Rep., 2017.

[6] J. Hinkel, D. Lincke, A. T. Vafeidis, M. Perrette, R. J. Nicholls, R. S. Tol, B. Marzeion, X. Fettweis, C. Ionescu, and A. Levermann, "Coastal flood damage and adaptation costs under 21st century sea-level rise," *Proceedings of the National Academy of Sciences*, vol. 111, no. 9, pp. 3292–3297, 2014.

[7] J. Zscheischler, S. Westra, B. J. Van Den Hurk, S. I. Seneviratne, P. J. Ward, A. Pitman, A. Aghakouchak, D. N. Bresch, M. Leonard, T. Wahl, and X. Zhang, "Future climate risk from compound events," *Nature Climate Change*, vol. 8, no. 6, pp. 469–477, 2018. [Online]. Available: http://dx.doi.org/10.1038/s41558-018-0156-3

[8] M. V. Bilskie, H. Zhao, D. Resio, J. Atkinson, Z. Cobell, and S. C. Hagen, "Enhancing flood hazard assessments in coastal Louisiana through coupled hydrologic and surge processes," *Frontiers in Water*, vol. 3, p. 609231, 2021.

[9] M. Loveland, A. Kiaghadi, C. N. Dawson, H. S. Rifai, S. Misra, H. Mosser, and A. Parola, "Developing a modeling framework to simulate compound flooding: When storm surge interacts with riverine flow," *Frontiers in Climate*, vol. 2, p. 609610, 2021.

[10] K. Kumbier, R. C. Carvalho, A. T. Vafeidis, and C. D. Woodroffe, "Investigating compound flooding in an estuary using hydrodynamic modelling: a case study from the Shoalhaven River, Australia," *Natural Hazards and Earth System Sciences*, vol. 18, no. 2, pp. 463–477, 2018.

[11] F. L. Santiago-Collazo, M. V. Bilskie, P. Bacopoulos, and S. C. Hagen, "An examination of compound flood hazard zones for past, present, and future low-gradient coastal land-margins," *Frontiers in Climate*, vol. 3, p. 684035, 2021.

[12] W. V. Sweet and J. Park, "From the extreme to the mean: Acceleration and tipping points of coastal inundation from sea level rise," *Earth's Future*, vol. 2, no. 12, pp. 579–600, 2014. [Online]. Available: http://doi.wiley.com/10.1002/2014EF000272

[13] K. Naseri and M. Hummel, "A Bayesian Copula-Based Nonstationary Framework for Compound Flood Risk Assessment along US Coastlines," *Journal of Hydrology*, p. 128005, 2022.

[14] K. E. Trenberth, L. Cheng, P. Jacobs, Y. Zhang, and J. Fasullo, "Hurricane Harvey Links to Ocean Heat Content and Climate Change Adaptation," *Earth's Future*, vol. 6, no. 5, pp. 730–744, 2018.

[15] K. Emanuel, "Assessing the present and future probability of Hurricane Harvey's rainfall," *Proceedings of the National Academy of Sciences of the United States of America*, vol. 114, no. 48, pp. 12 681–12 684, 2017.

[16] ——, "Increasing destructiveness of tropical cyclones over the past 30 years," *Nature*, vol. 436, no. 7051, pp. 686–688, 2005.

[17] ——, "Downscaling CMIP5 climate models shows increased tropical cyclone activity over the 21st century," *Proceedings of the National Academy of Sciences of the United States of America*, vol. 110, no. 30, pp. 12 219–12 224, 2013.

[18] A. H. Sobel, S. J. Camargo, T. M. Hall, C.-y. Lee, M. K. Tippett, and A. a. Wing, "Human Influence on Tropical Cyclone Intensity," *Science*, vol. 353, no. 6296, 2016.

[19] L. Herdman, L. Erikson, and P. Barnard, "Storm surge propagation and flooding in small tidal rivers during events of mixed coastal and fluvial influence," *Journal of Marine Science and Engineering*, vol. 6, no. 4, p. 158, 2018.

[20] Z. Xiao, Z. Yang, T. Wang, N. Sun, M. Wigmosta, and D. Judi, "Characterizing the non-linear interactions between tide, storm surge, and river flow in the Delaware Bay Estuary, United States," *Front. Mar. Sci.*, vol. 8, p. 715557, 2021.

[21] A. Gori, N. Lin, and J. Smith, "Assessing Compound Flooding From Landfalling Tropical Cyclones on the North Carolina Coast," *Water Resources Research*, vol. 56, no. 4, 2020.

[22] F. Ye, W. Huang, Y. J. Zhang, S. Moghimi, E. Myers, S. Pe'eri, and H. C. Yu, "A cross-scale study for compound flooding processes during Hurricane Florence," *Natural Hazards and Earth System Sciences*, vol. 21, no. 6, pp. 1703–1719, 2021.

[23] A. Gori, N. Lin, and D. Xi, "Tropical cyclone compound flood hazard assessment: From investigating drivers to quantifying extreme water levels," *Earth's Future*, vol. 8, no. 12, p. e2020EF001660, 2020.

[24] M. A. Abdelhafez, B. Ellingwood, and H. Mahmoud, "Vulnerability of seaports to hurricanes and sea level rise in a changing climate: A case study for mobile, al," *Coastal Engineering*, vol. 167, p. 103884, 2021.

[25] Y. Wang and R. Marsooli, "Dynamic modeling of sea-level rise impact on coastal flood hazard and vulnerability in new york city's built environment," *Coastal engineering*, vol. 169, p. 103980, 2021.

[26] D. L. Passeri, M. V. Bilskie, N. G. Plant, J. W. Long, and S. C. Hagen, "Dynamic modeling of barrier island response to hurricane storm surge under future sea level rise," *Climatic Change*, vol. 149, no. 3, pp. 413–425, 2018.

[27] M. Bilskie, S. Hagen, S. Medeiros, and D. Passeri, "Dynamics of sea level rise and coastal flooding on a changing landscape," *Geophysical Research Letters*, vol. 41, no. 3, pp. 927–934, 2014.

[28] M. E. Mousavi, J. L. Irish, A. E. Frey, F. Olivera, and B. L. Edge, "Global warming and hurricanes: the potential impact of hurricane intensification and sea level rise on coastal flooding," *Climatic Change*, vol. 104, no. 3, pp. 575–597, 2011.

[29] B. H. Strauss, P. M. Orton, K. Bittermann, M. K. Buchanan, D. M. Gilford, R. E. Kopp, S. Kulp, C. Massey, H. d. Moel, and S. Vinogradov, "Economic damages from hurricane sandy attributable to sea level rise caused by anthropogenic climate change," *Nature communications*, vol. 12, no. 1, pp. 1–9, 2021.

[30] L. Castrucci and N. Tahvildari, "Modeling the impacts of sea level rise on storm surge inundation in flood-prone urban areas of hampton roads, virginia," *Marine Technology Society Journal*, vol. 52, no. 2, 2018.

[31] F. Silveira, C. L. Lopes, J. P. Pinheiro, H. Pereira, and J. M. Dias, "Coastal floods induced by mean sea level rise—ecological and socioeconomic impacts on a mesotidal lagoon," *Journal of Marine Science and Engineering*, vol. 9, no. 12, p. 1430, 2021.

[32] X. Li, D. Fu, J. Nielsen-Gammon, S. Gangrade, S.-C. Kao, P. Chang, M. M. Hernández, N. Voisin, Z. Zhang, and H. Gao, "Impacts of climate change on future hurricane induced rainfall and flooding in a coastal watershed: A case study on hurricane harvey," *Journal of Hydrology*, vol. 616, p. 128774, 2023.

[33] D. P. Viero, G. Roder, B. Matticchio, A. Defina, and P. Tarolli, "Floods, landscape modifications and population dynamics in anthropogenic coastal lowlands: The polesine (northern italy) case study," *Science of the Total Environment*, vol. 651, pp. 1435–1450, 2019.

[34] S. Hanson, R. Nicholls, N. Ranger, S. Hallegatte, J. Corfee-Morlot, C. Herweijer, and J. Chateau, "A global ranking of port cities with high exposure to climate extremes," *Climatic change*, vol. 104, pp. 89–111, 2011.

[35] M. Ouyang, Y. Ito, and T. Tokunaga, "Local land subsidence exacerbates inundation hazard to the kujukuri plain, japan," *Proceedings of the International Association of Hydrological Sciences*, vol. 382, pp. 657–661, 2020.

[36] D. L. Galloway, D. R. Jones, and S. E. Ingebritsen, *Land subsidence in the United States*. Geological Survey (USGS), 1999, vol. 1182.

[37] H. Jiang, J. Zhang, Y. Liu, J. Li, and Z. N. Fang, "Does flooding get worse with subsiding land? investigating the impacts of land subsidence on flood inundation from hurricane harvey," *Science of the total environment*, vol. 865, p. 161072, 2023.

[38] Deltares. (2020) Delft3D Flexible Mesh Suite. [Online]. Available: https://www.deltares.nl/en/software/delft3d-flexible-mesh-suite/

[39] W. Huang, F. Ye, Y. J. Zhang, K. Park, J. Du, S. Moghimi, E. Myers, S. Pe'eri, J. R. Calzada, H. C. Yu, K. Nunez, and Z. Liu, "Compounding factors for extreme flooding around Galveston Bay during Hurricane Harvey," *Ocean Modelling*, vol. 158, no. 804, pp. 1–35, 2021.

[40] Y. J. Zhang, F. Ye, H. Yu, W. Sun, S. Moghimi, E. Myers, K. Nunez, R. Zhang, H. Wang, A. Roland, J. Du, and Z. Liu, "Simulating compound flooding events in a hurricane," *Ocean Dynamics*, vol. 70, no. 5, pp. 621–640, 2020.

[41] National Oceanic and Atmospheric Administration. (2022) Sea, lake, and overland surges from hurricanes (slosh). [Online]. Available: https://www.nhc.noaa.gov/surge/slosh.php

[42] Center for Computation and Technology and Louisiana Sea Grant, Louisiana State University. (2022) Coastal Emergency Risks Assessment. [Online]. Available: https://coastalrisk.live/

[43] Federal Emergency Management Agency, "Guidance for Flood Risk Analysis and Mapping: Coastal Water Levels," Tech. Rep., 2016.

[44] F. L. Santiago-Collazo, M. V. Bilskie, and S. C. Hagen, "A comprehensive review of compound inundation models in low-gradient coastal watersheds," *Environmental Modelling and Software*, vol. 119, no. June, pp. 166–181, 2019. [Online]. Available: https://doi.org/10.1016/j.envsoft.2019.06.002

[45] M. Karamouz, A. Razmi, S. Nazif, and Z. Zahmatkesh, "Integration of inland and coastal storms for flood hazard assessment using a distributed hydrologic model," *Environmental Earth Sciences*, vol. 76, no. 11, pp. 1–17, 2017.

[46] W. F. Silva-Araya, F. L. Santiago-Collazo, J. Gonzalez-Lopez, and J. Maldonado-Maldonado, "Dynamic modeling of surface runoff and storm surge during hurricane and tropical storm events," *Hydrology*, vol. 5, no. 1, pp. 1–28, 2018.

[47] R. Bakhtyar, K. Maitaria, P. Velissariou, B. Trimble, H. Mashriqui, S. Moghimi, A. Abdolali, A. J. Van der Westhuysen, Z. Ma, E. P. Clark, and T. Flowers, "A New 1D/2D Coupled Modeling Approach for a Riverine-Estuarine System Under Storm Events: Application to Delaware River Basin," *Journal of Geophysical Research: Oceans*, vol. 125, no. 9, 2020.

[48] W. B. Chen and W. C. Liu, "Modeling flood inundation induced by river flow and storm surges over a river basin," *Water*, vol. 6, no. 10, pp. 3182–3199, 2014.

[49] O. E. Wing, C. C. Sampson, P. D. Bates, N. Quinn, A. M. Smith, and J. C. Neal, "A flood inundation forecast of Hurricane Harvey using a continental-scale 2D hydrodynamic model," *Journal of Hydrology*, vol. 4, no. August, 2019.

[50] Y. Zhang and M. R. Najafi, "Probabilistic Numerical Modeling of Compound Flooding Caused by Tropical Storm Matthew Over a Data-Scarce Coastal Environment," *Water Resources Research*, vol. 56, no. 10, 2020.

[51] J. L. Goodall, B. F. Robinson, and A. M. Castronova, "Modeling water resource systems using a service-oriented computing paradigm," *Environmental Modelling & Software*, vol. 26, no. 5, pp. 573–582, 2011.

[52] M. Sulis, S. B. Meyerhoff, C. Paniconi, R. M. Maxwell, M. Putti, and S. J. Kollet, "A comparison of two physics-based numerical models for simulating surface water–groundwater interactions," *Advances in Water Resources*, vol. 33, no. 4, pp. 456–467, 2010.

[53] T. Campbell, R. Allard, R. Preller, L. Smedstad, A. Wallcraft, Sue Chen, Hao Jin, S. Gaberšek, R. Hodur, J. Reich, C. D. Fry, V. Eccles, Hwai-Ping Cheng, J.-R. C. Cheng, R. Hunter, C. DeLuca, and G. Theurich, "Integrated Modeling of the Battlespace Environment," *Computing in Science & Engineering*, vol. 12, no. 5, pp. 36–45, sep 2010.

[54] H. S. Tang, S. I. Chien, M. Temimi, C. A. Blain, Q. Ke, L. Zhao, and S. Kraatz, "Vulnerability of population and transportation infrastructure at the east bank of Delaware Bay due to coastal flooding in sea-level rise conditions," *Natural Hazards*, vol. 69, no. 1, pp. 141–163, 2013.

[55] F. Ye, Y. J. Zhang, H. Yu, W. Sun, S. Moghimi, E. Myers, K. Nunez, R. Zhang, H. V. Wang, A. Roland, K. Martins, X. Bertin, J. Du, and Z. Liu, "Simulating storm surge and compound flooding events with a creek-to-ocean model: Importance of baroclinic effects," *Ocean Modelling*, vol. 145, no. July 2019, p. 101526, 2020. [Online]. Available: https://doi.org/10.1016/j.ocemod.2019.101526

[56] C. Copeland, "Hurricane-damaged drinking water and wastewater facilities: Impacts, needs, and response." Congressional Research Service, the Library of Congress, 2005.

[57] S. A. Mejia Manrique, E. W. Harmsen, R. M. Khanbilvardi, and J. E. González, "Flood Impacts on Critical Infrastructure in a Coastal Floodplain in Western Puerto Rico during Hurricane María," *Hydrology*, vol. 8, no. 3, p. 104, 2021.

[58] K. J. Schwab, K. E. Gibson, D. L. Williams, K. M. Kulbicki, C. P. Lo, J. N. Mihalic, P. N. Breysse, F. C. Curriero, and A. S. Geyh, "Microbial and chemical assessment of regions within New Orleans, LA impacted by Hurricane Katrina," *Environmental Science & Technology*, vol. 41, no. 7, pp. 2401–2406, 2007.

[59] U.S. Environmental Protection Agency. (2019) EPA Region 6 Quickly Assessed Water Infrastructure after Hurricane Harvey but Can Improve Emergency Outreach to Disadvantaged Communities. [Online]. Available: https://www.epa.gov/sites/default/files/2019-07/documents/$_{e}paoig_{2}0190716_{1}9-p-0236.pdf$

[60] G. Wasileski, H. Rodríguez, and W. Diaz, "Business closure and relocation: a comparative analysis of the Loma Prieta earthquake and Hurricane Andrew," *Disasters*, vol. 35, no. 1, pp. 102–129, 2011.

[61] United States Census Bureau. (2021) Quickfacts. [Online]. Available: https:https://www.census.gov/quickfacts/fact/table/beaumontcitytexas,US/HSG650219

[62] Lower Neches Valley Authority, "Stakeholder Update: The Texas Clean Rivers Program," Tech. Rep., 2018.

[63] A. Sebastian, D. Bader, C. Nederhoff, T. Leijnse, J. Bricker, and S. Aarninkhof, "Hindcast of pluvial, fluvial, and coastal flood damage in Houston, Texas during Hurricane Harvey (2017) using SFINCS," *Natural Hazards*, vol. 109, no. 3, pp. 2343–2362, 2021.

[64] V. M. Santos, T. Wahl, R. Jane, S. K. Misra, and K. D. White, "Assessing compound flooding potential with multivariate statistical models in a complex estuarine system under data constraints," *Journal of Flood Risk Management*, vol. 14, no. 4, p. e12749, 2021.

[65] A. Couasnon, A. Sebastian, and O. Morales-Nápoles, "A copula-based bayesian network for modeling compound flood hazard from riverine and coastal interactions at the catchment scale: An application to the Houston Ship Channel, Texas," *Water*, vol. 10, no. 9, p. 1190, 2018.

[66] F. Liu, "Analyzing the influence of compound events on flooding in the downstream reach of the Houston Ship Channel," 2017.

[67] D. F. Muñoz, P. Abbaszadeh, H. Moftakhari, and H. Moradkhani, "Accounting for uncertainties in compound flood hazard assessment: The value of data assimilation," *Coastal Engineering*, vol. 171, p. 104057, 2022.

[68] E. S. Blake and D. A. Zelinsky, "National Hurricane Center Tropical Cyclone Report: Hurricane Harvey," National Oceanic and Atmospheric Administration, National Weather Service, Tech. Rep., 2018. [Online]. Available: https://www.nhc.noaa.gov/data/tcr/AL092017_Harvey.pdf

[69] D. F. Muñoz, H. Moftakhari, and H. Moradkhani, "Compound Effects of Flood Drivers and Wetland Elevation Correction on Coastal Flood Hazard Assessment," *Water Resources Research*, vol. 56, no. 7, pp. 1–21, 2020.

[70] D. F. Muñoz, H. Moftakhari, M. Kumar, and H. Moradkhani, "Compound effects of flood drivers, sea level rise, and dredging protocols on vessel navigability and wetland inundation dynamics," *Frontiers in Marine Science*, vol. 9, 2022.

[71] J. Veeramony, A. Condon, and M. van Ormondt, "Forecasting storm surge and inundation: model validation," *Weather and Forecasting*, vol. 32, no. 6, pp. 2045–2063, 2017.

[72] Deltares, "Delft3D Hydro-Morphodynamics User Manual," Deltares, Tech. Rep., 2022. [Online]. Available: https://content.oss.deltares.nl/delft3d/manuals/Delft3D-FLOW$_{U}ser_{M}anual.pdf$

[73] K. M. Thyng, R. D. Hetland, S. A. Socolofsky, N. Fernando, E. L. Turner, and C. Schoenbaechler, "Hurricane Harvey caused unprecedented freshwater inflow to Galveston Bay," *Estuaries and Coasts*, vol. 43, no. 7, pp. 1836–1852, 2020.

[74] Cooperative Institute for Research in the Atmosphere. (2021) The Tropical Cyclone Extended Best Track Dataset (EBTRK): Atlantic Basin Dataset 1851 to 2020. [Online]. Available: https://rammb2.cira.colostate.edu/wp-content/uploads/2020/11/EBTRK$_{A}L_{f}inal_{1}851-2020_{n}ew_{f}ormat_{v}3.0.1_{2}3-Aug-2021.txt$

[75] R. D. Knabb, D. P. Brown, and J. R. Rhome, "National Hurricane Center Tropical Cyclone Report: Hurricane Rita," National Oceanic and Atmospheric Administration, National Weather Service, Tech. Rep., 2006.

[76] M. Ebad Sichani, K. A. Anarde, K. M. Capshaw, J. E. Padgett, R. A. Meidl, P. Hassanzadeh, T. P. Loch-Temzelides, and P. B. Bedient, "Hurricane risk assessment of petroleum infrastructure in a changing climate," *Frontiers in Built Environment*, vol. 6, p. 104, 2020.

[77] R. Berg, "National Hurricane Center Tropical Cyclone Report: Hurricane Ike," National Oceanic and Atmospheric Administration, National Weather Service, Tech. Rep., 2009.

[78] National Weather Service. (2017) Hurricane Harvey and Its Impacts on Southeast Texas (August 25-29, 2017). [Online]. Available: https://www.weather.gov/hgx/hurricaneharvey

[79] T. M. Brown-Giammanco, I. M. Giammanco, and H. Pogorzelski, "Hurricane Harvey Wind Damage Investigation," Tech. Rep., 2018.

[80] Federal Emergency Management Agency and US Army Corps of Engineers, "Flood Insurance Study: Coastal Counties, Texas. Intermediate Submission 2: Scoping and Data Review," Tech. Rep., 2011.

[81] U.S. Geological Survey, "Enhanced National Land Cover Data 1992 (NLCDe 92)," Tech. Rep., 2010.

[82] National Center for Atmospheric Research. (2022) Research data archive: Computational and information system lab. [Online]. Available: https://rda.ucar.edu/datasets/ds608.0/index.htmlcgi-bin/datasets/

[83] ——. (2017) The Climate Data Guide: CCMP: Cross-Calibrated Multi-Platform wind vector analysis. [Online]. Available: https://climatedataguide.ucar.edu/climate-data/ccmp-cross-calibrated-multi-platform-wind-vector-analysis

[84] National Oceanic and Atmospheric Administration. (2022) Index of /aorc-historic. [Online]. Available: https://hydrology.nws.noaa.gov/aorc-historic/

[85] Iowa Environmental Mesonet. (2022) Multi-Radar Multi-Sensor Data Respository. [Online]. Available: https://mtarchive.geol.iastate.edu/2017/

[86] U.S. Geological Survey. (2022) National Water Information System: Web Interface. [Online]. Available: https://waterdata.usgs.gov/nwis/inventory?agency$_c ode = USGS site_n o =$ 08041780

[87] National Science Foundation. (2019) Hydroshare thredds service: Dataset. [Online]. Available: https://thredds.hydroshare.org/thredds/catalog/catalog.html

[88] National Oceanic and Atmospheric Administration. (2022) Tides and currents. [Online]. Available: https://tidesandcurrents.noaa.gov

[89] S. Muis, M. Verlaan, H. C. Winsemius, J. C. Aerts, and P. J. Ward, "A global reanalysis of storm surges and extreme sea levels," *Nature Communications*, vol. 7, no. 1, pp. 1–12, 2016.

[90] M.-H. Hsu, A. Y. Kuo, J.-T. Kuo, and W.-C. Liu, "Procedure to calibrate and verify numerical models of estuarine hydrodynamics," *Journal of Hydraulic Engineering*, vol. 125, no. 2, pp. 166–182, 1999.

[91] P. Abbaszadeh, D. F. Muñoz, H. Moftakhari, K. Jafarzadegan, and H. Moradkhani, "Perspective on uncertainty quantification and reduction in compound flood modeling and forecasting," *Iscience*, p. 105201, 2022.

[92] T. G. Asher, R. A. Luettich Jr, J. G. Fleming, and B. O. Blanton, "Low frequency water level correction in storm surge models using data assimilation," *Ocean Modelling*, vol. 144, p. 101483, 2019.

[93] National Oceanic and Atmospheric Administration, "Tide Prediction Error for the United States Stations," Tech. Rep., 2013.

[94] U.S. Geological Survey. (2011) Discharge measurement quality code. [Online]. Available: https://help.waterdata.usgs.gov/codes-and-parameters/discharge-measurement-quality-code

[95] J. C. Dietrich, S. Tanaka, J. J. Westerink, C. N. Dawson, R. Luettich, M. Zijlema, L. H. Holthuijsen, J. Smith, L. Westerink, and H. Westerink, "Performance of the unstructured-mesh, SWAN+ADCIRC model in computing hurricane waves and surge," *Journal of Scientific Computing*, vol. 52, no. 2, pp. 468–497, 2012.

[96] T. Wahl, S. Jain, J. Bender, S. D. Meyers, and M. E. Luther, "Increasing risk of compound flooding from storm surge and rainfall for major us cities," *Nature Climate Change*, vol. 5, no. 12, pp. 1093–1097, 2015.

[97] J. Zscheischler, O. Martius, S. Westra, E. Bevacqua, C. Raymond, R. M. Horton, B. van den Hurk, A. AghaKouchak, A. Jézéquel, M. D. Mahecha, D. Maraun, A. M. Ramos, N. N. Ridder, W. Thiery, and E. Vignotto, "A typology of compound weather and climate events," *Nature Reviews Earth Environment*, vol. 1, pp. 333–347, 2020. [Online]. Available: http://dx.doi.org/10.1038/s43017-020-0060-z

[98] M. I. Vousdoukas, L. Mentaschi, E. Voukouvalas, M. Verlaan, and L. Feyen, "Extreme sea levels on the rise along europe's coasts," *Earth's Future*, vol. 5, no. 3, pp. 304–323, 2017.

[99] S. Pfahl, P. A. O'Gorman, and E. M. Fischer, "Understanding the regional pattern of projected future changes in extreme precipitation," *Nature Climate Change*, vol. 7, no. 6, pp. 423–427, 2017.

[100] Y. Hirabayashi, R. Mahendran, S. Koirala, L. Konoshima, D. Yamazaki, S. Watanabe, H. Kim, and S. Kanae, "Global flood risk under climate change," *Nature climate change*, vol. 3, no. 9, pp. 816–821, 2013.

[101] H. Lee, K. Calvin, D. Dasgupta, G. Krinner, A. Mukherji, P. Thorne, C. Trisos, J. Romero, P. Aldunce, K. Barrett *et al.*, "Synthesis report of the intergovernmental panel on climate change," Tech. Rep., 2023.

[102] W. V. Sweet, B. D. Hamlington, R. E. Kopp, C. P. Weaver, P. L. Barnard, D. Bekaert, W. Brooks, M. Craghan, G. Dusek, T. Frederikse *et al.*, "Global and regional sea level rise scenarios for the united states: updated mean projections and extreme water level probabilities along us coastlines," 2022.

[103] K. Waddington, D. Khojasteh, L. Marshall, D. Rayner, and W. Glamore, "Quantifying the effects of sea level rise on estuarine drainage systems," *Water Resources Research*, vol. 58, no. 6, p. e2021WR031405, 2022.

[104] T. R. Knutson, J. J. Sirutis, G. A. Vecchi, S. Garner, M. Zhao, H.-S. Kim, M. Bender, R. E. Tuleya, I. M. Held, and G. Villarini, "Dynamical downscaling projections of twenty-first-century atlantic hurricane activity: Cmip3 and cmip5 model-based scenarios," *Journal of Climate*, vol. 26, no. 17, pp. 6591–6617, 2013.

[105] D. B. Wright, T. R. Knutson, and J. A. Smith, "Regional climate model projections of rainfall from us landfalling tropical cyclones," *Climate dynamics*, vol. 45, pp. 3365–3379, 2015.

[106] M. Liu, G. A. Vecchi, J. A. Smith, and T. R. Knutson, "Causes of large projected increases in hurricane precipitation rates with global warming," *npj Climate and Atmospheric Science*, vol. 2, no. 1, p. 38, 2019.

[107] A. Gori, N. Lin, D. Xi, and K. Emanuel, "Tropical cyclone climatology change greatly exacerbates us extreme rainfall–surge hazard," *Nature Climate Change*, vol. 12, pp. 171–178, 2022.

[108] H. R. Moftakhari, G. Salvadori, A. AghaKouchak, B. F. Sanders, and R. A. Matthew, "Compounding effects of sea level rise and fluvial flooding," *Proceedings of the National Academy of Sciences*, vol. 114, no. 37, pp. 9785–9790, 2017.

[109] E. Bevacqua, D. Maraun, M. I. Vousdoukas, E. Voukouvalas, M. Vrac, L. Mentaschi, and M. Widmann, "Higher probability of compound flooding from precipitation and storm surge in europe under anthropogenic climate change," 2019. [Online]. Available: https://www.science.org

[110] P. D. Bates, N. Quinn, C. Sampson, A. Smith, O. Wing, J. Sosa, J. Savage, G. Olcese, J. Neal, G. Schumann *et al.*, "Combined modeling of us fluvial, pluvial, and coastal flood hazard under current and future climates," *Water Resources Research*, vol. 57, no. 2, p. e2020WR028673, 2021.

[111] M. Deb, N. Sun, Z. Yang, T. Wang, D. Judi, Z. Xiao, and M. S. Wigmosta, "Interacting effects of watershed and coastal processes on the evolution of compound flooding during hurricane irene," *Earth's Future*, vol. 11, no. 3, p. e2022EF002947, 2023.

[112] Texas Water Development Board. (2023) Sabine-Neches Estuary. [Online]. Available: https://www.twdb.texas.gov/surfacewater/bays/major$_e$*stuaries*/*sabine*$_n$*eches*/*index.asp*

[113] U.S. Census Bureau. (2020) QuickFacts. [Online]. Available: https://www.census.gov/quickfacts/fact/table/

[114] National Oceanic and Atmospheric Administration. (2020) Relative sea level trends. [Online]. Available: https://tidesandcurrents.noaa.gov/sltrends/

[115] K. Emanuel, "Assessing the present and future probability of hurricane harvey's rainfall," *Proceedings of the National Academy of Sciences*, vol. 114, no. 48, pp. 12 681–12 684, 2017.

[116] N. Maymandi, M. A. Hummel, and Y. Zhang, "Compound coastal, fluvial, and pluvial flooding during historical hurricane events in the sabine-neches estuary, texas," *Water Resources Research*, p. e2022WR033144, 2022.

[117] Federal Emergency Management Agency. (2022) Flood assessment structure tool. [Online]. Available: https://www.fema.gov/sites/default/files/documents/fema$_f$*lood* − *assessment* − *structure* − *tool.pdf*

[118] U.S. Army Corps of Engineers. (2022) National structure inventory. [Online]. Available: https://www.hec.usace.army.mil/confluence/nsi/

[119] Federal Emergency Management Agency, "Hazus Flood Technical Manual," Tech. Rep., 2022.

[120] ——. (2023) Housing assistance program data. [Online]. Available: https://www.fema.gov/openfema-data-page/housing-assistance-program-data-owners-v2

[121] ——. (2023) Nfip redacted claims. [Online]. Available: https://www.fema.gov/openfema-data-page/fima-nfip-redacted-claims-v2

[122] S. J, "Eye of the storm: Report of the governor's commission to rebuild texas," US Geological Survey, Tech. Rep., 2018.

[123] C. N. Dawson, C. Del-Castillo-Negrete, A. Shukla, B. PACHEV, C. Kaiser, and E. Kutanoglu, "Adcirc simulation of synthetic storms in the gulf of mexico," 2021. [Online]. Available: https://www.designsafe-ci.org/data/browser/public/designsafe.storage.published/PRJ-2968/details-7112540539143646740-242ac114-0001-012

[124] J. A. Hall, C. P. Weaver, J. Obeysekera, M. Crowell, R. M. Horton, R. E. Kopp, J. Marburger, D. C. Marcy, A. Parris, W. V. Sweet *et al.*, "Rising sea levels: Helping decision-makers confront the inevitable," *Coastal Management*, vol. 47, no. 2, pp. 127–150, 2019.

[125] S. Vitousek, P. L. Barnard, C. H. Fletcher, N. Frazer, L. Erikson, and C. D. Storlazzi, "Doubling of coastal flooding frequency within decades due to sea-level rise," *Scientific reports*, vol. 7, no. 1, pp. 1–9, 2017.

[126] K. Crossett, B. Ache, P. Pacheco, and K. Haber, "National coastal population report, population trends from 1970 to 2020," *NOAA State of the Coast Report Series, US Department of Commerce, Washington*, 2013.

[127] G. A. Vecchi, T. L. Delworth, H. Murakami, S. D. Underwood, A. T. Wittenberg, F. Zeng, W. Zhang, J. W. Baldwin, K. T. Bhatia, W. Cooke *et al.*, "Tropical cyclone sensitivities to co 2 doubling: Roles of atmospheric resolution, synoptic variability and background climate changes," *Climate Dynamics*, vol. 53, pp. 5999–6033, 2019.

[128] S. Dangendorf, A. Arns, J. G. Pinto, P. Ludwig, and J. Jensen, "The exceptional influence of storm 'xaver'on design water levels in the german bight," *Environmental Research Letters*, vol. 11, no. 5, p. 054001, 2016.

[129] A. Arns, S. Dangendorf, J. Jensen, S. Talke, J. Bender, and C. Pattiaratchi, "Sea-level rise induced amplification of coastal protection design heights," *Scientific reports*, vol. 7, no. 1, p. 40171, 2017.

[130] P. Orton, N. Lin, V. Gornitz, B. Colle, J. Booth, K. Feng, M. Buchanan, M. Oppenheimer, and L. Patrick, "New york city panel on climate change 2019 report chapter 4: coastal flooding," *Annals of the New York Academy of Sciences*, vol. 1439, no. 1, pp. 95–114, 2019.

[131] J. M. Kruger, "Potential use of subsidence rates determined from gps-based height modernization measurements of ngs benchmarks in southeast texas for flood risk planning," in *AGU Fall Meeting Abstracts*, vol. 2019, 2019, pp. NH31E–0896.